UNIVERSITY OF CALIFORNIA
RIVERSIDE

Smart and Functional Interfaces for Sensitive SPR Biosensing Towards Biomedical Applications

A Dissertation submitted in partial satisfaction
of the requirements for the degree of

Doctor of Philosophy

in

Chemical and Environmental Engineering

by

Nor Akmaliza Rais

December 2019

Dissertation Committee:
Dr. Quan Cheng, Chairperson
Dr. Ashok Mulchandani
Dr. Richard Hooley

The Dissertation of Nor Akmaliza Rais is approved:

_____

_____

_____

Committee Chairperson

University of California, Riverside

PERSONAL ACKNOWLEDGEMENT

All good things must come to an end, so does my journey in UCR. I am looking forward to the next phase in my life, taking with me all the valuable academic and life experiences I gained since I came to UCR in Spring 2014. First and foremost, to Prof. Quan (Jason) Cheng, my Advisor and the Chairperson of my Dissertation Committee. I could not have achieved this without his trust, and he taught me what a good scientist (and mentor) should be. Being in his group we are provided the opportunity to explore research and build ourselves as independent researchers, while guiding us to accomplish the objectives. I am forever grateful to Dr. Cheng for the knowledges and allowing me to be an expert in biosensors technologies, the reason why I chose to leave the comfort of life in Malaysia and pursue a PhD. I gratefully acknowledge the other members of my Committee, Prof. Ashok Mulchandani and Prof. Richard Hooley, for their time and guidance from my Qualifying Exam until the completion of my study.

To the people I look forward to meeting every day (and nights!), my lab members in "Biosensors Technology and Fabrication Lab", the memories of us taking the spam calls would be one of those I will miss the most. When I joined the lab in Fall 2016, I met two most amazing people who had been so patient and generous with sharing their knowledges and taught me the skills I have now – Dr. Kristy McKeating and Dr. Sam Hinman. Then, there were Dr. Pete Shanta, Kelvin Tran, Daniel Shields, Zhengdong Yang, Alex Lambert, Bochao Li, Santino Valiulis, Daniel Stuart, Alex Malinick and Fatimah Abouhajar, the best lab companion I could ever wish for. Thank you for the help whenever I got stuck or needed someone to watch the experiments, and for the friendship. I wish everyone all the best in

their future endeavors! To all the visiting scholars and students which I am glad to get the chance to meet and share the experiences. To the undergraduate students whom I had supervised during their time in the lab; Vani Bhardwaj, Chathu Keerthisinghe and Alexander Martinez, thank you for believing in me and from you I learn so much about being a good teacher.

So many people I am thankful to, including the faculties and staffs in the Dept. of Chemical and Environmental Engineering and Dept. of Chemistry, for their support during my time in UCR. A special thanks to Prof. Nosang Myung, who introduced me to the sensor research opportunity in UCR. I would like to recognize the staffs at the International Affairs office who always make me feel at home and assisted in the matters of international students. To all my friends in UCR, it was always good to have some good times even with the stress of being students, I appreciate the acquaintance and the inspiration of the hard work put into the research works and academics to make this world a better place.

Nobody has been more important to me in the pursuit of this study, than the members of my family. I would like to thank my parents; my 'Abah' Rais Bin Sukimi and my 'Mak' Fatimah Binti Ibrahim, for their love, encouragement and accepting that I can't always be there for them. To my wonderful daughters; Adani and Arisha, I hope you learn that everything is possible if you have a strong determination. I love both of you, thank you so much for the understanding and for being here with me. Also, to my siblings, I appreciate their help and for being there when I needed them most. Last but not least, to my friends in the community whom I am extremely grateful to have around and provide the sense of having a family here, and the emotional support throughout this journey.

PROFESSIONAL ACKNOWLEDGEMENT

This work would not have been possible without the financial support of my sponsor Skim Pascasiswazah Majlis Amanah Rakyat (MARA), Malaysia. I am especially indebted to UCR Graduate Student Association (GSA) Travel Conference for providing the funding enabled me to present in Pittcon Conference and UC Chemical Symposium (UCCS) in Spring 2019. I would like to thank Dr. Wei Cheng from The Center for Clinical Molecular Medical detection, the First Affiliated Hospital of Chongqing Medical University, Chongqing, China, for the collaboration in the Malaria project. Also, special appreciation to the team in UCR cleanroom facility (CNSENF); Mark Heiden, Dr. Dong Yan and Frank Lee for their support and guidance. Finally, to the team in Dept. of Mechanical Engineering Machine Shop for always willing to help whenever I needed some machining and fabrication tasks.

COPYRIGHT ACKNOWLEDGEMENT

The text and figures in Chapter 3 is adapted from a published article "Antifouling Lipid Membranes over Protein A for Orientation-Controlled Immunosensing in Undiluted Serum and Plasma, *ACS Sens*. **2019**, 4, 7, 1774-1782". The authors listed in that publication has contributed in the following scopes. Samuel S. Hinman and Kristy S. McKeating initiated the research and performed the works related to lipids characterization and detection of IgG. The extensive washing experiment, comparison with traditional SAM and detection of Cholera Toxin was accomplished by Nor Akmaliza. The research was directed and supervised by Prof. Quan Cheng.

I dedicate this dissertation to my daughters,

Adani Khairunnisa and Arisha Humaira,

the reason I keep on going.

ABSTRACT OF THE DISSERTATION

Smart and Functional Interfaces for Sensitive SPR Biosensing Towards Biomedical Applications

by

Nor Akmaliza Rais

Doctor of Philosophy, Graduate Program in Chemical and Environmental Engineering
University of California, Riverside, December 2019
Dr. Quan Cheng, Chairperson

The aim of this thesis is to develop Surface Plasmon Resonance (SPR) methods that improve biosensing performance, in particular the sensitivity and selectivity of the analysis and their adaptation for biomedical applications to samples with complex background. This is of significant importance in translating the biosensor technologies to deliver the same results as the conventional methods but in a more accessible, efficient, and economical manner. The first study exploited SPR as a DNA biosensor for the detection of Malaria *Plasmodium falciparum* parasite with the hybridization chain reaction (HCR), which resulted in the formation of self-assembled target DNA nanostructures for signal enhancement. The sensitivity was further improved by using gold nanoparticles (AuNPs) for additional signal amplification. Tests with human blood plasma indicated the results were comparable to analyses in buffer, despite noticeable non-specific binding from the plasma. The concern of non-specific binding was systematically investigated in the second

study where an antifouling surface consists of supported lipid bilayer membranes (SLBs) and protein A was developed for detection of trace amount of proteins in undiluted human serum. Specifically, cholera toxin (CT) spiked into the serum was used as the target, and advanced interface was further extended to immunosensing of immunoglobulin G (IgG). In the third study, SPR biosensor was employed in combination of bright field microscopy to characterize cellular apoptosis. HeLa cells undergoing apoptosis induced by hydrogen peroxide (H_2O_2) were monitored by SPR and the signals were compared to microscopic analysis of the morphological changes. SPR study revealed a decreased signal as cell confluency decreases, with the rates increasing as H_2O_2 concentration increases. An abnormality was found at high concentrations when both apoptosis and necrosis were induced. A mathematical model was proposed to explain SPR response where a non-uniform adsorbed layer was partially responsible. The significance of this thesis is that a number of high performing biosensing approaches have been developed and demonstrated. In addition to the advantages of SPR (e.g. label-free, real-time biomolecules binding, and portability), these methods have paved the way towards realizing effective sensing in biomedical research, especially in the early detection of infectious diseases and in the treatment of cancers.

TABLE OF CONTENTS

LIST OF FIGURES

LIST OF TABLES

CHAPTER 1 : Motivation, Challenges and Introduction to SPR Biosensors for Biomedical Research

1.1 Medical and Clinical Diagnostics Processes

Medical and clinical diagnostics is the practice of detecting, identifying and monitoring a disease or medical disorder. A diagnostic process begins when a patient experiences a health problem and engages with health care system. The processes consist of gathering and interpreting information and working diagnosis which includes physical exam and diagnostic testing.[1] The diagnostic testing can be through clinical lab, medical imaging, and anatomy pathology where tissue samples are taken from a biopsy. Diagnostic testing is important for detecting infectious diseases such as tuberculosis, Malaria and HIV, as early detection helps in the patients' treatment and eradication of the diseases.[2] Most diagnostic techniques used for such diseases involves collecting patients' bodily fluids such as blood and urine, then taking them to laboratory for series of tests. Common techniques includes immunoassays such as ELISA, colorimetric, microscopy, protein Western blot, rapid immunotechniques sticks, and nucleic acid based test; which are laborious, slow, less sensitive, and sometimes ineffective, and expensive.[3] For more severe diseases like cancer, the diagnosis is more complicated that it requires more than blood lab tests or tissue samples test for the tumor biomarkers.[4] In addition to tests, the diagnosis of cancers also include 1) physical exam for lumps and other abnormalities, 2) imaging tests such as computerized tomography (CT) scan, bone scan, magnetic resonance imaging (MRI),

positron emission tomography (PET) scan, ultrasound and X-ray, and 3) sample cells biopsy.[5, 6]

Although many advanced and rapid diagnostic techniques for infectious diseases are being developed, an increased focus on customized and consumer-driven health care has also increased the demand for point of care diagnostic and home testing device kit which can take place of traditional laboratory-based testings.[3] This refers to a technology where the bulky equipment is miniaturized into a portable size and integrated with a data processing for faster results analysis and transfer of data via a wireless communication. In the case of cancers diagnosis, while the current diagnostic techniques cannot be replaced, oncology studies can benefit from a simple bioanalysis techniques to detect cancer biomarkers or even in monitoring of cancer cells toxicity effects for new drugs development.[7]

1.2 Biosensors for Biomedical Applications

Biosensors technology is actively researched in the medical field to diagnose infectious diseases and many types of cancers.[8, 9] One of the advantages of biosensors is that the detection of target molecule is achievable in very low quantities, thus allowing early detection of diseases.[10] A biosensor has been demonstrated to be working *in vitro* and *in vivo* environment for a precise detection of disease biomarker.[11] In another development, many strategies were attempted for biosensor platforms that are miniaturized,[9] wearable,[12] non-invasive,[13] portable,[14, 15] potential for point-of-care

testing,[16, 17] connected to smart phones[18] and integrated to the Internet-of-Things (IoT) data communication networks for continuous monitoring of patients conditions.[19]

In clinical diagnosis, biosensors have been used for the detection and monitoring of various analytes, such as glucose, urea, lactate, cholesterol, and uric acid in biological samples including blood, serum and urine.[20] Although many novel biosensors have been developed for research purposes, and while biosensing instruments can be easily found in labs, only two over-the-counter biosensors are available. Glucose meter is the best example of how biosensor contributes to a more effective healthcare, that patients can have immediate response to their medical condition without having to wait for lab results. For people who has diabetic condition, monitoring the glucose level in blood has become an important part in managing their life to avoid long-term complication. Today, technology trend of glucose meter is moving towards noninvasive and continuous glucose monitoring, both eliminate the need of drawing blood and provide real time measurement. Another successful biosensor is the pregnancy test kit using urine sample, which is affordable and easy to use. Most pregnancy test kit is a qualitative test; however, a quantitative type has already been available in the market, able to determine the weeks after conception. The glucose meter and pregnancy test show that it is feasible to produce biosensors that can directly impact the healthcare field. However, a lot more work has to be done to translate lab scale biosensors to a real world application[21].

1.3 Principles of Biosensors

Biosensors are analytical devices that consist of a biological recognition element and a suitable transducer, usually coupled to an appropriate data processing system.[22] Other than in the medical field, biosensors have also been used widely in other applications such as food quality assurance,[23] agriculture, pharmaceutical, defense and environmental monitoring.[24]

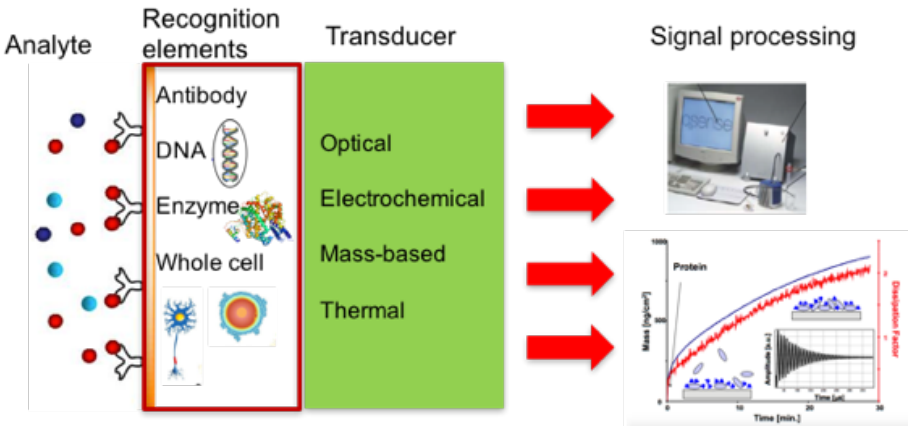

Figure 1.1 Schematic of biosensor

As is depicted in Figure 1.1, the biological recognition element of a biosensor can be antibody, DNA, enzyme, or whole cell. Recognition elements can be immobilized on a sensor support or sensor surface using different methods such as entrapment, encapsulation, adsorption, and covalent attachment. The transducer then converts the physico-chemical change, due to the interaction of molecules with the receptor, into a measurable output signal. The signal processing is the part of biosensor that process, amplify and quantify the transduced signal, before it is ready for display on the user

interface. Most transducers produce either optical or electrical signals that are usually proportional to the amount of the interaction between the analyte and its biorecognition element. The typical characteristics of biosensors are;[24]

a) Selectivity: The ability of bioreceptors to detect the specific analyte in a mixture of sample and contaminants. For example; specific interaction of antibody with a particular antigen
b) Reproducibility: The ability of the biosensor to generate identical responses for a duplicated experimental set-up.
c) Stability: The degree of susceptibility to ambient disturbances in and around the biosensing system.
d) Sensitivity: The minimum amount of analyte that can be detected by a biosensor defines its limit of detection (LOD) or sensitivity.
e) Linearity: The attribute that shows the accuracy of the measured response (for a set of measurements with different concentrations of analyte) to a straight line

Biosensors are most commonly classified based on the biorecognition element and the signal transduction. Based on the biological recognition element, biosensors have been classified into enzymatic, immunosensors, DNA biosensors, and whole-cell biosensors.[25, 26] Enzyme biosensors have been devised on immobilization methods, i.e. adsorption of enzymes by van der Waals forces, ionic bonding or covalent bonding. The commonly used enzymes for this purpose are oxidoreductases, polyphenol oxidases, peroxidases, and aminooxidases.[27, 28] Immunosensors were established on the fact that antibodies have high

affinity towards their respective antigens, i.e. the antibodies specifically bind to pathogens or toxins, or interact with components of the host's immune system. The DNA biosensors were devised on the property that single-strand nucleic acid molecule is able to recognize and bind to its complementary strand in a sample. The interaction is due to the formation of stable hydrogen bonds between the two nucleic acid strands (i.e., hybridization). The most widely used whole-cell biosensors are the microbial and mammalian cells tissues, often used to study toxicity, carcinogenicity, and mutagenicity of the cells towards chemicals or drugs under investigation.

Biosensors are also classified according to the transduction techniques; including electrochemical, optical, mass-based/ piezoelectric and thermal sensors. Electrochemical and optical are the two types of detection methods frequently used in biosensors. In electrochemical detection technique, the direct conversion of a biological reaction to an electronic signal is measured. The most common techniques include cyclic voltammetry, chronopotentiometry, impedance spectroscopy and field-effect transistor. Electrochemical sensing usually requires a reference electrode, a counter or auxiliary electrode and a working electrode. The recognition element is commonly enzymes due to their specific binding capabilities and biocatalytic activity, but other elements are used such as antibodies, nucleic acids, cells and microorganism.[22]

Optical biosensors are the most commonly reported class of biosensors, due to their advantages include high specificity, sensitivity, small size and cost effectiveness for the detection of wide range of analytes.[29] Unlike electrochemical methods, optical detection allows a safe non-electrical sensing of biological elements and do not require reference

electrode, making it a simple construction. An optical biosensor usually is a compact device containing the biorecognition elements, combined with optical transducer system that produce a signal which is proportionate to the concentration of measured analytes.

1.4 Surface Plasmon Resonance (SPR) Biosensors

SPR biosensors belong to the label-free optical biosensing technologies. Label-free assays measure the presence of analytes in their natural forms and the detected signal is directly by the interaction of the analytes with the transducer.[30] For labeled assays, either analytes or biorecognition molecules are labeled with signaling tags, such as fluorophores fluorophore, quantum dot or radioisotope, and the optical signal is then generated by a colorimetric, fluorescent or luminescent methods.[31] The label-free method is more preferred for biosensors due to its simplicity and shorter assay time, and has ability to perform measurements of molecular interaction in real-time, thus allowing continuous monitoring.[32] For disease diagnostics purposes, a label-free detection provides more room for small molecular targets, which can be less accessible when a label tag is present.

SPR biosensor has been successfully used for the detection of various analytes such as proteins,[33] DNA,[34] drugs,[35] and microbials such as E. Coli,[36] and bacteria.[37] Because of the advantages offered by SPR method, particularly its versatility for detection of many analytes, label-free, real time monitoring, potential rapid response,[38] the recent development of SPR focuses on more advance medical and healthcare applications. These

include disease biomarkers, [36] pharmaceutical research such as in drug development and drug delivery,[39, 40] and development of portable SPR. [41, 42]

1.4.1 Principle of SPR Detection

The SPR method is based on an optical measurement of a refractive index change associated with the binding of analyte molecules in a sample to the capture molecules immobilized on the SPR sensor surface.[43] An SPR system is typically constructed with a light source, a prism, a sensor chip and a detector that measures the output of the reflected incident light (the Kretschmann Configuration, Figure 1.2). This system is usually combined with a fluidic flow carrying the analyte to be reacted with the ligand immobilized on the sensor surface. In this method, a light source passes through a prism, reflects off the backside of the sensor chip surface and into a detector. At a certain incident angle, known as resonance angle, light is absorbed by the electrons in the metal film on the sensor chip causing them to resonate. This resonating electron are also known as surface plasmons, regarded as an evanescent wave propagating along a metal-dielectric interface.[44] This wave is evanescent meaning it decays exponentially the further it gets from the metal surface, providing a high surface sensitivity to the surrounding environment. The depth of the evanescent wave which is useful for measurement is within 300 nm of the sensor surface.[45] The wavelength of the evanescent field is the same as the wavelength of the incident light at a total internal reflectivity (TIR) condition.

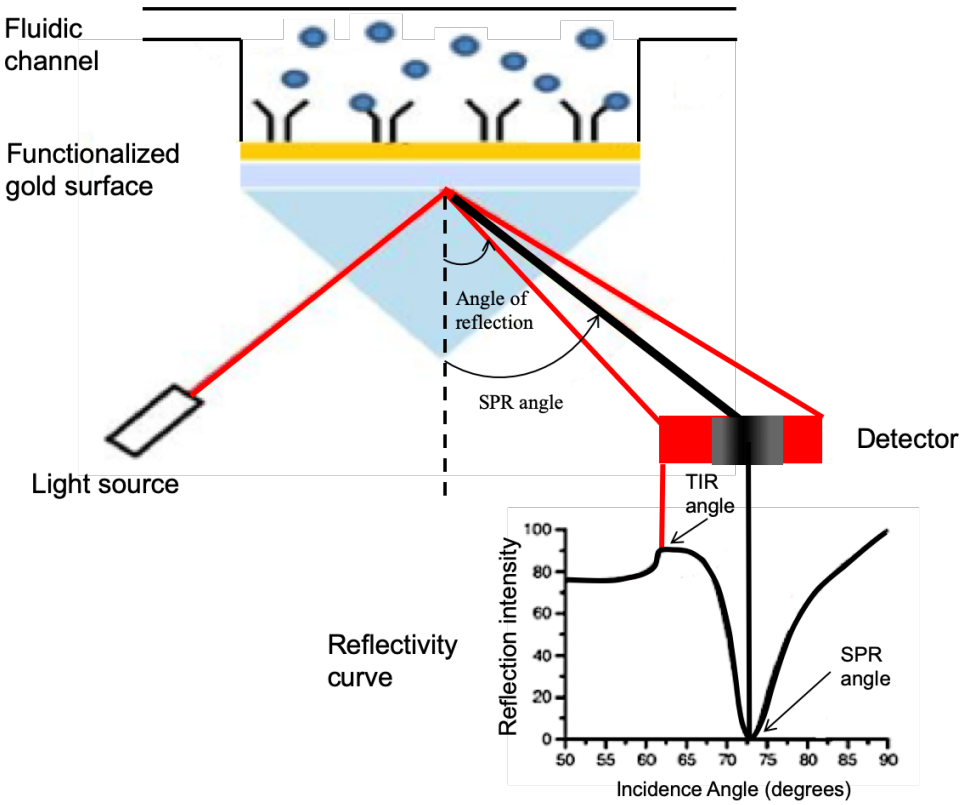

Figure 1.2 SPR Detection: Intensity profile and the shift of SPR angle

With the metal layer acting as a resonator, a coupling can occur between the plasmon of the free electron in the metal and the bound electromagnetic field of the total internally reflected photons. Through the coupling, the energy from the photons is transferred into surface plasmons, resulting in an intensity lost in the reflected beam, which appears as a dark band. This can be seen as a drastic dip in the SPR reflectivity curve showing the resonance angle as the minimum angle. The change in reflected light intensity or resonance angle is converted to SPR angle shift, θ (Figure 1.3, edited from ref. 36). The shape and location of the SPR dip can be used to convey information about the sensor

surface (e.g. mass and density) and any molecular interaction that caused a change to the refractive index of the medium.

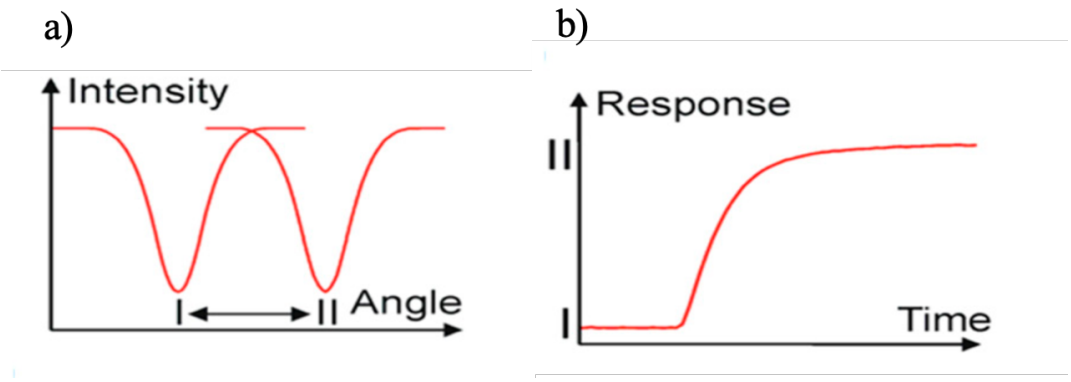

Figure 1.3 SPR reflectivity curve and sensorgram

1.4.2 Signal from Molecular Bindings and Interactions

The binding of the biomolecules on the sensor surface results in the change of the refractive index, therefore it can be detected by SPR. This happens as photons have a different velocity in different media, and the energy of the plasmons is changed when the composition of the medium changes, consequently, change the angle of incident light at which the resonance occurs. Therefore, a shift in the reflectivity is a direct method of detection, which avoids the drawbacks of labelling method. SPR also enables the continuous observation of binding interaction between molecules by monitoring this change in SPR response over time; the curve is known as sensorgram (Figure 1.4a, edited from ref. 46). The sensitivity of SPR biosensors can be measured by developing a calibration curve, in which the SPR measurements are repeated at different concentrations

of analytes and the results of resonance angle shift per concentration is plotted (Figure 1.4b). This analysis is used to identify the limit of detection (LOD) as well as the linear range of the sensing system.

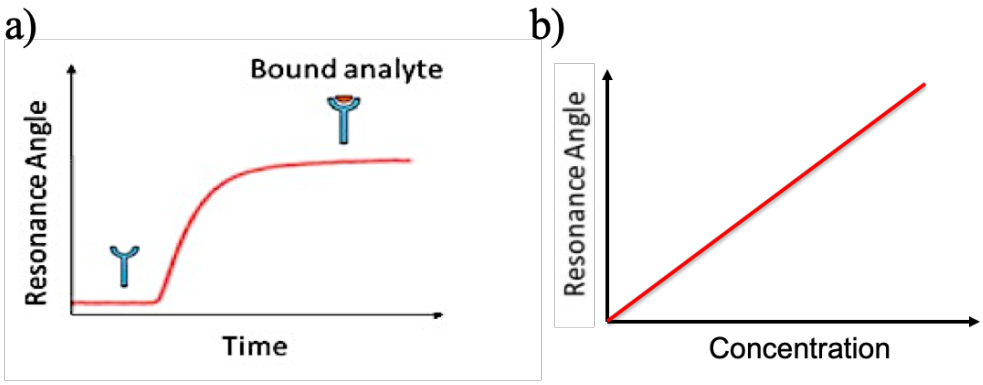

Figure 1.4 (a) The change in reflected light intensity is converted to SPR angle shift in a sensorgram showing a real-time monitoring of the binding process (b) Sensitivity or calibration curve obtained after measuring the response of different analyte concentrations

1.5 Theoretical basis of SPR

The working principal of the SPR technique is based on utilizing visible light to excite free electrons on a surface of a metal. This causes surface plasmons to travel along the metal surface, creating an evanescent field to the adjacent medium in contact with the metal. The fundamentals of this techniques are based on the reflectivity and refractivity of lights travelling from and to materials having different refractive indexes.

1.5.1 Total Internal Reflection and Evanescent Waves

Refraction is the bending of a wave when it enters material where it will travel at a different speed (Figure 1.5). Consider an upper material having a refractive index, n_2, that is greater than the refractive index of the lower material, n_1. When an incident light travel from a material of greater refractive index into a material with lower refractive index, the light bends away from the normal line so that $\theta_2 > \theta_1$. The angle θ_2 is called the angle of refraction. If the angle of incident, θ_1, further increases, more light is reflected and refracted. When the light reaches the right angle of incident, then the light travels right along the boundary so that θ_2 becomes 90^o. The angle of incident when this condition occurs is called the critical angle, θ_c. When the angle of incident is bigger than the critical angle ($\theta_1 > \theta_c$), where $\sin(\theta_c) = n_2/n_1$, none of the light travels along the boundary but all of it is internally reflected. This phenomenon is known as the Total Internal Reflection (TIR), when the incident wave cannot pass through the boundary and is totally reflected to the incident medium.

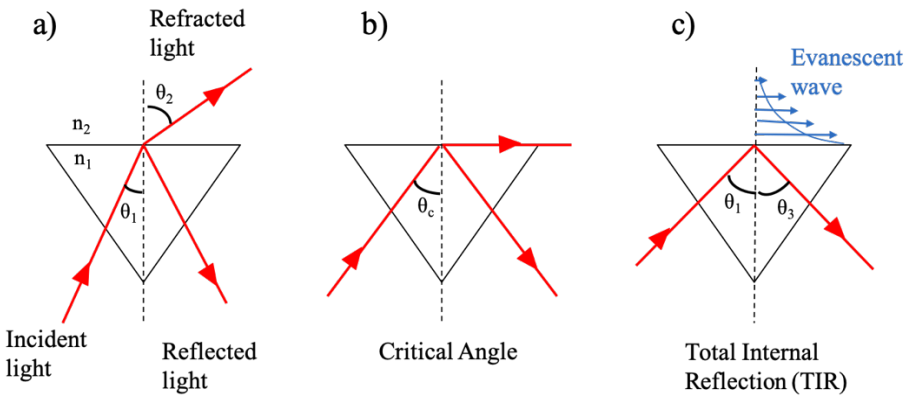

Figure 1.5 a) Refracted and reflected light, b) Critical Angle and c) Total Internal Reflection (TIR)

Evanescent waves are then formed in the lower refractive index medium n_2 under the condition of TIR. The amplitude of this type of standing waves decays exponentially with the distance to the interface of the media 1 and 2. The magnitude of the parallel wave vector of the evanescent wave, k_{ev}, is given by:

$$k_{ev} = \frac{\omega}{c} n_1 \, sin\theta \qquad \text{Equation 1.}$$

Where ω and c are the angular frequency and the speed of light in vacuum, respectively. For practical purpose, Equation 1 can also be expressed in terms of wavelength, λ:

$$k_{ev} = \frac{2\pi}{\lambda} n_1 \, sin\theta \qquad \text{Equation 1a.}$$

For non-absorbing media, the dielectric constant equals the square of the refractive index, $\varepsilon = n^2$, where ε is the dielectric constant (or permittivity) and n is the refractive index. Therefore, for plane polarized light under TIR condition, the wave vector projection of the photons on the metal surface can also be expressed as:

$$k_{ev} = \frac{\omega}{c}\sqrt{\varepsilon_o}\, sin\theta \quad \text{or} \quad k_{ev} = \frac{2\pi}{\lambda}\sqrt{\varepsilon_o}\, sin\theta \qquad \text{Equation 2.}$$

1.5.2 Surface Plasmons

When a metal surface is coupled to a prism where the electron is excited, this configuration produces surface plasmon. Surface plasmon is defined as an electromagnetic wave propagating at the interface between a metal and a dieletric.[44, 47] Maxwell's theory of surface plasmons describes the free electrons of a metal as an electron liquid of high density (i.e. plasma) and density fluctuations on a surface of this liquid as surface plasmons. Plasmons can also be thought as the particle name of this electromagnetic wave that has mass and velocity. The surface plasmon wave vector function consists of complex dielectric permittivity of the dielectric that is the medium next to the metal, denoted by ε_1 and the complex dielectric permittivity of the metal, denoted by ε_2. For photon-plasmon interaction, only the parallel vector component of surface plasmons matters. This is because plasmons are confined to the plane of the gold film.

The following equation defines the wave vector of a parallel surface plasmon wave, k_{SP}:

$$k_{SP} = \frac{\omega}{c}\sqrt{\frac{\varepsilon_1\varepsilon_2}{\varepsilon_1+\varepsilon_2}} \qquad \text{or} \qquad k_{SP} = \frac{2\pi}{\lambda}\sqrt{\frac{n_2^2 n_g^2}{n_2^2+n_g^2}} \qquad \text{Equation 3.}$$

Where n_g is the refractive index of the gold film.

Surface plasmons are not present inherently on these interfaces. Instead they can be created via excitation by e.g. light. The most common approach to excitation of surface plasmons are the Kretschmann geometry [48] and Otto geometry (Figure 1.6).[49]

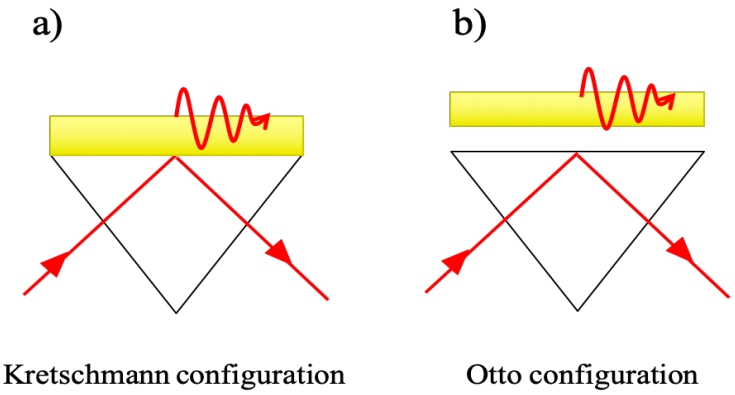

Figure 1.6 Excitation of surface plasmons in the a) Kretschmann and b) Otto configuration

In the Kretcshmann configuration, the metal film is placed directly onto the glass prism. The light illuminates the glass block, and an evanescent wave penetrates through the metal

film. The plasmon is excited at the outer side of the film. This configuration is used in most practical applications.

1.5.3 Excitation of Surface Plasmon Resonance

For surface plasmon resonance to occur, a coupling method between the surface plasmons and photons is required. In Kretschmann configuration, the prism itself acts as a coupler (Figure 1.7). The metal surface is positioned next to the prism and surface plasmons are generated at the metal-dielectric interface.[50] Wave vector coupling (i.e. surface plasmon resonance) takes place when photon wave vector projection on the metal k_{ev} equals the parallel vector component k_{SP} of surface plasmon:

$$k_{ev} = k_{SP}$$

$$\frac{\omega}{c}\sqrt{\varepsilon_o}\, sin\theta = \frac{\omega}{c}\sqrt{\frac{\varepsilon_1\varepsilon_2}{\varepsilon_1+\varepsilon_2}} \quad \text{or}$$

$$\frac{2\pi}{\lambda} n_1 sin\theta = \frac{\omega}{c}\frac{2\pi}{\lambda}\sqrt{\frac{n_2^2 n_g^2}{n_2^2+n_g^2}} \qquad \text{Equation 4.}$$

Thus, using Equation 4, the angle required for the resonance, θ_{SPR}, is related to n_2 when n_1 and n_g are fixed, giving the equation:

$$\theta_{SPR} = sin^{-1}\left(\frac{1}{n_1}\sqrt{\frac{n_2^2 n_g^2}{n_2^2+n_g^2}}\right) \qquad \text{Equation 5.}$$

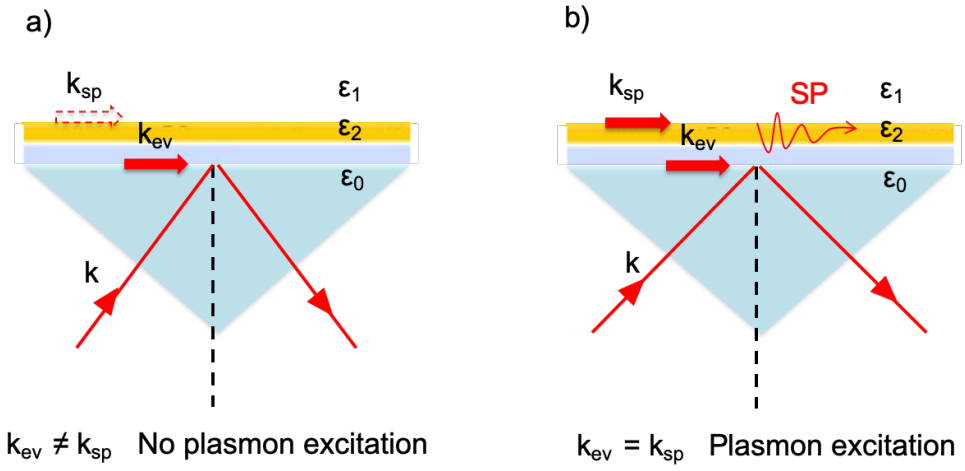

Figure 1.7 Schematic of the Kretschmann configuration of the SPR used in this study. When the projected wave vector of the incident light does not match the vector of surface plasmons no excitation occurs (a). At a certain incident light angle the projected wave vector of the incident light matches the wave vector of surface plasmons (b).

The excitation is possible when using p-polarized light (i.e. polarization occurs parallel to the plane of incidence), while s-polarized light (i.e. polarization occurs perpendicular to the plane of incidence) cannot excite electronic surface plasmons.[51] Typical metals that support surface plasmons are silver[52] and gold, but other metals such as aluminum and copper,[53] have been used. Gold is mostly selected, because of its chemical

inertness, high wavelength surface plasmons and the methods to functionalize the surface with various biomolecules using self-assembled chemistry have been established.

1.6 Challenges in SPR biosensors

The works presented in this thesis are focused on improving current sensors and designing new sensing interface for the application of SPR in biomedical research. In the following sections, the challenges and proposed solutions that break the limitations of SPR biosensors are described.

1.6.1 Non-specific Binding (NSB)

Non-specific absorption or binding of unwanted analyte either on the sensing surface or on the capture ligand has always been a challenge in optimizing the design of surface-based and label-free biosensors (Figure 1.8). When this occurs, an optimum sensitivity and selectivity cannot be achieved, because it causes an elevated background signal that cannot be discriminated from the specific binding.[54] Ideally, the biomolecules of interest must bind with high affinity and selectively to the sensitive area.[55] Non-specific binding occurs from many reasons, mainly the combination of biomolecules-substrate interaction, substrate stickiness, non-specific electrostatic and hydrophobic binding to charged surface, and adsorption of molecules in free spaces.[56] This is especially important in clinical applications, where actual bodily fluids are used as test samples, and it contains many proteins that prone to adsorb nonspecifically to the sensing surface. There are many strategies to reduce or eliminate this type of NSB, grouped into two categories; physical

and chemical blocking methods. The most popular and simplest method to prevent NSB is to use blocker proteins that adsorb to surfaces so that only the analyte binds only to the capture ligand (Figure 1.8b). The examples of the blocker proteins are serum albumins (BSA), [57] and casein.[58] Although BSA is easily accessible, it is not the preferred method to prevent NSB, as addition of BSA often causes a nonuniform layer and some proteins can still adsorbed on to a BSA layer.[59] Chemical method such as the self-assembled monolayers (SAMs) offers better resistance to NSB, in which the alkanethiol SAMs (Figure 1.9a) are one of the most popularly used bioreceptor linker molecules, due to two major advantages: plentiful functional groups to immobilize bioreceptors and a dense monolayer that allows little NSB.[60, 61] In our studies, SAMs prepared from thiolated poly-(ethylene glycol) (PEG) and 11-mercaptoundecanoic acid (MUA) (Figure 1.9b) were mostly used, as the terminal hydroxyl groups provide functionalities needed for amine containing biomolecules with the standard EDC/NHS coupling method.[62]

In addition to the traditional SAMs, we developed an SPR surface using DNA self-assembled monolayers (DNA-SAMs) for a direct immobilization of DNA on the gold surface.[63, 64] In this method, the surface is also backfilled with a short chain alkanethiolates, such as mercaptohexanol (Figure 1.10, edited from ref. 65). The reason for this dense molecular packing is to avoid the interaction of the nitrogen-containing base pairs of DNA with the substrate, causing the DNA chain to collapse.[65] Furthermore, the filling of mercaptohexanol in the gap assists in the formation of the SAMs by erecting the DNA strands on the surface. This also prevents NSB to occur, as well as promoting a controlled orientation for the interaction of the DNA with subsequent biomolecules.

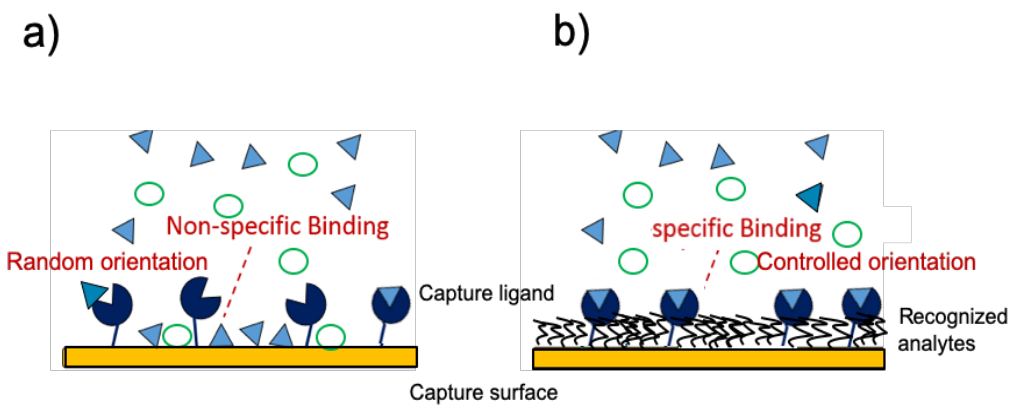

Figure 1.8 Schematic representation of the non-specific binding and random/uncontrolled orientation of capture ligand. (a) Some ligand molecules are unavailable for analyte binding as a result of random orientation and non-specific binding occurs between the analytes and the surface, (b) Specific binding of analytes to the controlled orientation ligand while the surface is covered with a blocking agent

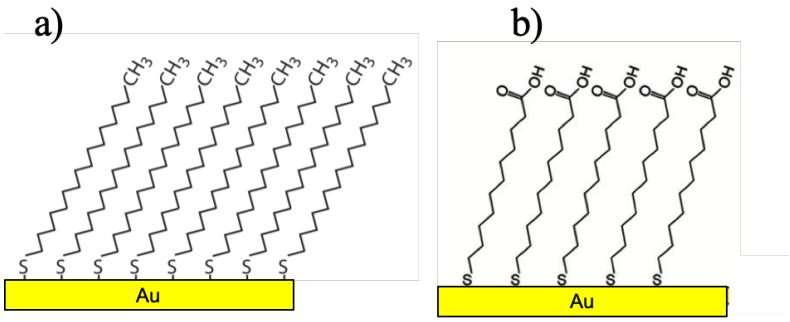

Figure 1.9 Schematic representation of SAM surfaces on gold, modified with (a) alkanethiol (showing hexadecanethiol, HDT) and (b) MUA

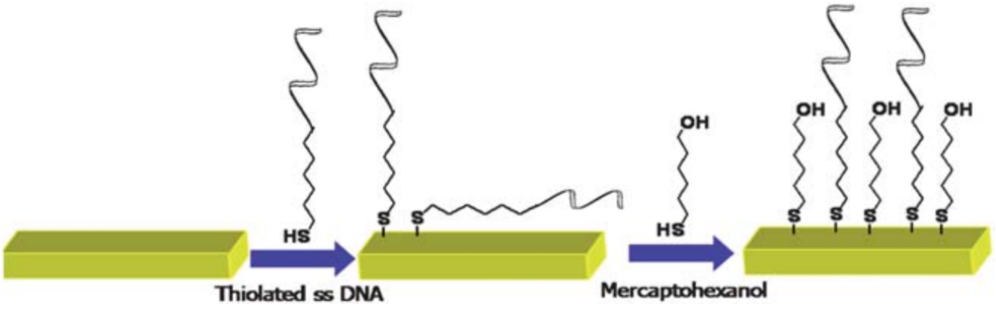

Figure 1.10 Schematic representation of DNA-SAMs on gold substrate followed by incubation with mercaptohexanol to assist the formation of the self-assembled monolayer

1.6.2 Uncontrolled Orientation

The efficiency of biosensing surface depends highly on the efficiency of the binding between the capture ligands and the analytes. Although the surface can be entirely covered with capture ligands, it is known that not all of them will bind to the analytes due to steric hindrance. One reason is the random orientation or nonsite-specific immobilization of the ligands on the surface, resulted from a passive non-covalent adsorption (Figure 1.11b).[66] This is particularly a concern for antibodies, which are used in immunoassays, as randomly adsorbed antibodies have poor affinity towards their antigen.[67] Naturally, this uncontrolled orientation reduces the performance of a biosensor. Therefore, to achieve maximum binding, the capture ligands must be oriented in a way that their binding active sites are entirely exposed to the solution and accessible (Figure 1.11a). A controlled ligand orientation can be achieved by an affinity-based binding between a target analyte and its surface immobilized partner. Most used examples are the Fc region of immunoglobulin G (IgG) to protein A and protein G, biotin to avidin, histidine to metal chelates such as Ni-

nitriloacetic acid (NTA), and carbohydrate residues to lectin.[64, 68] Our interest has been in the IgG-protein A system, in which the position of the antibody binding site (Fab region) remains accessible for binding with the antigen where the Fc region of the antibody binds specifically to protein A due to a strong affinity.[69] As shown in Figure 1.11a, the presence of protein A produces a uniform assembly and controlled orientation of IgG leads to an effective binding with the antigens, compared to the random orientation. We demonstrated the use of thiolated protein A in Chapter 3, combined with a supported lipid bilayer membranes (SLBs) for a successful immunosensing on an antifouling surface. Other than the antibody-protein A system, we also employed other site-selective methods like biotin-strepavidin and antibody-antigen as linkers that bind the analytes to the biorecognition elements.[70]

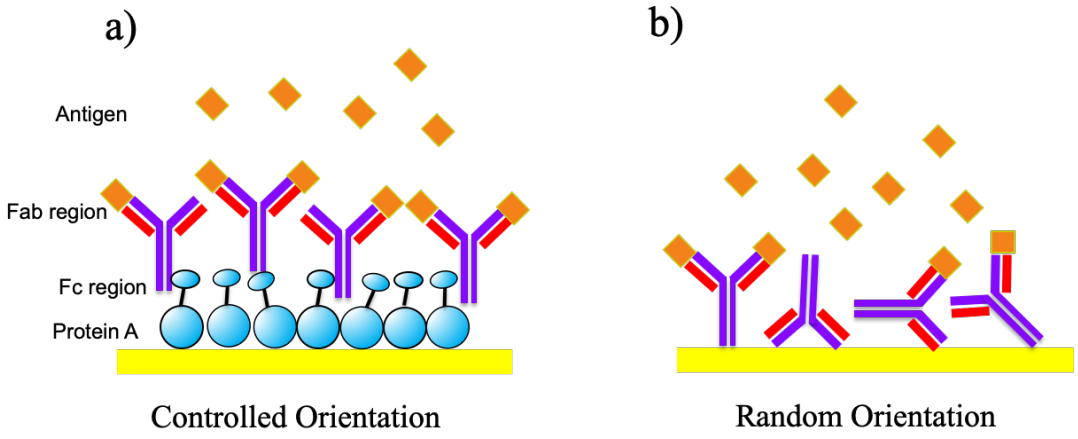

Figure 1.11 Schematic representation of (a) Controlled orientation of IgG binds to Fc binding domain of protein A and (b) Random orientation in absence of protein A

1.6.3 Surface Fouling from Complex Media

The use of SPR biosensors in medical diagnostic would require the analysis of actual clinical samples, mainly of blood plasma or serum. Blood plasma is the yellowish colored liquid that make up 55% of the whole blood, while serum consists of plasma without fibrinogen.[71] Both contains various proteins, antibodies, antigens, and hormones; all have the potential to adsorb on the biosensor surfaces nonspecifically. This effect, also known as "fouling", causes a disturbance to the SPR signal from the intended target analyte, as the nonspecific contents accumulate on the surface, which then alter the refractive index measured by SPR. Much research has been done in developing antifouling surfaces, while still maintaining the excellent binding recognitions. Other than the PEG based SAMs, the zwitterionic surfaces and polymer brushes also exhibit antifouling property, due to their net neutral surface charge and closely-packed polymer chains, respectively.[72] We studied different types of phospholipids, specifically phosphatidylcholine (EPC and POPC) and phosphatidylglycerol (POPG) as antifouling surfaces when formed as a supported lipid bilayer membrane on a protein A surface.

The phospholipid is the type of lipids that construct cell membrane, forming lipid bilayers because of their amphiphilic property.[73] A solid supported lipid bilayer membrane (SLB) is usually constructed from lipid vesicle fusion followed by adsorption on a hydrophilic surface, which then rupture to form a continuous surface of supported membrane as shown in Figure 1.12.[74] Other advantages of SLB includes easy incorporation of proteins, small molecules, nanoparticles and other species on the membrane surface or

inserted into the membrane, which can be used to study biomolecules interaction on cell membrane surfaces.[75]

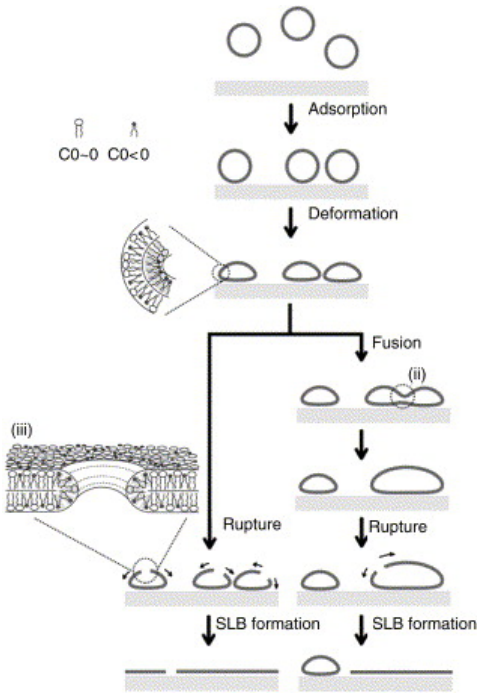

Figure 1.12 Possible mechanisms of supported bilayer formation. Vesicles adsorb, deform, and rupture to form an SLB. Under some conditions, vesicle-vesicle fusion occurs as an intermediate preceding vesicle rupture. Reprinted from Ref. 54, Copyright 2006, with permission from Elsevier

1.6.4 Weak Signal and Low Sensitivity

The growing interest of biosensors for biomedical applications is mostly focused on detecting ultra-low concentrations of target analyte like disease biomarkers,[76, 77] and low molecular weight molecules such as DNA, RNA and small molecules.[31] This is particularly important when diagnosing infectious diseases at an early stage. Therefore, one of the major challenges is to develop biosensors with sufficient sensitivity and low detection limit

by amplifying the signal through different strategies. In SPR biosensors, signal amplifications were achieved by enhancing the small changes in refractive index so that a large resonance angle output is obtained. Established methods such as sandwich assays (Figure 1.13a) (for examples antibody-antibody,[78] avidin-antibody-strepavidin,[79] aptamer-antibody[80]) and gold nanoparticles[81] (AuNPs) (Figure 13b) (figures edited from ref. 84 and 85) have been used to improve SPR detection. The main advantage of AuNPs is the versatility for conjugation with many biomolecules including DNA, proteins, antibodies and cells.[82] Nanoparticles, in general, increase SPR sensitivity based on the pseudo mass increase.[36] In more recent developments, nucleic acid amplification methods such as rolling circle amplification (RCA) and loop-mediated isothermal amplification (LAMP), have been widely utilized for biosensing including for infectious diseases or cancers.[83] However, the limitation of using nucleic acid methods is it requires high temperature operation (30 – 65 ^{o}C) because of the enzymes involve in the mechanisms. In our studies, we employed signal amplification via AuNPs and a room temperature DNA self-assembly, which are demonstrated for detection of Malaria and for immunosensing purposes.

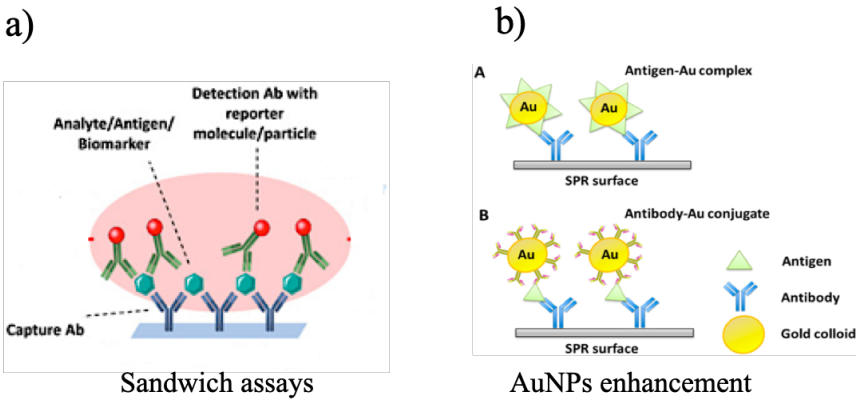

Figure 1.13 Schematic representation of (a) sandwich assay and (b) AuNPs enhancement strategies.

1.6.5 Cell-based SPR

Although the advantages of SPR, especially the real time and label-free features, are very much attractive for the studies of living cells, the progress of using SPR in this field is not as rapid as other biomolecules. Main reason is the nature of SPR technique itself, as the sensitive evanescent field in the SPR setup is limited to around 300 nm depth from the surface, and thus is not sufficient to detect interactions of the whole cells. However, there are a lot of unknown features on the interactions at the cell-substrate interface that remain to be explored. Our interest is to develop an SPR method for monitoring the signal based on the cell's uniformity, morphology and detachment process from the surface. This is particularly useful for cancer cells toxicity and therapeutic studies, as the process of apoptosis changes the morphology of the cells. Therefore for adhered

cells any changes happened at the cell membrane within 300 nm from the substrate can be monitored by SPR.

1.7 Objectives and Scope of Dissertation

The goals of this dissertation are to demonstrate the great potential of SPR biosensors in medical applications, mainly for diagnosis of infectious diseases and cancers. This was achieved through advanced SPR surface chemistry, biomolecular binding interaction, signal amplification, antifouling surfaces, novel interface and combination of at least two of these strategies. The challenges in biosensing development were scrutinized in order to find the gaps in realizing SPR biosensors to a level more superior than current bioanalytical methods. The overarching goals of the proposed work is to enable integration of SPR into a portable field-used biosensing system complete with sample preparation, detection platform, data processing and user interface.

Chapter 2 of this thesis is on the development of a dual signal amplification method, which comprised of AuNPs and DNA hybridization chain reaction (HCR) to improve the sensitivity of DNA biosensor for the detection of malaria parasite. The motivation for this work was primarily the urgent need for early detection of malaria and portable biosensors that can be brought into hardly accessible malarial regions. The highlights of this work are the simple DNA detection scheme with room temperature operating condition, and the use of complex media to mimic the actual clinical test does not compromise the sensing performance.

In Chapter 3, we demonstrated an SPR immunosensor with antifouling surface and controlled capture antibody orientation, using lipid bilayers interface and affinity-based recognition via protein A, respectively. The latter enables the antibodies active site to be fully accessible to antigen binding. The mobility of different types of lipid after bilayer membrane was characterized using Fluorescence Recovery After Photobleaching (FRAP) and the results were related to the membranes' antifouling property. As the proof-of-concept, IgG and Cholera toxin (CT) were used as the detection model systems.

Chapter 4 describes how SPR can be used to monitor HeLa cells morphological changes and detachment from substrate surfaces, when the cells on the SPR chips undergo apoptotic phase after being treated with a cell death inducer, in this work, hydrogen peroxide (H_2O_2). The SPR signals were comparable to cell confluency, which is a direct cellular parameter for apoptotic cells. An interesting finding during the period of this work is the mathematical model analysis that relates SPR signal to the thickness of cells layer and refractive indexes in the vicinity of sensing surface. Although cell-based SPR offers huge potential in cancer diagnosis and cells toxicology studies, it remains underrated and is less explored than other SPR biosensors.

We conclude the work done and provide some insights towards the future of SPR biosensors for medical applications in Chapter 5.

1.8 References

1. Balough, E. P.; Miller, B. T.; Ball, J. R.; National Academies of Sciences, E., and Medicine, *Improving Diagnosis in Health Care*. The National Academies Press: Washington, DC, **2015**; p 472.

2. Srivastava, S.; Singh, P. K.; Vatsalya, V.; Karch, R. C., Developments in the Diagnostic Techniques of Infectious Diseases: Rural and Urban Prospective. *Advances in infectious diseases* **2018,** *8* (3), 121-138.

3. Ivanov, A., Barriers to the Introduction of New Medical Diagnostic Tests. *Laboratory Medicine* **2013,** *44* (4), e132-e136.

4. Koo, M. M.; Hamilton, W.; Walter, F. M.; Rubin, G. P.; Lyratzopoulos, G., Symptom Signatures and Diagnostic Timeliness in Cancer Patients: A Review of Current Evidence. *Neoplasia (New York, N.Y.)* **2018,** *20* (2), 165-174.

5. Hamilton, W., Cancer diagnosis in primary care. *The British journal of general practice : the journal of the Royal College of General Practitioners* **2010,** *60* (571), 121-128.

6. Loud, J. T.; Murphy, J., Cancer Screening and Early Detection in the 21(st) Century. *Seminars in oncology nursing* **2017,** *33* (2), 121-128.

7. Mesaros, C.; Blair, I. A., Oncology bioanalysis: from biomarkers to drug discovery. *Biomarkers in Medicine* **2015,** *9* (9), 819-820.

8. Metkar, S. K.; Girigoswami, K., Diagnostic biosensors in medicine – A review. *Biocatalysis and Agricultural Biotechnology* **2019,** *17*, 271-283.

9. Patel, S.; Nanda, R.; Sahoo, S.; Mohapatra, E., Biosensors in Health Care: The Milestones Achieved in Their Development towards Lab-on-Chip-Analysis. *Biochemistry research international* **2016,** *2016*, 3130469-3130469.

10. Giepmans, B. N. G.; Adams, S. R.; Ellisman, M. H.; Tsien, R. Y., The Fluorescent Toolbox for Assessing Protein Location and Function. *Science* **2006,** *312* (5771), 217.

11. Malima, A.; Siavoshi, S.; Musacchio, T.; Upponi, J.; Yilmaz, C.; Somu, S.; Hartner, W.; Torchilin, V.; Busnaina, A., Highly sensitive microscale in vivo sensor enabled by electrophoretic assembly of nanoparticles for multiple biomarker detection. *Lab on a Chip* **2012,** *12* (22), 4748-4754.

12. Crean, C.; McGeouge, C.; O'kennedy, R., 11 - Wearable biosensors for medical applications. In *Biosensors for Medical Applications*, Higson, S., Ed. Woodhead Publishing: 2012; pp 301-330.

13. Micheli, L.; Moscone, D.; Palleschi, G., 10 - Biosensors for non-invasive measurements. In *Biosensors for Medical Applications*, Higson, S., Ed. Woodhead Publishing: 2012; pp 263-300.

14. Srinivasan, B.; Tung, S., Development and Applications of Portable Biosensors. *Journal of Laboratory Automation* **2015,** *20* (4), 365-389.

15. Breault-Turcot, J.; Masson, J. F., Nanostructured substrates for portable and miniature SPR biosensors. (1618-2650 (Electronic)).

16. Vashist, S. K., Point-of-Care Diagnostics: Recent Advances and Trends. *Biosensors* **2017,** *7* (4), 62.

17. Baryeh, K.; Takalkar, S.; Lund, M.; Liu, G., 1 - Introduction to medical biosensors for point of care applications. In *Medical Biosensors for Point of Care (POC) Applications*, Narayan, R. J., Ed. Woodhead Publishing: 2017; pp 3-25.

18. Liu, Y.; Liu, Q.; Chen, S.; Cheng, F.; Wang, H.; Peng, W., Surface Plasmon Resonance Biosensor Based on Smart Phone Platforms. *Scientific Reports* **2015,** *5* (1), 12864.

19. Pateraki, M.; Fysarakis, K.; Sakkalis, V.; Spanoudakis, G.; Varlamis, I.; Maniadakis, M.; Lourakis, M.; Ioannidis, S.; Cummins, N.; Schuller, B.; Loutsetis, E.; Koutsouris, D., Chapter 2 - Biosensors and Internet of Things in smart healthcare applications: challenges and opportunities. In *Wearable and Implantable Medical Devices*, Dey, N.; Ashour, A. S.; James Fong, S.; Bhatt, C., Eds. Academic Press: 2020; Vol. 7, pp 25-53.

20. Malhotra, B. D.; Chaubey, A., Biosensors for clinical diagnostics industry. *Sensors and Actuators B: Chemical* **2003,** *91* (1–3), 117-127.

21. Lee, M. T., Over-the-Counter Biosensors: Past, Present, and Future. *Sensors* **2008,** *8* (9).

22. Grieshaber, D.; MacKenzie, R.; Vörös, J.; Reimhult, E., Electrochemical Biosensors - Sensor Principles and Architectures. *Sensors (Basel, Switzerland)* **2008,** *8* (3), 1400-1458.

23. Scognamiglio, V.; Arduini, F.; Palleschi, G.; Rea, G., Biosensing technology for sustainable food safety. *TrAC Trends in Analytical Chemistry* **2014,** *62*, 1-10.

24. Bhalla, N.; Jolly, P.; Formisano, N.; Estrela, P., Introduction to biosensors. *Essays in Biochemistry* **2016,** *60* (1), 1-8.

25. Alhadrami, H. A. A.-O. h. o. o., Biosensors: Classifications, medical applications, and future prospective. (1470-8744 (Electronic)).

26. Mehrotra, P., Biosensors and their applications - A review. *Journal of oral biology and craniofacial research* **2016,** *6* (2), 153-159.

27. Wang, J., Electrochemical Glucose Biosensors. *Chemical Reviews* **2008,** *108* (2), 814-825.

28. Akyilmaz, E.; Yorganci, E.; Asav, E., Do copper ions activate tyrosinase enzyme? A biosensor model for the solution. *Bioelectrochemistry* **2010,** *78* (2), 155-160.

29. Damborský, P.; Švitel, J.; Katrlík, J., Optical biosensors. *Essays in Biochemistry* **2016,** *60* (1), 91-100.

30. Hunt, H. K.; Armani, A. M., Label-free biological and chemical sensors. (2040-3372 (Electronic)).

31. Sin, M. L. Y.; Mach, K. E.; Wong, P. K.; Liao, J. C., Advances and challenges in biosensor-based diagnosis of infectious diseases. *Expert Review of Molecular Diagnostics* **2014,** *14* (2), 225-244.

32. Fan, X.; White, I. M.; Shopova, S. I.; Zhu, H.; Suter, J. D.; Sun, Y., Sensitive optical biosensors for unlabeled targets: A review. *Analytica Chimica Acta* **2008,** *620* (1), 8-26.

33. Jung, S.-H.; Jung, J.-W.; Suh, I.-B.; Yuk, J. S.; Kim, W.-J.; Choi, E. Y.; Kim, Y.-M.; Ha, K.-S., Analysis of C-Reactive Protein on Amide-Linked N-Hydroxysuccinimide−Dextran Arrays with a Spectral Surface Plasmon Resonance Biosensor for Serodiagnosis. *Analytical Chemistry* **2007,** *79* (15), 5703-5710.

34. Lee, S. J.; Youn, B.-S.; Park, J. W.; Niazi, J. H.; Kim, Y. S.; Gu, M. B., ssDNA Aptamer-Based Surface Plasmon Resonance Biosensor for the Detection of Retinol Binding Protein 4 for the Early Diagnosis of Type 2 Diabetes. *Analytical Chemistry* **2008,** *80* (8), 2867-2873.

35. Baird, C. L.; Courtenay, E. S.; Myszka, D. G., Surface plasmon resonance characterization of drug/liposome interactions. *Analytical Biochemistry* **2002,** *310* (1), 93-99.

36. Nguyen, H. H.; Park, J.; Kang, S.; Kim, M., Surface Plasmon Resonance: A Versatile Technique for Biosensor Applications. *Sensors* **2015,** *15* (5).

37. Dudak, F. C.; Boyacı, İ. H., Rapid and label-free bacteria detection by surface plasmon resonance (SPR) biosensors. *Biotechnology Journal* **2009,** *4* (7), 1003-1011.

38. Homola, J., Present and future of surface plasmon resonance biosensors. *Analytical and Bioanalytical Chemistry* **2003,** *377* (3), 528-539.

39. Miyazaki, C. M.; Shimizu, F. M.; Ferreira, M., 6 - Surface Plasmon Resonance (SPR) for Sensors and Biosensors. In *Nanocharacterization Techniques*, William Andrew Publishing: 2017; pp 183-200.

40. McKeating, K. S.; Aube, A.; Masson, J.-F., Biosensors and nanobiosensors for therapeutic drug and response monitoring. *Analyst* **2016,** *141* (2), 429-449.

41. Masson, J.-F., Surface Plasmon Resonance Clinical Biosensors for Medical Diagnostics. *ACS Sensors* **2017,** *2* (1), 16-30.

42. Wang, D.-S.; Fan, S.-K., Microfluidic Surface Plasmon Resonance Sensors: From Principles to Point-of-Care Applications. *Sensors* **2016,** *16* (8).

43. Piliarik, M.; Vaisocherová, H.; Homola, J., Surface Plasmon Resonance Biosensing. In *Biosensors and Biodetection*, Rasooly, A.; Herold, K. E., Eds. Humana Press: Totowa, NJ, 2009; pp 65-88.

44. Raether, H., Surface plasmons on smooth surfaces. In *Surface Plasmons on Smooth and Rough Surfaces and on Gratings*, Raether, H., Ed. Springer Berlin Heidelberg: Berlin, Heidelberg, 1988; pp 4-39.

45. Van Der Merwe, P. A., Surface plasmon resonance. *Protein-ligand interactions: hydrodynamics and calorimetry* **2001,** *1*, 137-170.

46. Linman, M. J.; Cheng, Q. J., Surface Plasmon Resonance: New Biointerface Designs and High-Throughput Affinity Screening. In *Optical Guided-wave Chemical and Biosensors I*, Zourob, M.; Lakhtakia, A., Eds. Springer Berlin Heidelberg: Berlin, Heidelberg, 2009; pp 133-153.

47. Maier, S. A., Plasmonics : fundamentals and applications. Springer: New York, 2007.

48. Kretschmann, E.; Raether, H., Notizen: Radiative Decay of Non Radiative Surface Plasmons Excited by Light. In *Zeitschrift für Naturforschung A*, 1968; Vol. 23, p 2135.

49. Otto, A., Excitation of nonradiative surface plasma waves in silver by the method of frustrated total reflection. *Zeitschrift für Physik A Hadrons and nuclei* **1968,** *216* (4), 398-410.

50. Homola, J., Surface Plasmon Resonance Based Sensors. *Surface Plasmon Resonance Based Sensors* **2006**.

51. Peterson, A. W.; Halter, M.; Plant, A. L.; Elliott, J. T., Surface plasmon resonance microscopy: Achieving a quantitative optical response. *The Review of scientific instruments* **2016,** *87* (9), 093703-093703.

52. Wang, G.; Wang, C.; Yang, R.; Liu, W.; Sun, S., A Sensitive and Stable Surface Plasmon Resonance Sensor Based on Monolayer Protected Silver Film. *Sensors (Basel, Switzerland)* **2017,** *17* (12), 2777.

53. Tanabe, I.; Tanaka, Y. Y.; Watari, K.; Hanulia, T.; Goto, T.; Inami, W.; Kawata, Y.; Ozaki, Y., Far- and deep-ultraviolet surface plasmon resonance sensors working in aqueous solutions using aluminum thin films. *Scientific reports* **2017,** *7* (1), 5934-5934.

54. Lichtenberg, J. Y.; Ling, Y.; Kim, S., Non-Specific Adsorption Reduction Methods in Biosensing. *Sensors (Basel, Switzerland)* **2019,** *19* (11), 2488.

55. Reimhult, E.; Höök, F., Design of surface modifications for nanoscale sensor applications. *Sensors (Basel, Switzerland)* **2015,** *15* (1), 1635-1675.

56. Ahluwalia, A.; Giusto, G.; De Rossi, D., Non-specific adsorption on antibody surfaces for immunosensing. *Materials Science and Engineering: C* **1995,** *3* (3), 267-271.

57. Riquelme, M. V.; Zhao, H.; Srinivasaraghavan, V.; Pruden, A.; Vikesland, P.; Agah, M., Optimizing blocking of nonspecific bacterial attachment to impedimetric biosensors. *Sensing and Bio-Sensing Research* **2016,** *8*, 47-54.

58. Tacha, D. E.; McKinney, L., Casein Reduces Nonspecific Background Staining in Immunolabeling Techniques. *Journal of Histotechnology* **1992,** *15* (2), 127-132.

59. Ratner, B. D.; Hoffman, A. S.; Schoen, F. J.; Lemons, J. E., Introduction - Biomaterials Science: An Evolving, Multidisciplinary Endeavor. In *Biomaterials Science (Third Edition)*, Ratner, B. D.; Hoffman, A. S.; Schoen, F. J.; Lemons, J. E., Eds. Academic Press: 2013; pp xxv-xxxix.

60. Wink, T.; J. van Zuilen, S.; Bult, A.; P. van Bennekom, W., Self-assembled Monolayers for Biosensors. *Analyst* **1997,** *122* (4), 43R-50R.

61. Choi, K. H.; Sajid, M.; Aziz, S.; Yang, B.-S., Wide range high speed relative humidity sensor based on PEDOT:PSS–PVA composite on an IDT printed on piezoelectric substrate. *Sensors and Actuators A: Physical* **2015,** *228*, 40-49.

62. Fischer, M. J. E., Amine Coupling Through EDC/NHS: A Practical Approach. In *Surface Plasmon Resonance: Methods and Protocols*, Mol, N. J.; Fischer, M. J. E., Eds. Humana Press: Totowa, NJ, 2010; pp 55-73.

63. Wang, S.; Cai, X.; Wang, L.; Li, J.; Li, Q.; Zuo, X.; Shi, J.; Huang, Q.; Fan, C., DNA orientation-specific adhesion and patterning of living mammalian cells on self-assembled DNA monolayers. (2041-6520 (Print)).

64. Rusmini, F.; Zhong, Z.; Feijen, J., Protein Immobilization Strategies for Protein Biochips. *Biomacromolecules* **2007,** *8* (6), 1775-1789.

65. Singh, V.; Zharnikov, M.; Gulino, A.; Gupta, T., DNA immobilization, delivery and cleavage on solid supports. *J. Mater. Chem.* **2011,** *21*, 10602-10618.

66. Shen, M.; Rusling, J.; Dixit, C. K., Site-selective orientated immobilization of antibodies and conjugates for immunodiagnostics development. *Methods (San Diego, Calif.)* **2017,** *116*, 95-111.

67. Tajima, N.; Takai, M.; Ishihara, K., Significance of Antibody Orientation Unraveled: Well-Oriented Antibodies Recorded High Binding Affinity. *Analytical Chemistry* **2011,** *83* (6), 1969-1976.

68. Sassolas, A.; Blum Lj Fau - Leca-Bouvier, B. D.; Leca-Bouvier, B. D., Immobilization strategies to develop enzymatic biosensors. (1873-1899 (Electronic)).

69. Valsecchi, C.; Jones, T.; Wang, C.; Lochbihler, H.; Menezes, J. W.; Brolo, A. G., Low-Cost Leukemic Serum Marker Screening Using Large Area Nanohole Arrays on Plastic Substrates. *ACS Sensors* **2016,** *1* (9), 1103-1109.

70. Wilchek, M.; Bayer Ea Fau - Livnah, O.; Livnah, O., Essentials of biorecognition: the (strept)avidin-biotin system as a model for protein-protein and protein-ligand interaction. (0165-2478 (Print)).

71. Varacallo, M. J., *Physiology, Blood Plasma*. StatPearls Publishing: Treasure Island (FL), 2019.

72. Vaisocherová, H.; Brynda, E.; Homola, J., Functionalizable low-fouling coatings for label-free biosensing in complex biological media: advances and applications. *Analytical and Bioanalytical Chemistry* **2015,** *407* (14), 3927-3953.

73. Castellana, E. T.; Cremer, P. S., Solid supported lipid bilayers: From biophysical studies to sensor design. *Surface Science Reports* **2006,** *61* (10), 429-444.

74. Hamai, C.; Yang, T.; Kataoka, S.; Cremer, P. S.; Musser, S. M., Effect of Average Phospholipid Curvature on Supported Bilayer Formation on Glass by Vesicle Fusion. *Biophysical Journal* **2006,** *90* (4), 1241-1248.

75. Perez, L.; Ghang, Y.-J.; Williams, P. B.; Wang, Y.; Cheng, Q.; Hooley, R. J., Cell and Protein Recognition at a Supported Bilayer Interface via In Situ Cavitand-Mediated Functional Polymer Growth. *Langmuir* **2015,** *31* (41), 11152-11157.

76. Whiley, L.; Legido-Quigley, C., Current strategies in the discovery of small-molecule biomarkers for Alzheimer's disease. *Bioanalysis* **2011,** *3* (10), 1121-1142.

77. Hwang, H.; Hwang, B.-Y.; Bueno, J., Biomarkers in Infectious Diseases. *Disease Markers* **2018,** *2018*, 2.

78. Wang, S.; Zhao, S.; Wei, X.; Zhang, S.; Liu, J.; Dong, Y., An Improved Label-Free Indirect Competitive SPR Immunosensor and Its Comparison with Conventional ELISA for Ractopamine Detection in Swine Urine. *Sensors (Basel, Switzerland)* **2017,** *17* (3), 604.

79. Wei, J.; Mu, Y.; Song, D.; Fang, X.; Liu, X.; Bu, L.; Zhang, H.; Zhang, G.; Ding, J.; Wang, W.; Jin, Q.; Luo, G., A novel sandwich immunosensing method for measuring cardiac troponin I in sera. *Analytical Biochemistry* **2003,** *321* (2), 209-216.

80. Wu, B.; Jiang R Fau - Wang, Q.; Wang Q Fau - Huang, J.; Huang J Fau - Yang, X.; Yang X Fau - Wang, K.; Wang K Fau - Li, W.; Li W Fau - Chen, N.; Chen N Fau - Li, Q.; Li, Q., Detection of C-reactive protein using nanoparticle-enhanced surface plasmon resonance using an aptamer-antibody sandwich assay. (1364-548X (Electronic)).

81. Matsishin, M.; Rachkov, A.; Lopatynskyi, A.; Chegel, V.; Soldatkin, A.; El'skaya, A., Selective Amplification of SPR Biosensor Signal for Recognition of rpoB Gene Fragments by Use of Gold Nanoparticles Modified by Thiolated DNA. *Nanoscale research letters* **2017,** *12* (1), 252-252.

82. Merkoçi, A., Nanoparticles-based strategies for DNA, protein and cell sensors. *Biosensors and Bioelectronics* **2010,** *26* (4), 1164-1177.

83. Zhou, H., Nucleic Acid Amplification Strategies for Biosensing, Bioimaging, and Biomedicine. In *Nucleic Acid Amplification Strategies for Biosensing, Bioimaging and Biomedicine*, Zhang, S.; Bi, S.; Song, X., Eds. Springer Singapore: Singapore, 2019; pp 3-14.

84. Lara, S.; Perez-Potti, A., Applications of Nanomaterials for Immunosensing. *Biosensors* **2018,** *8* (4), 104.

85. Lyon, L. A.; Musick, M. D.; Natan, M. J., Colloidal Au-Enhanced Surface Plasmon Resonance Immunosensing. *Analytical Chemistry* **1998,** *70* (24), 5177-5183.

CHAPTER 2 : SPR Biosensor for the Detection of Malaria *Plasmodium falciparum* DNA with Signal Amplifications

ABSTRACT

Malaria remains a deadly disease to this date despite recent advances in its diagnosis, treatment and management. For the diagnosis, PCR detects a specific DNA sequence and is highly sensitive but has disadvantages such as high cost, need of specialist, and poor field deployability. We report here a DNA-based surface plasmon resonance biosensing of *Plasmodium falciparum*, the most fatal parasite associated with malaria. Direct detection of the parasite DNA by an immobilized capture probe complementary to the target DNA was achieved with unremarkable performance. To improve the sensitivity and limit of detection, we introduced signal amplification strategies using the concept of DNA self-assemblies via hybridization chain reaction (HCR), which triggers formation of DNA nanostructures, and a further signal amplification by gold nanoparticles (AuNPs). We achieved a linear sensitivity range from 0.1 nM to 0.1 μM of target DNA, with higher signal and lower detection limit were obtained after the AuNPs enhancement step. The sensitivity was not compromised when the detection was conducted in human blood plasma, which was used to mimic actual diagnostic sample. Overall this method demonstrates great potential of SPR in clinical application, and successively to foster an effective treatment and control of Malaria.

2.1 Introduction

Malaria is a dangerous disease caused by blood-borne parasites of the genus *Plasmodium* that live and reproduce in two types of hosts; female *Anopheles* mosquitoes and humans. In this cyclical infection, the parasites are transmitted into the human bloodstream, then travel to the liver to mature before multiplying in the red blood cells and continue the cycle by infecting more cells.[1] Most human infections are caused by *Plasmodium falciparum,* which also causes severe organ damage, respiratory distress, coma, and anemia, often leading to fatality.[2, 3] In the recent World Health Organization (WHO) Malaria Report, 219 million cases and 435 000 related deaths have occurred in 2017 based on data from 87 countries and areas with ongoing malaria transmission.

Although malaria parasites achieve maturity in 48 hours, an early diagnosis remains a challenge, as the density of this parasite is very low at this stage and therefore not detectable by the traditional malaria diagnostic methods, namely blood film microscopy or the immunoassay rapid diagnostic tests (RDTs).[4] Molecular diagnostic methods based on malarial DNA amplification such as polymerase chain reaction (PCR) and nucleic acid sequence-based amplification (NASBA)[5, 6] have proven to be more sensitive and specific (thus, allowing multiplex detection) than the RDTs.[7] However, the nucleic acid detection methods require well-equipped laboratories and trained technicians, which are inaccessible in the poor endemic regions.[8]

Evidently, there is a need for a more advance method beyond the current diagnosis and clinical detection of malaria. Biosensors have been developed to provide highly sensitive, rapid, specific, simple and field deployable detection of biomolecules in various

applications.[9, 10] In the case of malaria, recent development of biosensors have focused on targeting parasite-related biomarkers such as *Plasmodium falciparum* histidine rich protein II (*Pf*HRP-II), *Plasmodium falciparum* lactate dehydrogenase (*Pf*LDH), heme, and hemozoin.[11, 12] Biosensors for the direct detection of the malaria parasite's DNA unfortunately are still lacking and are very much needed for diagnosis in the early stages of infection. Previously, a quartz crystal microbalance (QCM) biosensor was developed for the detection of post-PCR amplified DNA of P. *falciparum* and P. *vivax* that was extracted from patient blood samples.[13, 14]

In our study, we further improve the sensitivity and practicality of the malaria DNA biosensor by employing surface plasmon resonance (SPR), a surface-sensitive, label-free optical transduction biosensor.[15, 16] Compared to labeled optical biosensors such as fluorescence and colorimetry, SPR offers several advantages that includes real-time measurement, simplified design, universal detection, field-deployability and great potential in clinical applications.[17-20] Numerous studies on SPR biosensors have been reported on the detection of proteins,[21, 22] antibodies,[23] microRNA,[24, 25] DNA,[26] and cancer biomarkers.[27, 28]

To achieve the goals, we developed an SPR biosensor for a highly sensitive direct detection of P. *falciparum* DNA based on a concept of DNA self-assembly, via hybridization chain reaction (HCR),[29-31] with signal amplification using gold nanoparticles (AuNPs).[26] The self-assembly assay of HCR, which usually consists of two single stranded DNAs complementary to each other can hybridize and form long DNA nanostructures and has been utilized as amplification technique for sensitive detection of nucleic acid

implemented in room temperature.[32] A further SPR signal amplification using nanoparticles is often integrated with DNA self-assembly approach, for example AuNPs,[33, 34] aggregation of network of AuNPs,[35] DNA modified AuNPs,[36] and magnetic nanoparticles.[37] AuNPs was chosen because it is proven to be effective in SPR signal enhancement due to high refractive index and the electronic coupling interaction between the localized SPR (LSPR) of AuNPs and the resonance wave of the gold film on the sensor chip.[38]

Our biosensor was also tested in human blood plasma to mimic clinical samples, and the non-specific binding on the sensor surface was systematically assessed to ensure the sensing performance is not compromised by the complex media and AuNPs. The graphical representations in Figure 2.1, shows how our biosensor fill the gaps in malaria diagnosis. The potential benefits of this study are numerous; the amplification methods can be applied to other DNA-based biosensors in drug discovery, biomedicine, food safety and environmental monitoring,[39] and combining with SPR features this biosensing strategy is an exciting opportunity to realize compact and portable biosensors for field use.

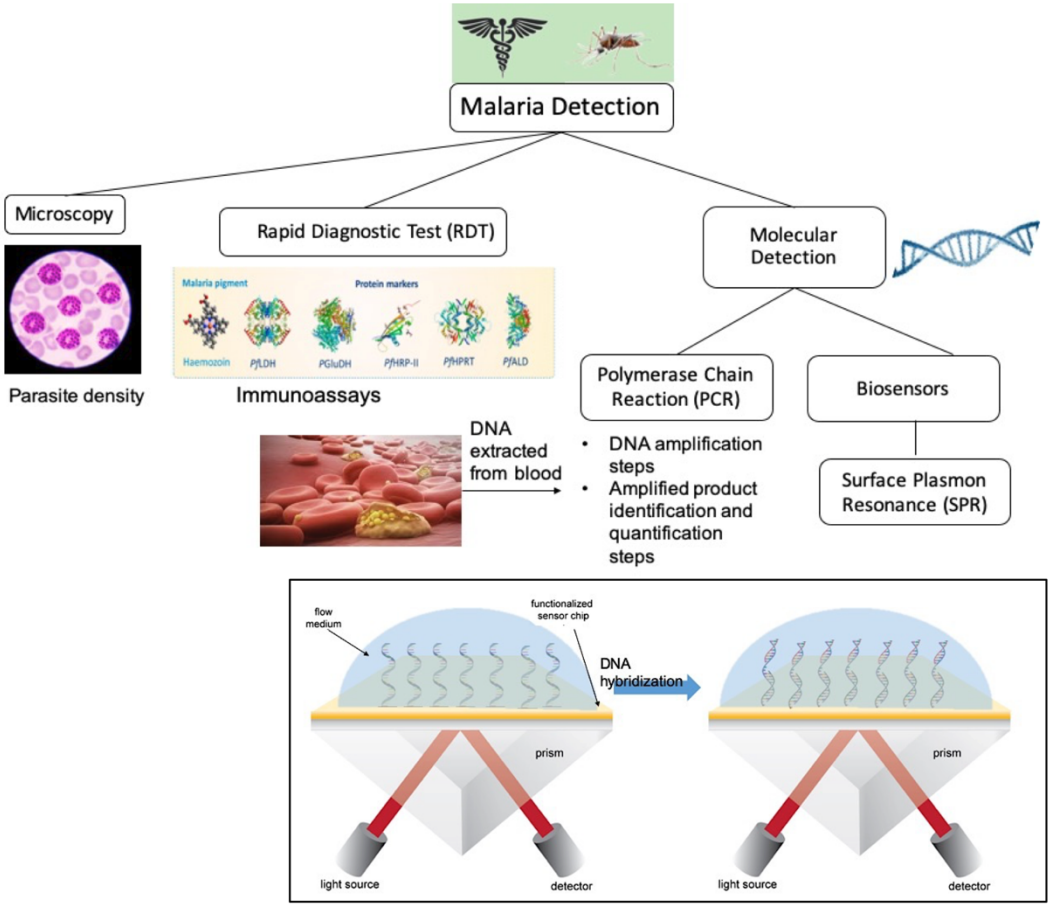

Figure 2.1 Schematic representation of malaria diagnostics including biosensors for the DNA level detection. The boxed figure illustrates the principle of SPR for direct detection of target DNA by the immobilized capture probe

2.2 Experiment Section

2.2.1 Materials

Sulfuric acid (H_2SO_4), Hydrogen peroxide (H_2O_2), Hydrochloric acid (HCl), Nitric acid (HNO_3), Sodium phosphate dibasic (Na_2HPO_4), Potassium phosphate monobasic (KH_2PO_4), Sodium Chloride (NaCl) and Potassium Chloride (KCl) were from Fisher Chemical. Sodium citrate tribasic dehydrate, Trizma Base Gold (III) chloride trihydrate ($HAuCl_4$), 6-mercapto-1-hexanol (MCH), and Tween 20 was from Sigma. Thiolated poly-thymine (T_{20}-SH) and Biotinylated poly-thymine (Biotin-T20-SH) reconstituted to 100 μM in H_2O, and the probe sequences are listed in Table 2.1 were from IDT. The probes were stored in IDTE buffer (10 mM Tris, 0.1 mM EDTA, pH 8.0) (100 μM) at 4^{o}C, and dissolved in Tris buffer (pH 7.4) prior to use in SPR. Strepavidin was from Thermo Scientific and reconstituted in PBS 1x. Citrated human blood plasma (Catalog no. P9523) contains 4% trisodium citrate as anticoagulant was purchased from Sigma. The hybridization buffer (pH 7.5) contained 40 mM Tris, 250 mM NaCl, 40 mM KCl and PBS 1x 10 mM (pH 7.4) were used. The pH of buffer solutions was adjusted with HCl. All buffers were filtered and degassed before storage and use. Nanopure water ($\geq$ 18 MΩ.com), purified through a Barnstead E-Pure filtration system (Thermo Scientific, Rockford, IL) was used for all reagent preparations.

Table 2.1 DNA sequences employed in this work

Name	5′-3′
Capture	**GAATGTTGATTTTATAT** TTTTTT- (CH2)6-SH2
Target	**ATATAAAATCAACATTC** *CCTAAGAAATGCTACA*
H1	**biotin-**TTTTTTAGTTCTGCGTCGTGATGG *TGTAGCATTTCTTAGG*
H2	CCATCACGACGCAGAACT *CCTAAGAAATGCTACA* TATATA**-biotin**

*The italic and underlined parts are complementary sequences, respectively

2.2.2 Apparatus

Gold chips were fabricated using an E-beam evaporator Temescal BJD 1800 in the UCR Center for Nanoscale Science and Engineering (CNSE) facility. All absorbance spectra were obtained using a Cary 50 UV-Vis spectrophotometer (Agilent Technologies, Santa Clara, CA). SPR spectroscopy measurements were carried out in room temperature using a commercial instrument from NanoSPR (Addison, IL) consisting of a dual channel fluidic setup (30 µL), a glass prism, and a 650 nm light source. Centrifugation was carried out using Eppendorf Centrifuge 5415C.

2.2.3 Gel electrophoresis

All oligonucleotides were dissolved in Tris-ethylene diamine tetraacetic acid buffer (pH 8.0, 10 mM Tris-HCl, 1mM EDTA) prior to use or stored at −20 °C. The hybridization buffer (pH 7.5) contained 40 mM Tris, 250 mM NaCl, 40 mM KCL. The self-assembly of HCR amplification reaction was ascertained by 8% native polyacrylamide gel electrophoresis in 1 × TBE (90 mM Tris-HCl, 90 mM boric acid, 2 mM EDTA, pH 7.9) buffer at constant voltage of 100 V for 40 min. The gel electrophoresis was carried out on

a DYY-6C electrophoresis analyzer (Liuyi Instrument Company, China) and imaged on a Bio-Rad ChemDocXRS (Bio-Rad Laboratories, USA).

2.2.4 Gold Nanoparticles Synthesis and Conjugation.

Gold nanoparticles were prepared using a standard citrate reduction method.[40] Briefly, to synthesize 13 nm gold nanoparticles, $HAuCl_4$ was dissolved in 500 mL of distilled water in glassware previously cleaned with Aqua Regia (3:1 HCl to HNO_3), giving a final concentration of 1 M $HAuCl_4$. This solution was heating until boiling with vigorous stirring, then a 50 mL of 38.8 mM solution of sodium citrate tribasic dihydrate was added, and the solution was boiled for another 15 min before being allowed to cool to room temperature. These nanoparticles were functionalized with thiolated oligonucleotides consisting of biotinylated poly-thymine, and poly-thymine in a 1:1 ratio according to a protocol previously reported in our group.[41] The synthesized gold nanoparticles were used as-is before the addition of 5 nmol DNA-Biotin (100 µM, H_2O) to 2 mL of concentrated gold nanoparticles. Immediately, 40 µL of citrate-HCL (500 mM, pH 3.0) was added before the addition of 20 µL of 10% (v/v) Tween 20. Finally, 250 µL of 5M NaCl was added to the mixture and the nanoparticles solution was stored overnight at 4 °C. Each addition step was followed by vortex and sonication. Excess reagents were removed from the nanoparticle solution by centrifugal filtration (Amicon, MWCO 50 kDa), washed five times with PBS, and the resulting Au-DNA-Biotin conjugates was stored at 4°C after addition of 250 µL buffer. UV-Vis was performed to determine the concentration of gold nanoparticles and to assess the conjugation result.

2.2.5 Gold chip preparation

The SPR chips were fabricated by depositing a 2 nm thick chromium layer (0.5 Å/s), followed by a 50 nm thick gold layer (1 Å/s), at $5x10^{-6}$ Torr via an e-beam evaporator. For the cleaning of the glass slides, 80 mL of piranha solution consisting of 3:1 v/v H_2SO_4 and 30% H_2O_2 was prepared in a 100 mL beaker. In a separate round glass container, BK-7 glass microscope slides (refractive index = 1.5167) ware arranged after which the piranha solution was poured into and boiled for 30 min or until all bubbles disappear. The container was removed from the hot plate and cooled to room temperature. After that, the slides were thoroughly rinsed with DI water and blow dried under compressed air.

2.2.6 Sensing chip preparation

Prior to immobilization of the thiolated capture probes onto the gold chips via the Au-S bond, the chips were rinsed thoroughly with ethanol and then air dried. In the first step, 500 µL of 1 µM thiolated capture probe diluted in immobilization solution (Tris buffer, pH 7.5) was pipetted onto the gold chip then incubated for 2 hours. Next, 500 µL of 1mM 6-mercapto-1-hexanol (MCH) was incubated on the gold chip for 1 hour. MCH, a short-chain thiol with hydrophilic hydroxy group, is co-assembled with probe DNA for reducing the non-specific binding of DNA and making the DNA chain erect on the gold surface.[42] The chips were rinsed with DIW and dried with N_2 after each step.

2.2.7 SPR of DNA detection and amplification

Prior to the experiments, a thin layer of matching fluid (Immersion Fluid from Cargille Laboratories) was applied to the sensing chips. All biological components were diluted prior to injection with hybridization buffer, to achieve the final concentrations. The hybridization buffer was also used as the running buffer at a flow rate of 5.0 mL / h. After 30 mins of steady baseline as monitored using SPR, the detection of target DNA and the amplification steps was carried out by injecting the probes and other binding molecules into the channels, in sequence, accordingly. All steps were separated by a buffer wash of at least 15 minutes. The measurements were repeated for at least three times, where the angle shift ($\Delta\theta$) was calculated after subtracting the non-specific binding in control channels from specific binding in the experiment channels after rinsing.

2.3 Results and Discussions

2.3.1 Characterization of the proposed assay

The feasibility of the HCR system was verified using polyacrylamide gel electrophoresis (PAGE). The results confirm the formation of DNA assemblies from the hybridization assay. As shown in Figure 2.2, the mixture of capture, target and H1 DNA hybridized with each other (lane 6) while in the presence of H2 longer DNA fragments are formed (lane 7 and 8).

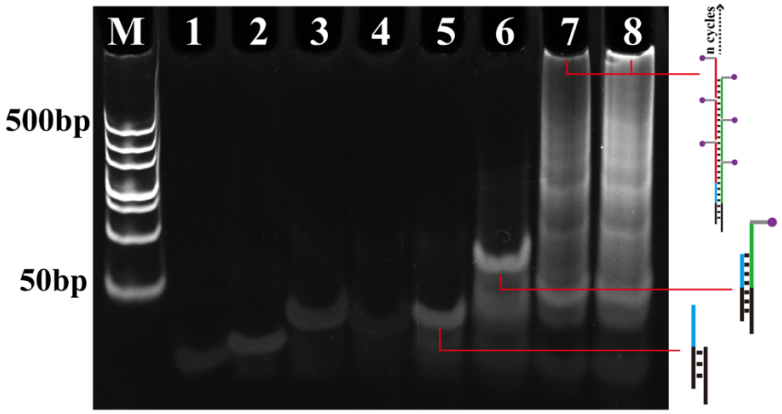

Figure 2.2 8% native polyacrylamide gel electrophoresis analysis of hybridization chain reaction corresponding to hybridization of different chains. Lane 1-4 represent Capture, Target, H1 and H2, respectively. Lane 5: Capture and Target; Lane 6: Capture, Target and H1; Lane 7, 8: hybridization chain reaction with 1 μM and 2 μM H1, H2, respectively.

2.3.2 UV-Vis Analysis of Conjugated Gold Nanoparticles.

The presence of protein conjugated to the AuNPs were analyzed using UV-Vis spectroscopy (Figure 2.3) and the size of gold nanoparticles was determined from the data[43]. We used AuNPs of 13 nm in diameter because smaller nanoparticle are more stable in solution, easier to prepare, and have well-established bioconjugation protocols compared to larger nanoparticles (> 15 nm).[44] In addition, a smaller diameter allows for more biotinylated AuNP binding to streptavidin and has less non-specific binding, resulting in a larger SPR signal. The unconjugated 13 nm AuNPs exhibit maximum UV absorbance at a wavelength of 520 nm, which is consistent with values typically reported for this size; and we calculated the concentration of our AuNPs to be 3 nM. For conjugation to DNA

the gold nanoparticle solution was used at the synthesized concentration. After conjugation, the increased particle size caused a red-shift to 525 nm in the maximum absorbance peak,[38, 45] and the concentration for Au-DNA-Biotin (1:1) was calculated to be 10 nM. A second maximum peak at 260 nm confirms the presence of protein. All dilutions prior to SPR measurements were achieved by addition of Tris buffer.

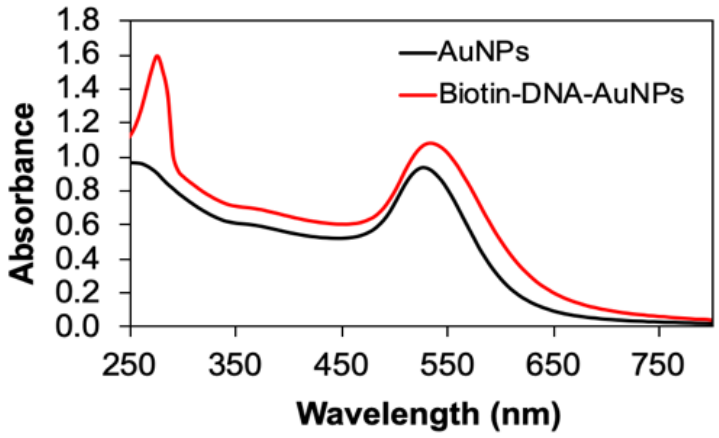

Figure 2.3 Absorbance spectra of 13 nm AuNPs before and after DNA-Biotin conjugation

2.3.3 Analysis of target DNA hybridization on sensing surface

With the confirmation of capture, and the target DNA probes hybridizing as intended, it is imperative that the hybridization translates to a binding signal on SPR as well. For this purpose, we constructed a biosensor for the detection of target DNA when it hybridizes with the capture probe. The chip is docked into SPR equipment followed by 30 min baseline, after which 0.1 µM of target DNA was injected only in the experiment channel (Figure 2.4). After 90 minutes of incubation time, the flow pump was turned on for the rinsing step. A shift in resonance angle was observed resulted from the specific

binding of the probes, while the signal remains in the control channel. Although the binding is validated, a small angle shift ($\Delta\theta = 0.02^{o}$) was observed, consistent with a mass of the hybridized structure of less than 50 bp as seen in Lane 5 of Figure 2.2. This small angle shift justified a need for signal amplification to improve sensitivity and to detect at even lower concentration.

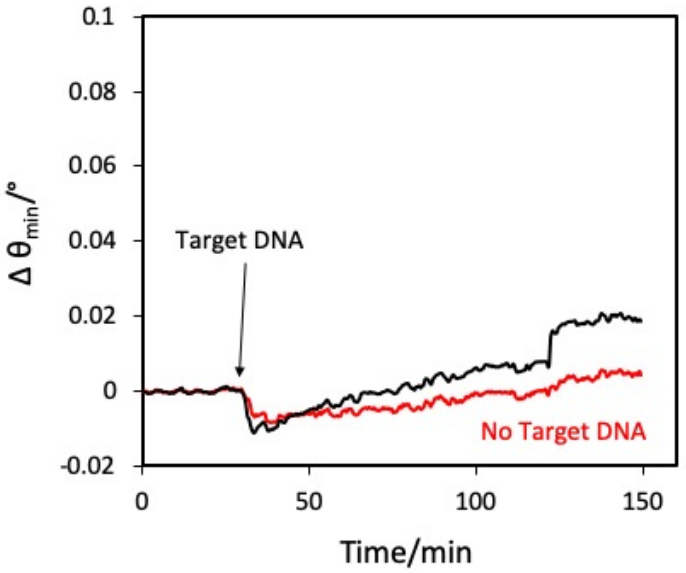

Figure 2.4 SPR sensorgrams representing detection of target 0.1 μM DNA

2.3.4 Feasibility of biosensing strategy with HCR amplification

In this amplification strategy, HCR probes (H1 and H2) were introduced after incubation of target DNA. One terminal of target DNA binds to the capture probe and the other terminal triggers HCR through hybridization with H1. The remaining sequence of H1 is complementary to H2, subsequently triggering linear amplification and building up DNA nanostructures. We again used SPR to determine the binding signal of this scheme. In the

experiment channel, a pre-mixed 0.1 μM target DNA, 1 μM H1 and 1 μM H2 was injected into the flow channel and incubated for 90 min. In the control channel, only H1 and H2 was injected. After rinsing, an increase of angle shift ($\Delta\theta = 0.03°$) was observed with HCR molecules while we observed no change in the absence of target DNA (Figure 2.5A).

2.3.5 Optimization of HCR Condition

In order to evaluate optimum conditions for this assay, several experiments were conducted with the aim to improve the hybridization process as to achieve higher SPR signal. From literatures, the formation of HCR molecules is one of the important factors in getting the most benefit from this amplification strategy. For example, different DNA base pairs that are most efficient to produce highest SPR signal was studied,[46] and it is known that surface plasmon wave is sensitive within 300 nm from the metal surface.[47] The efficiency of the self-assembled DNA can also be affected by steric hindrance when the nanostructures are too close to each other.[48] Other factors to be considered include hybridization reaction time and the volume ratio between HCR probes.[31, 46] In this work, the hybridization reaction was evaluated by comparing one-step reaction to two-step reaction, where two-step reaction would trigger the formation of larger HCR product. In two-step reaction, target DNA is injected first and let incubated and rinsed, before H1 and H2 probes are injected for the self-assembly to happen. While target DNA, H1 and H2 are premixed and injected at the same time in one-step reaction. The result of two-step reaction of 0.1 μM target DNA is shown in Figure 2.5B. By comparing to the one-step reaction, a

higher angle shift was observed for the two-step reaction ($\Delta\theta = 0.04°$), consistent with the above discussion. Therefore, the two-step reaction was chosen for the rest of this study.

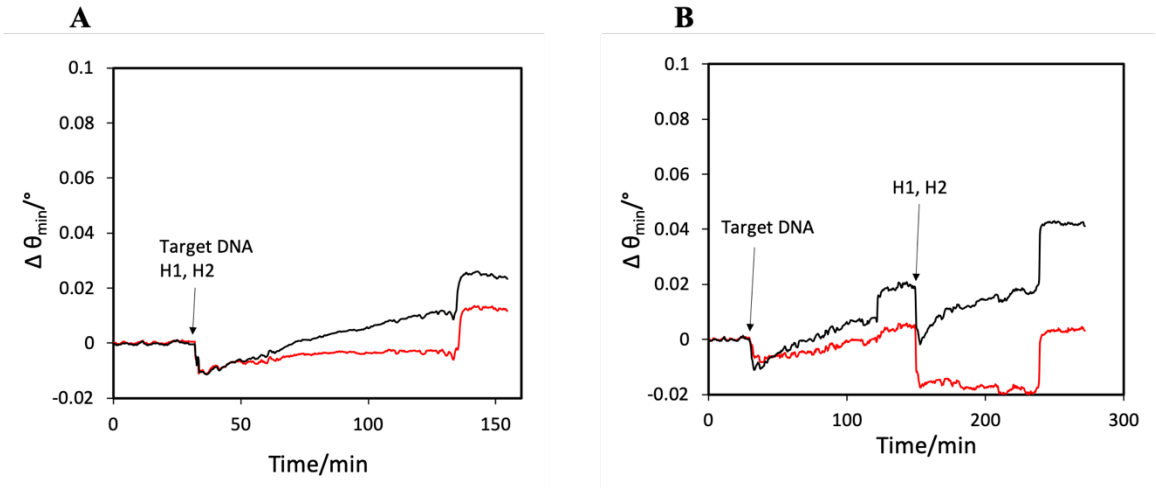

Figure 2.5 Sensorgrams from a typical SPR experiment of 0.1 µM target DNA with HCR molecules H1 and H2 for linear DNA amplification strategy using one-step (A) and two-step (B) method. Red line indicates control channel without target DNA

2.3.6 HCR amplification capability

To further explore if the proposed HCR assay can produce higher signal through better DNA hybridization efficiency, other factors such as hybridization process temperature and concentration of HCR probes were studied. Although experiments involving DNA-based HCR were mostly done at room temperature[49, 50] it is worth investigating the effect of temperature on hybridization efficiency, as optimal hybridization of DNA occur at temperature higher than room temperature, which is between 37 to 42°C. All the oligonucleotides used in this experiment have melting temperature around 42-63°C,

which allows to study the hybridization behavior at temperature higher than room temperature.[51] Some works reported heat treatment of probes mixture at 95°C for 5 min and cooled to room temperature slowly, after which partly hybridized probes were obtained.[31, 52] Based on this information, the following experiments were conducted, and their results are shown in Figure 2.6, by pretreating mixture of H1 and H2, offline, at (A) 45°C for 4 hours and (B) 95°C for 10 min, respectively, prior to injection into SPR. In the control channel, non-treated H1 and H2 was injected for comparison. A 1 μM target DNA was used while other steps we done following the same procedure for two-step reaction. From these results, it can be concluded that heat treatment of H1 and H2 probes has no effect, as the resonance angle shift between the two channels are similar after the HCR step.

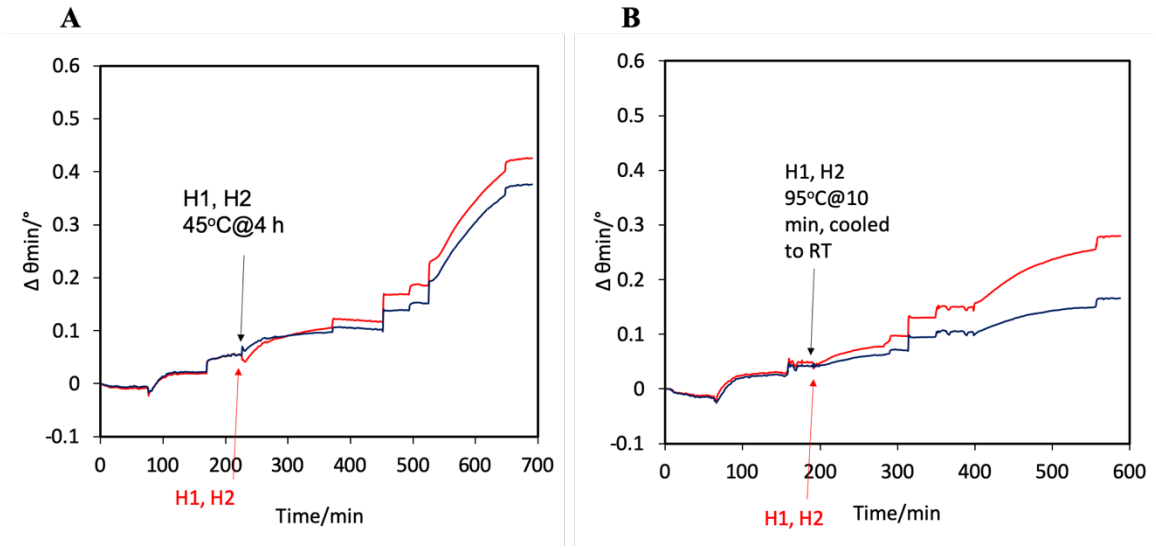

Figure 2.6 Effect of heat treatment on HCR molecules formation

To validate the HCR amplification, further experiments were conducted to compare the result from gel electrophoresis to SPR signal. As shown in Figure 2.7, the sensorgram of two SPR channels containing the same mixture of target and HCR probes as in Lane 6 and 7 of gel electrophoresis were obtained with 1 μM target DNA. In the presence of target DNA with H1 and H2, making a complete HCR system, a high SPR signal ($\Delta\theta = 0.18°$) was obtained because the self-assembled hybridization molecules have high molecular weights thus the signal was enhanced comparably and also because the target DNA could bind to many AuNPs due to the HCR molecules. Inversely, with the absence of H2, the increase of signal was almost negligible after HCR step. To evaluate the effect of the H1 and H2 concentrations, one channel was injected with 1 μM of H1 and H2 and another channel with 2 μM of H1 and H2, while target DNA was fixed to 1 μM for both channels. These parameters are comparable to Lane 7 and 8 in the gel electrophoresis, and the sensorgram is shown in Figure 2.8. No significant difference was observed between the two channels after HCR step, thus a higher concentration of H1 and H2 has no effect on signal amplification. Possible explanation to this is that the volume ratio of H1 and H2 is 1:1 and that 1 μM is the optimum concentration, as the same findings were reported by other studies.[30, 34] Therefore 1 μM of H1 and H2 was chosen for the amplification study.

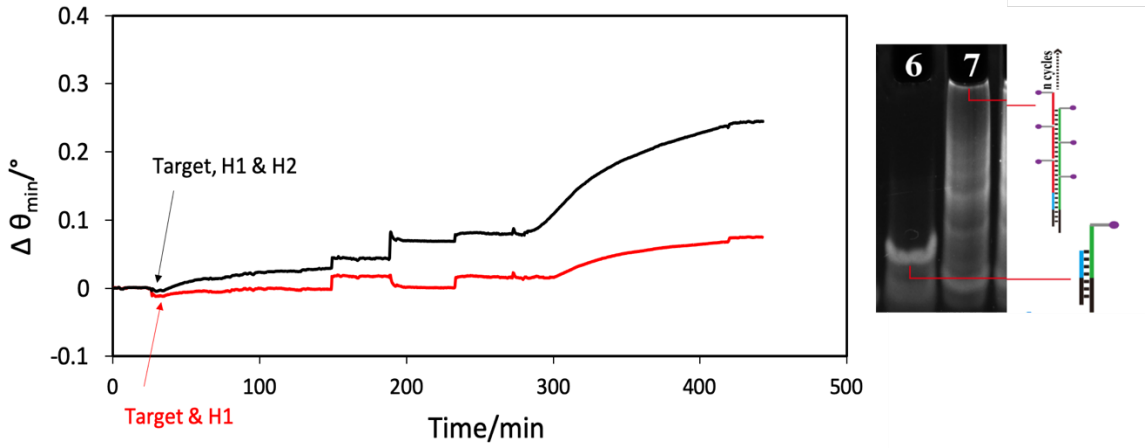

Figure 2.7 Sensorgram represent Red Line-Lane 6: Capture, Target and H1; Black Line-Lane 7: hybridization chain reaction with 1 μM H1, H2.

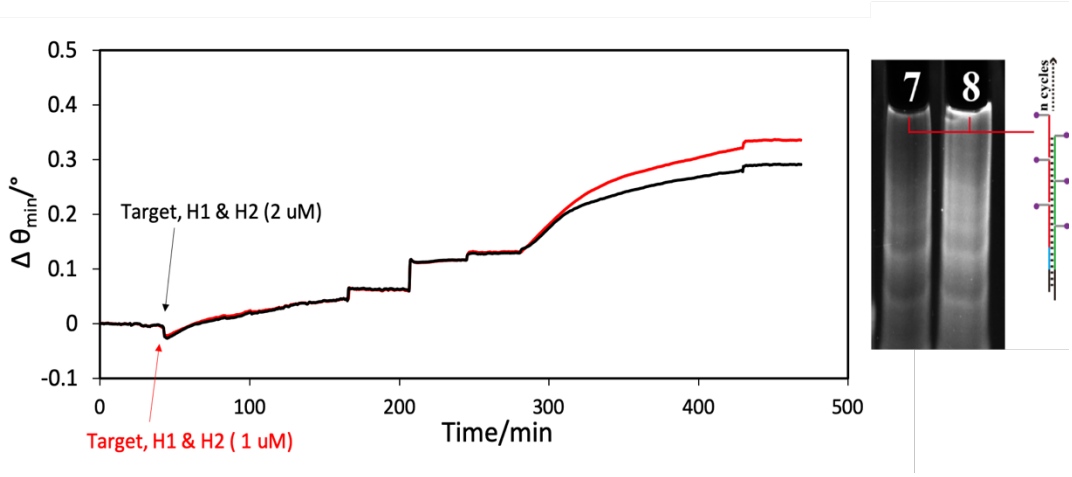

Figure 2.8 Sensorgram represent Red Line-Lane 7, Black Line-Lane 8: hybridization chain reaction with 1 μM and 2 μM H1, H2, respectively.

2.3.7 Further amplification using gold nanoparticles (AuNPs)

While HCR is proven to amplify the detection, a more sensitive strategy is required to improve the sensitivity and limit of detection (LOD) of this biosensor. We chose to incorporate AuNPs because it is proven to be effective in SPR signal enhancement due to high refractive index and the electronic coupling interaction between the localized SPR of AuNPs and the resonance wave of the gold film on the sensor chip.[38] In this work, an SPR sensing strategy consists of thiolated capture DNA, target DNA, HCR probes H1 and H2 with biotin end terminal, streptavidin and biotin-labelled gold nanoparticles was employed (Figure 2.9). Additional amplification was achieved when the biotinylated AuNPs binds to H1 and H2 assemblies via a streptavidin bridge. The result was plotted in a sensorgram (Figure 2.10) showing real-time binding of the biomolecules. In step 1, 0.1 μM target DNA, was injected into experiment channel and incubated for 90 min. After rinsing, 1 μM H1 and 1 μM H2 were injected in both experiment and control channels. Next, 100 μg/mL streptavidin was injected, incubated and rinsed followed by 1.0 nM of 13 nm biotinylated-AuNPs. After final rinse, a high SPR signal was observed in experiment channel ($\Delta\theta$ = 0.40°) while in control channel a non-specific binding was observed ($\Delta\theta$ = 0.04°) but sufficient to say no significant increase in resonance angle was seen in the absence of target DNA. The higher SPR response in experiment channel after step 2 is gained by the DNA nanostructures, while no response in control channel as HCR molecules were not formed. In step 3, no SPR signal is obtained in control channel due to absence on biotin, while the signal increase in experiment channel as streptavidin binds to biotin on the terminal end of H1 and H2. Evidently, a much higher response was observed from AuNPs enhancement in

step 4 compare to step 2 and 3 for experiment channel. To find out if the sensing scheme is highly sensitive, we conducted SPR with lower concentration of target DNA. From the sensorgram in Figure 2.11, a smaller angle shift was obtained ($\Delta\theta = 0.28°$) when the target DNA was reduced to 1.0 nM. In the following discussions, we compare the sensitivities when amplified by HCR and AuNPs.

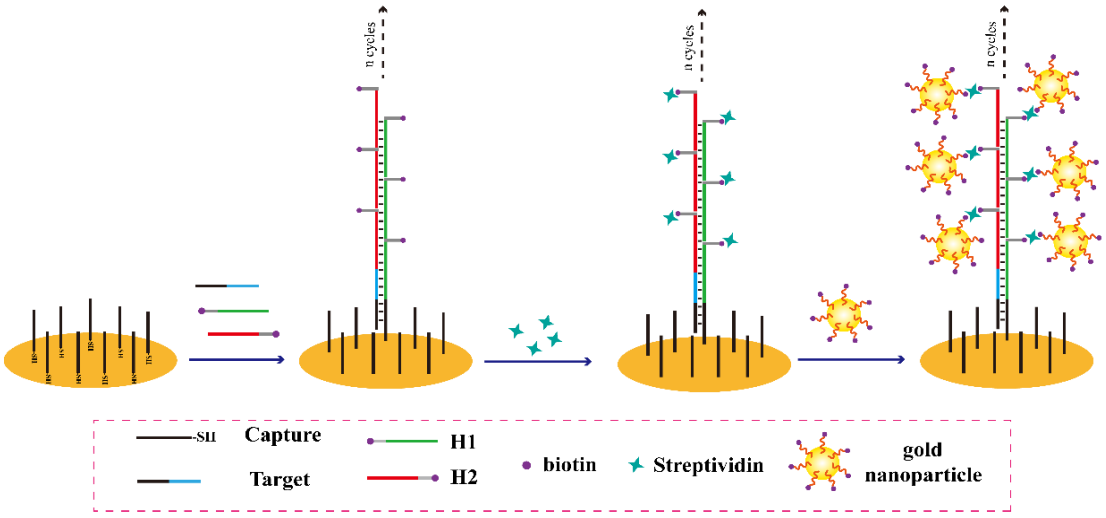

Figure 2.9 Schematic representation of Plasmodium falciparum detection assay using SPR based on DNA self-assembly and AuNPs amplification

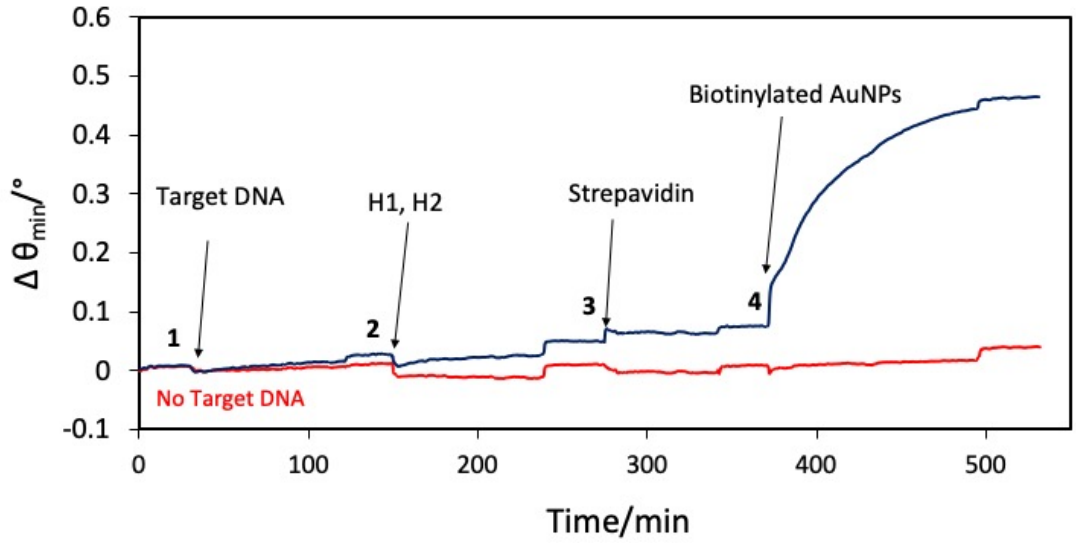

Figure 2.10 Sensorgrams from a two-step SPR experiment of 0.1 μM target DNA with HCR molecules H1 and H2 for linear DNA amplification strategy and AuNPs signal enhancement.

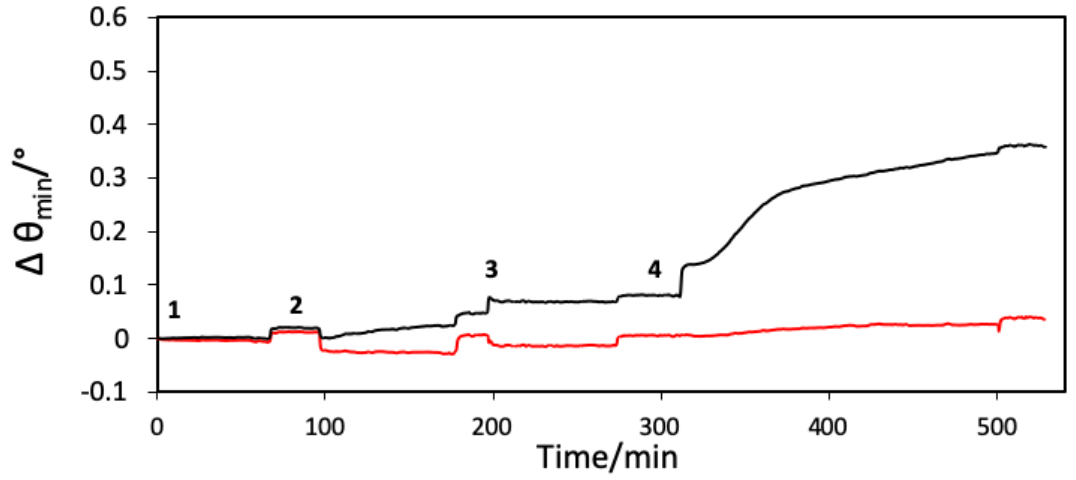

Figure 2.11 Sensorgram from a two-step hybridization, for 1.0 nM target DNA concentration

2.3.8 Sensitivity of detection in buffer medium

To evaluate the analytical performance of our SPR biosensor using either HCR or AuNPs, the angle shifts from different concentrations of target DNA were measured following a two-step reaction. On the experiment channel, target DNA from 0.1 nM to 1.0 μM were injected on separate experiments; non target DNA was injected in the control channel in order to assess non-specific binding. Increasing amounts of target DNA led to a proportional increase in the SPR signal, the sensorgrams and calibration curves are shown in Figure 2.12, after (A) HCR and (B) AuNPs amplification. The calibration curve for HCR showed a linear correlation from 1.0 nM to 0.1 μM, with R^2 value of 0.9927. Because the SPR signal produces a systematic amount of noise, any shift below 0.02^o is not meaningful therefore was not included in the calibration curve. In the case of AuNPs, the resonance angle shift reached a plateau after 0.1 μM (small insert). The curve was re-plotted to show the dynamic range from 0.1 nM to 0.1 μM and an R^2 value of 0.9719 was obtained. From these results, we determined the amplification method by AuNPs is ten times higher than HCR.

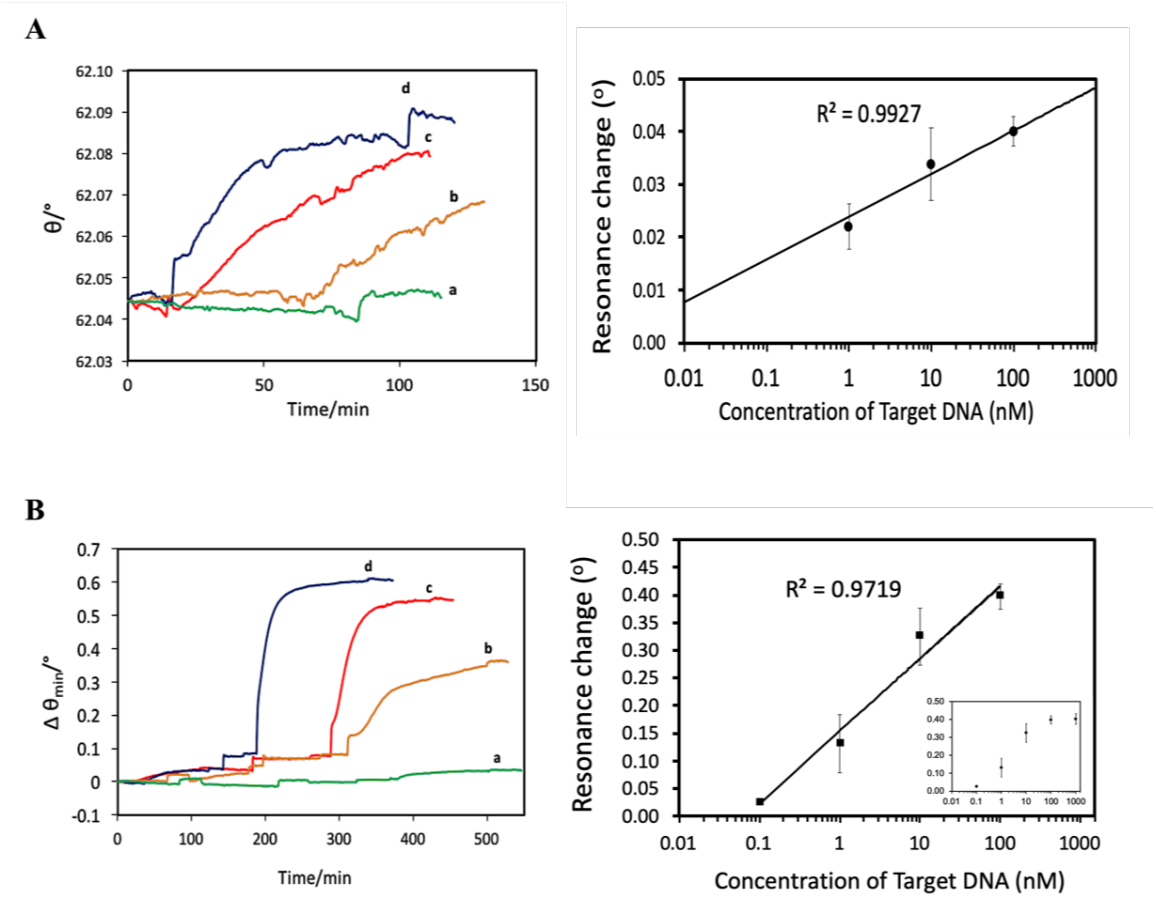

Figure 2.12 SPR sensorgrams and calibration curves for (A) (B) HCR and (C) (D) AuNPs amplified detection of Plasmodium falciparum DNA. The curves from a to b represent 0.1 nM, 1.0 nM, 10 nM and 0.1 μM, respectively.

2.3.9 Analysis of detection in complex media

To further evaluate the biosensor's performance in complex media to mimic clinical samples, the target DNA was spiked into blood plasma (Figure 2.13, step 1a) instead of the buffer; all further steps were performed as described previously. Two control experiments were conducted to assess if using complex media will compromise the assay. First, we

assessed the non-specific binding in the absence of target DNA. The sensorgrams show that there is an angle shift of 0.1° on the channel injected with plasma, due to the proteins and other components that non-specifically bind on the sensor surface, while on the buffer channel the signal remains at baseline as no binding occurred. However, after AuNPs amplification step, no significant difference between both channels was observed, showing that the assay is not compromised by the complex components. In the second control experiment (Figure 2.14), both channels were spiked with 0.1 µM target DNA, however only one channel was injected with H1 and H2. Subsequently, after streptavidin was introduced only the channel with HCR displayed a signal increase and the same was observed after AuNPs amplification. No binding was observed on the channel without H1 and H2 due to lack of biotin, preventing binding of streptavidin and biotinylated AuNPs.

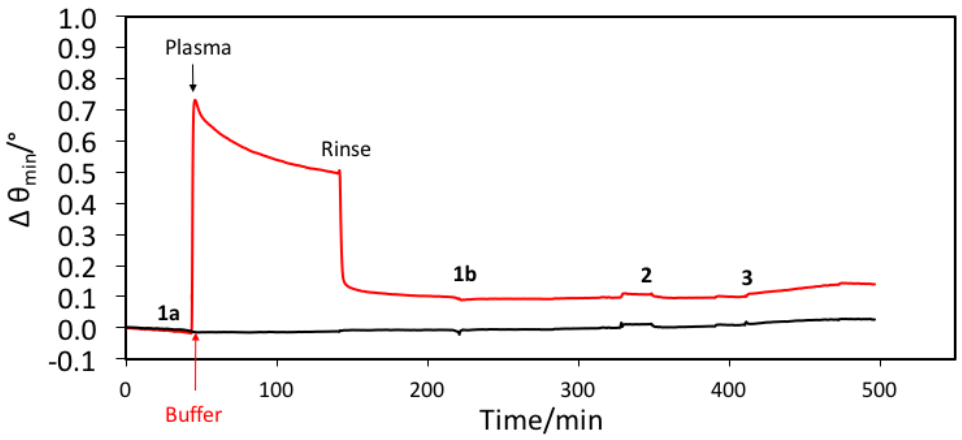

Figure 2.13 Control experiment - No target DNA in samples

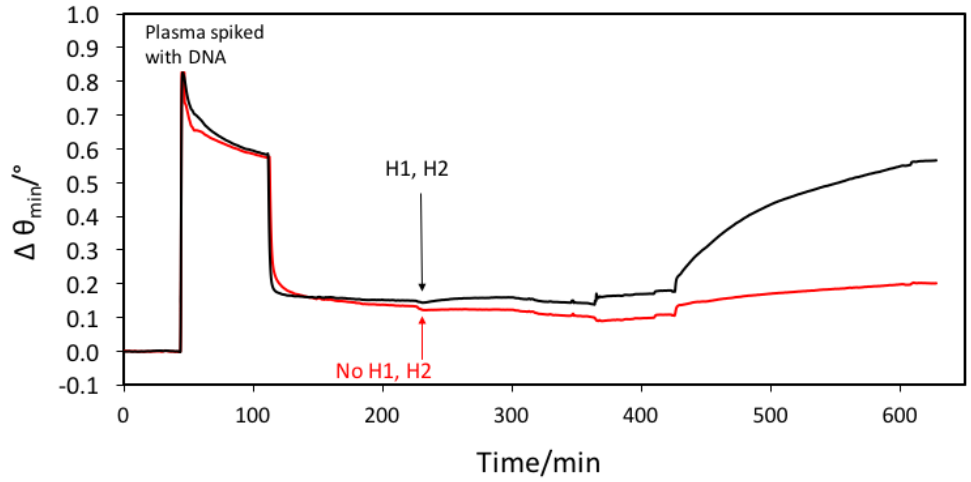

Figure 2.14 Control experiment - No H1 and H2 in control channel

2.3.10 Sensitivity of detection in blood plasma

In clinical diagnosis of Malaria, the blood of suspected patients is drawn and brought to the lab for several tests including the blood film microscopy, RDTs or PCR. The blood film test being the main method used to spot and count malaria parasites in blood would usually takes 1-3 days and the process is repeated for the patients during treatment, until the result becomes negative. This clearly signifies the need for more sensitive, fast and early detection, before the patient reaches a dangerous untreatable level of this disease. To show the feasibility of this biosensing strategy in clinical application, we compared the biosensor performance when tested in blood plasma versus in buffer samples. Here, SPR measurements using plasma sample were conducted and the sensorgram is shown in Figure 2.15. Briefly, the sensor chip incubated with capture DNA was left in running buffer for 30 min before the plasma spiked with target DNA was injected (step 1a). In the control

channel, the same volume of buffer is spiked into plasma, while the other steps are identical to the experiment channel. As seen in both channels, there is a large SPR increase after injection of plasma due to a high refractive index of the bulk solution, after reaching a plateau we incubated the solution for 90 min. After the running buffer was turned on, the signal decreased but did not return to baseline due to binding of other components in the plasma. The subsequent injections were H1 and H2, followed by streptavidin and the biotinylated AuNPs. The experiments were repeated with different concentrations of target DNA, and Figure 2.16A shows that the resonance angle increased gradually as the target DNA concentration increased from 0.1 nM to 0.1 μM after the final rinse. For all sensorgrams only the experiment channel showed a large increase of signal after AuNPs amplification. To compare sensitivity with the buffer sample, calibration curves of both conditions are plotted in the same graph shown in Figure 2.16B. The graph shows the sensitivity of detection in blood plasma is comparable to buffered sample, that this method has great potential for clinical application with further improvement.

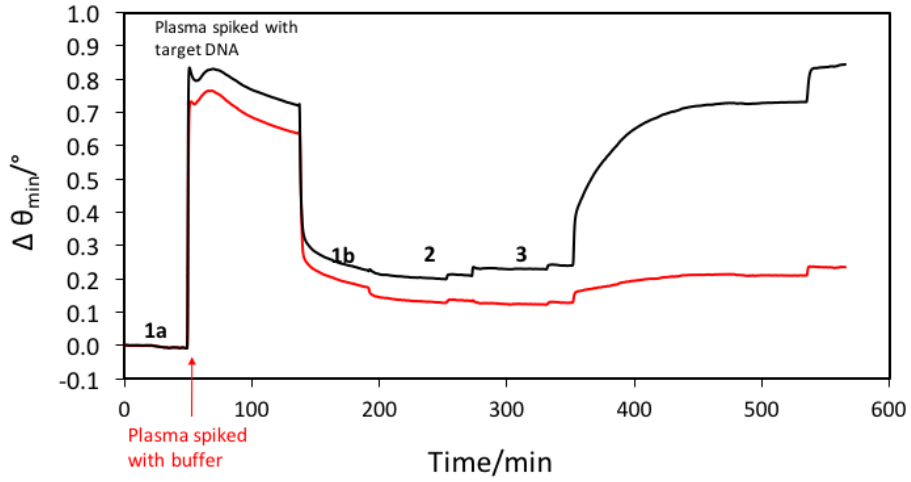

Figure 2.15 Sensorgram of target DNA spiked in plasma

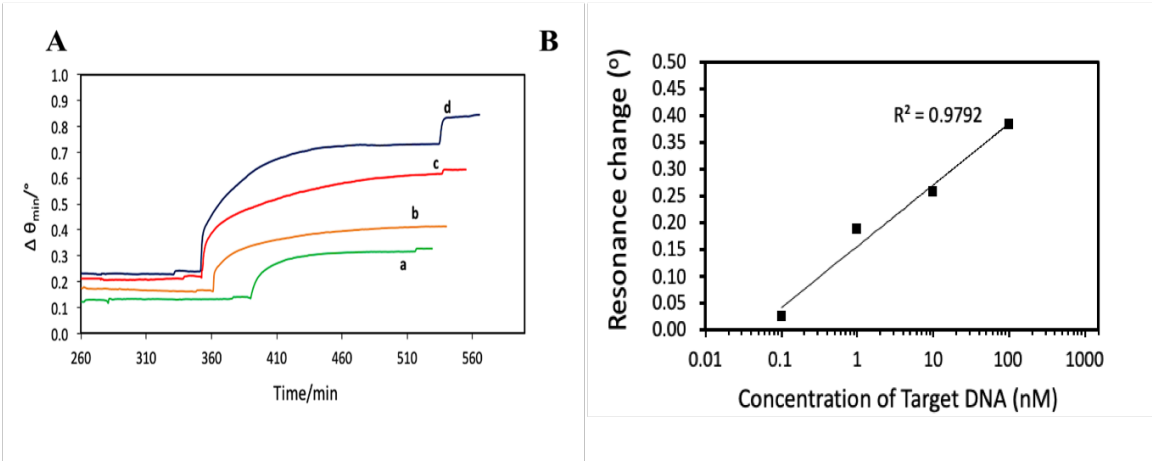

Figure 2.16 Sensorgrams of different concentration of target DNA spiked in plasma. (A) resonance change after AuNPs amplification. The curves from a to b represent 0.1 nM, 1.0 nM, 10 nM and 1 μM, respectively. (B) Calibration curve

2.3.11 Comparison to other SPR malaria biomarkers and malaria DNA biosensor

Although many biosensors have been developed for malaria detection, most of the published works use enzymatic protein biomarkers such as *Plasmodium falciparum* histidine rich protein II (PfHRP-II or HPR-II), *Plasmodium falciparum* lactate dehydrogenase (PfLDH) and the parasite waste product such as hemozoin.[12] To date, very few biosensors have been developed for molecular detection of the parasite's DNA and the reasons are very clear, DNA that has to be extracted from blood, while the other biomarkers are abundantly present in blood and urine of infected patients. However, the detection method using biomarkers is not sensitive to low parasite density and can only be detected at least 7 days after the parasites are transferred to the human blood stream. This means that the current methods are not effective for early detection of Malaria, even the most used diagnostic like RDTs. Thus, the use of DNA as a new biosensor target allows highly sensitive and low limit of detection, which means the disease can be detected at an earlier stage of infection.

An SPR based biosensor has the advantage of highly sensitive detection for many biomolecules. In the development of malaria biosensors, we grouped the sensors into two categories based on the target biomarkers; non-DNA and DNA target biomarkers. From the literature, we found SPR biosensors have been developed using heme (a toxin released by the parasites)[53] and the retromer protein complex,[54] and *Pf*HRP-II.[55] During these experiments the sensing antigens were recognized using apo-hemoglobin and antibodies, and the binding occurred in buffered media. For all biosensors, the antigens were prepared in labs and not extracted from actual clinical sample. This is understandable as SPR chips

are prone to surface fouling and the measurement produces a very large non-specific binding signal when complex media such as blood, plasma, serum and urine are used. Although this interference from complex media seems to hinder the progress of SPR for clinical application, the use of undiluted complex media with SPR has been demonstrated.[56] Recently, our group has reported an antifouling sensor surface utilizing a supported lipid bilayer when used with human serum and plasma.[57]

In the development of Malaria DNA based biosensors we did not note any previous research using SPR. Nevertheless, other biosensing methods were found, such as Malaria DNA detection by frequency and phase change using QCM[13, 14] and Mach-Zehnder Interferometer (MZI).[58] In these methods, DNA was extracted from patient blood samples and from malaria parasites cultured in lab. In the QCM biosensor, the extracted DNA was amplified using PCR before the target DNA is allowed to bind with the immobilized complementary probes. For the MZI biosensor, the DNA amplification step was done on the sensing chip at 37^{o}C. Again, for both methods actual clinical sample was not used during the detection step. However, the results are a good indicator that a biosensor for detection of malaria at the molecular level is more sensitive than microscopy and can move us towards the sensitivity achieved by RDTs and PCR, with more advance features than those conventional methods including detection of more than one Plasmodium species at the same time.

In our SPR biosensor, the detection and amplification occur on the same surface, via simple DNA binding and hybridization at room temperature, before further amplification using AuNPs. The measurement was done in buffer and undiluted blood plasma, and we

achieved detection as low as 1 picomolar compared to micromolar detection from the QCM method. The DNA amplification using HCR method is also versatile for other biosensing detection of low abundance DNA, for example in biochemical studies, forensic investigations and pathogen detections.[31] However, our method lacks comparison to other clinical methods such as microscopy, RDTs and PCR, which is useful as a benchmark to any developed biosensor. In addition, the specificity of our biosensor against other *Plasmodium* species was not evaluated. While we did not use blood sample from infected patients, using undiluted blood plasma can mimic actual clinical diagnostics and further improvement can be made from this initial data. Nonetheless, our method has several advantages : it eliminates the need to pre-amplify the target DNA using complex instruments, the detection and amplification result is analyzed on the same platform, it provides real-time measurement of all binding interactions, is universally applicable to other detection of DNA and has potential for detection using clinical samples and to be developed into a portable instrument.

2.3.12 Potential of our biosensor for clinical detection and integration into a portable instrument

An ideal DNA biosensor for clinical application, not only for malaria but for other diseases, must be comprised of 1) a sample preparation chamber where the biofluid of interest is either diluted or separated, and where the DNA can be extracted, 2) a sensing chip immobilized with the recognition element, 3) an efficient binding mechanism between the target DNA and the recognition element, 4) a transducer system that recognizes the

binding and transforms the biomolecule interactions into a measurable signal, 5) a proper amplification method (if required) for the sensitivity to be in a useful clinical detection range, and 6) data processing that informs the user of the detection result for proper diagnosis and prognosis to be made based on the patient sample. The challenge is however to fully integrate and miniaturize all the above, in a cost-effective way, into a simple automated device for it to be field deployable or for use in point-of-care diagnostic.

For our SPR biosensor to be integrated as the main sensing platform in a portable diagnostic equipment; important parts of the platform are a prism, a gold chip and a flow cell with at least two channels. A microfluidic chamber for sample collection, sample dilution, components separation and DNA extraction are needed before the extracted target DNA can be introduced into the SPR flow cell. A sample-processing module that is able to perform the task has been developed,[58] although the system is not fully integrated with the sensing part, the system shows capability to extract DNA that was previously spiked into a blood sample.

Another consideration is whether the sensing chip is reusable or one-time use, although the latter is not preferable due to cost, but a very good antifouling surface or cleaning procedure has to be established between usages when applying a single chip for multiple measurements. A multiplex system for detection of multiple *Plasmodium* species is desirable, therefore the target-recognition element has to be highly specific and multiple probes have to be immobilized on the surface. Another factor to consider is a calibration process to avoid signal drift over time and to make sure results are accurate and reproducible; this could include auto-calibration or manual calibration with a known

sample, and in our case the calibration includes a shift after subtracting the non-specific binding. Finally, we need a data processing system that interprets the binding signal into a digital electronic signal that is proportional to the concentration of target DNA and then translates the result to a user interface showing positive or negative detection of malaria parasites from the patient sample.

2.4 Conclusion

In this study, we developed a simple and sensitive SPR DNA biosensor for a molecular level detection of Malaria that is vital for early diagnosis of this disease. We showed that the DNA detection coupled with HCR and gold nanoparticles amplification strategies increase the sensitivity, thus enabling picomolar range of detection. Compared to existing methods, our biosensor has several advantages, as discussed above. Although actual clinical samples were not used, we performed a systematic evaluation using human blood plasma to access the non-specific bindings that is a known challenge in biosensor especially SPR.

Our future direction includes evaluation of sensing capability and selectivity in a clinical standard requirement, using infected blood samples instead of the spiked blood plasma. More evaluations are needed to compare with conventional methods such as microscopy, RDTs and PCR. Overall, with our findings and from other existing studies in DNA biosensor, the future of a complete biosensor system for clinical diagnosis is brighter now than ever, not only for Malaria but also for other applications that could benefit from

this development. Future research should also be looking into integration of a microfluidic or lab-on-a-chip for sample preparation, and miniaturization of the detection and transduction system.

2.5 References

1. Cowman, A. F.; Healer, J.; Marapana, D.; Marsh, K., Malaria: Biology and Disease. *Cell* **2016,** *167* (3), 610-624.

2. Wilson, D. W.; Goodman, C. D.; Sleebs, B. E.; Weiss, G. E.; de Jong, N. W. M.; Angrisano, F.; Langer, C.; Baum, J.; Crabb, B. S.; Gilson, P. R.; McFadden, G. I.; Beeson, J. G., Macrolides rapidly inhibit red blood cell invasion by the human malaria parasite, Plasmodium falciparum. *BMC Biology* **2015,** *13* (1), 52.

3. Wahlgren, M.; Goel, S.; Akhouri, R. R., Variant surface antigens of Plasmodium falciparum and their roles in severe malaria. *Nature Reviews Microbiology* **2017,** *15*, 479.

4. Tangpukdee, N.; Duangdee, C.; Wilairatana, P.; Krudsood, S., Malaria diagnosis: a brief review. *The Korean journal of parasitology* **2009,** *47* (2), 93-102.

5. Johnston, S. P.; Pieniazek, N. J.; Xayavong, M. V.; Slemenda, S. B.; Wilkins, P. P.; da Silva, A. J., PCR as a Confirmatory Technique for Laboratory Diagnosis of Malaria. *Journal of Clinical Microbiology* **2006,** *44* (3), 1087.

6. Mfuh, K. O.; Achonduh-Atijegbe, O. A.; Bekindaka, O. N.; Esemu, L. F.; Mbakop, C. D.; Gandhi, K.; Leke, R. G. F.; Taylor, D. W.; Nerurkar, V. R., A comparison of thick-film microscopy, rapid diagnostic test, and polymerase chain reaction for accurate diagnosis of Plasmodium falciparum malaria. *Malaria Journal* **2019,** *18* (1), 73.

7. Byrnes, S. A.; Weigl, B. H., Selecting analytical biomarkers for diagnostic applications: a first principles approach. *Expert Review of Molecular Diagnostics* **2018,** *18* (1), 19-26.

8. Roth, J. M.; Korevaar, D. A.; Leeflang, M. M. G.; Mens, P. F., Molecular malaria diagnostics: A systematic review and meta-analysis. *Critical Reviews in Clinical Laboratory Sciences* **2016,** *53* (2), 87-105.

9. Bahadır, E. B.; Sezgintürk, M. K., Applications of commercial biosensors in clinical, food, environmental, and biothreat/biowarfare analyses. *Analytical Biochemistry* **2015,** *478*, 107-120.

10. Mehrotra, P., Biosensors and their applications – A review. *Journal of Oral Biology and Craniofacial Research* **2016,** *6* (2), 153-159.

11. Jain, P.; Chakma, B.; Patra, S.; Goswami, P., Potential Biomarkers and Their Applications for Rapid and Reliable Detection of Malaria. *BioMed Research International* **2014,** *2014*, 20.

12. Ragavan, K. V.; Kumar, S.; Swaraj, S.; Neethirajan, S., Advances in biosensors and optical assays for diagnosis and detection of malaria. *Biosensors and Bioelectronics* **2018,** *105*, 188-210.

13. Ittarat, W.; Chomean, S.; Sanchomphu, C.; Wangmaung, N.; Promptmas, C.; Ngrenngarmlert, W., Biosensor as a molecular malaria differential diagnosis. *Clinica Chimica Acta* **2013,** *419*, 47-51.

14. Wangmaung, N.; Chomean, S.; Promptmas, C.; Mas-oodi, S.; Tanyong, D.; Ittarat, W., Silver quartz crystal microbalance for differential diagnosis of Plasmodium falciparum and Plasmodium vivax in single and mixed infection. *Biosensors and Bioelectronics* **2014,** *62*, 295-301.

15. Homola, J., Surface Plasmon Resonance Sensors for Detection of Chemical and Biological Species. *Chemical Reviews* **2008,** *108* (2), 462-493.

16. V, K., DNA Biosensors-A Review. *Journal of Bioengineering & Biomedical Science* **2017,** *07*.

17. Sang, S.; Wang, Y.; Feng, Q.; Wei, Y.; Ji, J.; Zhang, W., Progress of new label-free techniques for biosensors: a review. *Critical Reviews in Biotechnology* **2016,** *36* (3), 465-481.

18. Sin, M. L. Y.; Mach, K. E.; Wong, P. K.; Liao, J. C., Advances and challenges in biosensor-based diagnosis of infectious diseases. *Expert Review of Molecular Diagnostics* **2014,** *14* (2), 225-244.

19. Masson, J.-F., Surface Plasmon Resonance Clinical Biosensors for Medical Diagnostics. *ACS Sensors* **2017,** *2* (1), 16-30.

20. Gorodkiewicz, E.; Lukaszewski, Z., Recent Progress in Surface Plasmon Resonance Biosensors (2016 to Mid-2018). *Biosensors* **2018,** *8* (4), 132.

21. Wang, R.; Lajevardi-Khosh, A.; Choi, S.; Chae, J., Regenerative Surface Plasmon Resonance (SPR) biosensor: Real-time measurement of fibrinogen in undiluted human serum using the competitive adsorption of proteins. *Biosensors and Bioelectronics* **2011,** *28* (1), 304-307.

22. Pimkova, K.; Bockova M Fau - Hegnerova, K.; Hegnerova K Fau - Suttnar, J.; Suttnar J Fau - Cermak, J.; Cermak J Fau - Homola, J.; Homola J Fau - Dyr, J. E.; Dyr, J. E., Surface plasmon resonance biosensor for the detection of VEGFR-1--a protein marker of myelodysplastic syndromes. (1618-2650 (Electronic)).

23. Jongerius-Gortemaker, B. G. M.; Goverde, R. L. J.; van Knapen, F.; Bergwerff, A. A., Surface plasmon resonance (BIACORE) detection of serum antibodies against Salmonella enteritidis and Salmonella typhimurium. *Journal of Immunological Methods* **2002,** *266* (1), 33-44.

24. Vaisocherová, H.; Šípová, H.; Víšová, I.; Bocková, M.; Špringer, T.; Laura Ermini, M.; Song, X.; Krejčík, Z.; Chrastinová, L.; Pastva, O.; Pimková, K.; Dostálová Merkerová, M.; Dyr, J. E.; Homola, J., Rapid and sensitive detection of multiple microRNAs in cell lysate by low-fouling surface plasmon resonance biosensor. *Biosensors and Bioelectronics* **2015,** *70*, 226-231.

25. Li, J.; Lei, P.; Ding, S.; Zhang, Y.; Yang, J.; Cheng, Q.; Yan, Y., An enzyme-free surface plasmon resonance biosensor for real-time detecting microRNA based on allosteric effect of mismatched catalytic hairpin assembly. *Biosensors and Bioelectronics* **2016,** *77*, 435-441.

26. Mariani, S.; Scarano, S.; Spadavecchia, J.; Minunni, M., A reusable optical biosensor for the ultrasensitive and selective detection of unamplified human genomic DNA with gold nanostars. *Biosensors and Bioelectronics* **2015,** *74*, 981-988.

27. Eletxigerra, U.; Martinez-Perdiguero, J.; Barderas, R.; Pingarrón, J. M.; Campuzano, S.; Merino, S., Surface plasmon resonance immunosensor for ErbB2 breast cancer biomarker determination in human serum and raw cancer cell lysates. *Analytica Chimica Acta* **2016,** *905*, 156-162.

28. Uludag, Y.; Tothill, I. E., Cancer Biomarker Detection in Serum Samples Using Surface Plasmon Resonance and Quartz Crystal Microbalance Sensors with Nanoparticle Signal Amplification. *Analytical Chemistry* **2012,** *84* (14), 5898-5904.

29. Dirks, R. M.; Pierce, N. A., Triggered amplification by hybridization chain reaction. (0027-8424 (Print)).

30. Ding, X.; Yan, Y.; Li, S.; Zhang, Y.; Cheng, W.; Cheng, Q.; Ding, S., Surface plasmon resonance biosensor for highly sensitive detection of microRNA based on DNA

super-sandwich assemblies and streptavidin signal amplification. *Analytica Chimica Acta* **2015,** *874*, 59-65.

31. Ding, X.; Cheng, W.; Li, Y.; Wu, J.; Li, X.; Cheng, Q.; Ding, S., An enzyme-free surface plasmon resonance biosensing strategy for detection of DNA and small molecule based on nonlinear hybridization chain reaction. *Biosensors and Bioelectronics* **2017,** *87*, 345-351.

32. Ding, X.; Yan, Y.; Li, S.; Zhang, Y.; Cheng, W.; Cheng, Q.; Ding, S., Surface plasmon resonance biosensor for highly sensitive detection of microRNA based on DNA super-sandwich assemblies and streptavidin signal amplification. (1873-4324 (Electronic)).

33. Wang, Q.; Liu, R.; Yang, X.; Wang, K.; Zhu, J.; He, L.; Li, Q., Surface plasmon resonance biosensor for enzyme-free amplified microRNA detection based on gold nanoparticles and DNA supersandwich. *Sensors and Actuators B: Chemical* **2016,** *223*, 613-620.

34. Wei, X.; Duan X Fau - Zhou, X.; Zhou X Fau - Wu, J.; Wu J Fau - Xu, H.; Xu H Fau - Min, X.; Min X Fau - Ding, S.; Ding, S., A highly sensitive SPRi biosensing strategy for simultaneous detection of multiplex miRNAs based on strand displacement amplification and AuNP signal enhancement. (1364-5528 (Electronic)).

35. Krishnan, S.; Mani, V.; Wasalathanthri, D.; Kumar, C. V.; Rusling, J. F., Attomolar Detection of a Cancer Biomarker Protein in Serum by Surface Plasmon Resonance Using Superparamagnetic Particle Labels. *Angewandte Chemie International Edition* **2011,** *50* (5), 1175-1178.

36. Bai, Y.; Feng, F.; Zhao, L.; Wang, C.; Wang, H.; Tian, M.; Qin, J.; Duan, Y.; He, X., Aptamer/thrombin/aptamer-AuNPs sandwich enhanced surface plasmon resonance sensor for the detection of subnanomolar thrombin. *Biosensors and Bioelectronics* **2013,** *47*, 265-270.

37. Li, X.; Wang Y Fau - Wang, L.; Wang L Fau - Wei, Q.; Wei, Q., A surface plasmon resonance assay coupled with a hybridization chain reaction for amplified detection of DNA and small molecules. (1364-548X (Electronic)).

38. Liu, X.; Yang, Y.; Mao, L.; Li, Z.; Zhou, C.; Liu, X.; Zheng, S.; Hu, Y., SPR quantitative analysis of direct detection of atrazine traces on Au-nanoparticles: Nanoparticles size effect. *Sensors and Actuators B: Chemical* **2015,** *218*, 1-7.

39. Vigneshvar, S.; Sudhakumari, C. C.; Senthilkumaran, B.; Prakash, H., Recent Advances in Biosensor Technology for Potential Applications - An Overview. *Frontiers in bioengineering and biotechnology* **2016,** *4*, 11-11.

40. Frens, G., Controlled nucleation for the regulation of the particle size in monodisperse gold suspensions. *Nature* **1973,** *241* (105), 20-22.

41. Hinman, S. S.; McKeating, K. S.; Cheng, Q., DNA Linkers and Diluents for Ultrastable Gold Nanoparticle Bioconjugates in Multiplexed Assay Development. *Analytical Chemistry* **2017,** *89* (7), 4272-4279.

42. Zhang, L.; Li, Z.; Zhou, X.; Yang, G.; Yang, J.; Wang, H.; Wang, M.; Liang, C.; Wen, Y.; Lu, Y., Hybridization performance of DNA/mercaptohexanol mixed monolayers on electrodeposited nanoAu and rough Au surfaces. *Journal of Electroanalytical Chemistry* **2015,** *757*, 203-209.

43. Haiss, W.; Thanh, N. T. K.; Aveyard, J.; Fernig, D. G., Determination of Size and Concentration of Gold Nanoparticles from UV−Vis Spectra. *Analytical Chemistry* **2007,** *79* (11), 4215-4221.

44. Kwon, M. J.; Lee, J.; Wark, A. W.; Lee, H. J., Nanoparticle-Enhanced Surface Plasmon Resonance Detection of Proteins at Attomolar Concentrations: Comparing Different Nanoparticle Shapes and Sizes. *Analytical Chemistry* **2012,** *84* (3), 1702-1707.

45. Deng, H.; Xu, Y.; Liu, Y.; Che, Z.; Guo, H.; Shan, S.; Sun, Y.; Liu, X.; Huang, K.; Ma, X.; Wu, Y.; Liang, X.-J., Gold Nanoparticles with Asymmetric Polymerase Chain Reaction for Colorimetric Detection of DNA Sequence. *Analytical Chemistry* **2012,** *84* (3), 1253-1258.

46. Guo, B.; Cheng, W.; Xu, Y.; Zhou, X.; Li, X.; Ding, X.; Ding, S., A simple surface plasmon resonance biosensor for detection of PML/RARα based on heterogeneous fusion gene-triggered nonlinear hybridization chain reaction. *Scientific reports* **2017,** *7* (1), 14037-14037.

47. Nguyen, H. H.; Park, J.; Kang, S.; Kim, M., Surface Plasmon Resonance: A Versatile Technique for Biosensor Applications. *Sensors* **2015,** *15* (5).

48. Liu, X.; Niazov-Elkan, A.; Wang, F.; Willner, I., Switching Photonic and Electrochemical Functions of a DNAzyme by DNA Machines. *Nano Letters* **2013,** *13* (1), 219-225.

49. Zhang, B.; Liu, B.; Tang, D.; Niessner, R.; Chen, G.; Knopp, D., DNA-Based Hybridization Chain Reaction for Amplified Bioelectronic Signal and Ultrasensitive Detection of Proteins. *Analytical Chemistry* **2012,** *84* (12), 5392-5399.

50. Ang, Y. S.; Yung, L.-Y. L., Rational design of hybridization chain reaction monomers for robust signal amplification. *Chemical Communications* **2016,** *52* (22), 4219-4222.

51. Fiche, J. B.; Buhot, A.; Calemczuk, R.; Livache, T., Temperature Effects on DNA Chip Experiments from Surface Plasmon Resonance Imaging: Isotherms and Melting Curves. *Biophysical Journal* **2007,** *92* (3), 935-946.

52. Xuan, F.; Hsing, I. M., Triggering Hairpin-Free Chain-Branching Growth of Fluorescent DNA Dendrimers for Nonlinear Hybridization Chain Reaction. *Journal of the American Chemical Society* **2014,** *136* (28), 9810-9813.

53. Briand, V. A.; Thilakarathne, V.; Kasi, R. M.; Kumar, C. V., Novel surface plasmon resonance sensor for the detection of heme at biological levels via highly selective recognition by apo-hemoglobin. *Talanta* **2012,** *99*, 113-118.

54. Iqbal, M. S.; Siddiqui, A. A.; Banerjee, C.; Nag, S.; Mazumder, S.; De, R.; Saha, S. J.; Karri, S. K.; Bandyopadhyay, U., Detection of retromer assembly in Plasmodium falciparum by immunosensing coupled to Surface Plasmon Resonance. (1570-9639 (Print)).

55. Sikarwar, B.; Sharma, P. K.; Srivastava, A.; Agarwal, G. S.; Boopathi, M.; Singh, B.; Jaiswal, Y. K., Surface plasmon resonance characterization of monoclonal and polyclonal antibodies of malaria for biosensor applications. *Biosensors and Bioelectronics* **2014,** *60*, 201-209.

56. Phillips, K. S.; Han, J. H.; Cheng, Q., Development of a "Membrane Cloaking" Method for Amperometric Enzyme Immunoassay and Surface Plasmon Resonance Analysis of Proteins in Serum Samples. *Analytical Chemistry* **2007,** *79* (3), 899-907.

57. McKeating, K. S.; Hinman, S. S.; Rais, N. A.; Zhou, Z.; Cheng, Q., Antifouling Lipid Membranes over Protein A for Orientation-Controlled Immunosensing in Undiluted Serum and Plasma. *ACS Sensors* **2019,** *4* (7), 1774-1782.

58. Liu, Q.; Nam, J.; Kim, S.; Lim, C. T.; Park, M. K.; Shin, Y., Two-stage sample-to-answer system based on nucleic acid amplification approach for detection of malaria parasites. *Biosensors and Bioelectronics* **2016,** *82*, 1-8.

CHAPTER 3 : Nanoparticle Enhanced SPR Detection of Cholera Toxin (CT) on an Antifouling Lipid Membrane in Undiluted Serum

ABSTRACT

Countless development of biosensors has been reported with the aim to make the devices readily available for clinical diagnostics. However, the analysis of clinically relevant biomarkers in complex matrices, such as human blood serum and plasma, has always been a challenge. These samples contain high concentration of proteins and other components that not only risks false analysis from non-specific binding but also causes surface fouling from the absorption of the unwanted protein components. Here we present a novel surface chemistry with antifouling property and an ultrasensitive detection with nanoparticle enhancement strategy, universal enough for many biomarker targets and other sensing methods. In this biosensor design, we utilized a biomimetic interface of supported lipid bilayers (SLBs) formed over a protein A coated gold chip. The membrane formation was followed by a subsequent interaction of analytes spiked in undiluted human serum to the capture element on sensor surface and the real-time binding was analyzed by Surface Plasmon Resonance (SPR) spectroscopy. Using Cholera Toxin (CT) as our proof-of-concept, we achieved a sensitive detection after a complete removal of non-specifically bound components in human serum, as monitored by SPR measurement. As protein A allows for an orientation-controlled binding to variety of antibodies, this interface unlocks more potential of antifouling applications to a wider biosensing field, including immunosensing. Therefore, in addition to CT, we tested the surface for detection of

Immunoglobulin G (IgG). For both analytes, the SPR signal was enhanced using gold nanoparticles allowing detection in low concentrations without compromising the antifouling property of the sensing surface.

3.1 Introduction

Currently, there are many issues around the world related to human health and diseases, that require a good detection and diagnosis system. An effective and early diagnosis is needed to provide proper treatments and for monitoring of diseases. In the case of infectious diseases, early detection is crucial to prevent fatality and a mass outbreak. For this reason, many ongoing developments in biomedical analysis are moving towards better diagnosis tools not only for the standards laboratory diagnosis but for more advanced clinically relevant devices. This includes for detecting diseases caused by bacteria (e.g. sepsis,[1] urinary tract infections,[2] sexually transmitted infections[3]), mycobacteria (e.g. tuberculosis[4]), virus (e.g hepatitis[5], HIV[6]), fungi (e.g. candidiasis[7]) and parasite (e.g. malaria[8]). For complex diseases such as cancer, pathological methods such as tissue biopsy are often needed to confirm a cancer diagnosis. However, by the time patients are diagnosed with breast, lung, colon, or ovarian cancer, more than 60% already have cells metastasize in other art of their body.[9]

Therefore, there is a need for highly specific and sensitive detection method that recognize the early sign of a diseases through their biomarkers.[10, 11] The biological biomarkers (biomarkers) are defined as the “cellular, biochemical or molecular alterations

that are measurable in biological media such as human tissues, cells, or fluids."[12] In particular, the disease biomarkers, can be proteins and protein fragments, DNA/RNA, or specific small molecules, are presence in the patient's body at a specific time and can be different types at different stages. Therefore, a biomarker can be used as a measurable indicator of a presence or severity of the diseases. Direct biomarker analysis within blood and serum holds great promise for monitoring of patient homeostasis, disease state, and drug or environmental exposure, provided that it can be performed in a sensitive, reproducible, and efficient fashion.[13] Some examples of common biomarkers are presented in Table 3.1.

Table 3.1 Common disease biomarkers

Disease	Biomarker	Location
Malaria	Histidine rich protein II (PfHRP-II), Hemozoin	Blood
Tuberculosis	Lipoarabinomannan (LAM) Mtb DNA, Ag85b	Urine Blood
Alzheimer's	amyloid-β, tau proteins	Plasma, cerebrospinal fluid
Parkinson's	Dopamine α-synuclein	Blood, cerebrospinal fluid
Breast cancer	Human epidermal growth factor receptor 2 (HER2)	Serum, breast tumor
Prostate	Prostate-specific antigen (PSA)	Seminal plasma

Biosensors technologies are widely employed as devices for diagnosis and for monitoring of diseases progression, with the advantages of being simple, sensitive and rapid detection, require small sample volume, and have shown potential in miniaturization

to a portable instrument. Surface Plasmon Resonance (SPR) is an example of surface sensitive biosensor, utilizing optical detection platform capable of measuring biomolecular interactions in real time and recent developments resulted in the construction of small portable devices for field use.[14] SPR has been successfully applied in the analysis of a number of clinical targets[15,16] including various disease biomarkers,[17-20] cancer biomarkers,[21] hormones,[22] and therapeutic drugs.[14, 23, 24]

However, the analysis or direct detection of biomarkers are carried out in a complex media such as blood serum or plasma, as opposed to buffered solution as commonly practiced in biosensors analysis. Human body fluids contain a wide range of complex proteins that causes a non-specific accumulation of biomolecules onto a biosensor surface, which hinders the progress of biosensors, not only SPR, towards accurate measurements necessary for a clinical application. Therefore, the design of novel interfaces that minimize these non-specific interactions is of the utmost importance.

Various surface chemistries intended to minimize these non-specific interactions and the resulting background signals have undergone aggressive development.[25, 26] Sample dilution may be performed to minimize the concentration of non-target molecules, though this strategy correspondingly minimizes target concentration and is not always practical.[27] Surface blocking with adsorbed, non-reactive compounds (*e.g.*, bovine serum albumin, Tween-20, and commercially available mixtures) has seen many notable successes for a variety of clinical targets within human bodily fluids.[28-32] Integrated chemical derivatization strategies may reduce assay time further through elimination of these blocking steps, and have included the use of polysaccharides (*e.g.*, carboxymethylated

dextran),[26, 33] polymeric monolayers (*e.g.*, polyethylene glycol),[25, 26], peptides,[34] ionic liquids,[35] and zwitterionic compounds.[36, 37] The latter category covers a wide variety of molecules, though phosphocholine based interfaces have demonstrated particularly notable successes in reducing non-specific adsorption onto glass and gold surfaces.[37-40] As a major component of the eukaryotic cellular membrane, this surface moiety is not only capable of mimicking this biological environment, but is remarkably resistant against fouling from extracellular constituents.[37, 40]

We have previously reported on the utility of supported lipid membranes for a variety of biosensing applications,[41-44] including the development of a membrane cloaking method for carrying out indirect immunoassays in undiluted animal serum.[45] For that experimental design, a supported lipid membrane was formed over an antibody functionalized gold surface, which was removed along with all superimposed serum contaminants using a mild surfactant once the crude sample was allowed to interact with the sensor. With all nonspecific components stripped away, the remaining signal could be attributed to the target compound, and furthermore, the antibody-antigen complex remained accessible to further signal enhancement mechanisms.

In addition to the surface fouling from carrying out the analysis in complex media, a specific interaction between the recognition element and the analyte is highly sought, as less effective binding caused by a steric hindrance or random orientation of the biomolecules resulted in signal interference and sensitivity reduction. For the attachment of biomolecules using the traditional coupling techniques such as electrostatic adsorption or covalent crosslinking (*e.g.*, using EDC/NHS, BS^3, *etc.*), as is common practice, the

attachment efficiency and orientation are dependent upon accessible functional groups and localized areas of charge on the biomolecules surface, which are highly variable. For example, in a non-ideal scenario of immunosensing, the antibody of interest may be attached with the fragment antigen-binding (Fab) region unexposed, or in worst case, not attached at all, rendering the constructed sensor incapable of measuring its intended target. Oriented immobilization of antibodies to a sensor surface can be universally achieved through the use of proteins with Fc (fragment crystallizable) binding domains such as protein A, G, or L.[46-48] However, given the broad affinity of these proteins for nearly all immunoglobulins, they represent a class of functionalization techniques extremely prone to surface fouling, and are therefore seldom seem in biosensing applications that are carried out in undiluted biofluids.

Herein we build upon this strategy, to further improve the practical utility supported lipid membranes as an antifouling surface for analysis in complex matrices through investigation of different lipid constituents on a protein A coated sensor surface for an orientation controlled biosensing (Figure 3.1). Surface plasmon resonance (SPR) was chosen for characterization and optimization of this interface,[49] since as a label-free optical detection method, all species bound to the sensor surface can be detected, whether they are labelled or unlabeled, target or contaminant.[50] Fluorescence microscopy and photobleaching assays were conducted to better understand the interactions between these lipids and the underlying protein A coated surface.

As a proof-of-concept, we utilized this interface for the detection of Cholera toxin (CT), a protein complex secreted by the gram-negative bacterium Vibrio Cholerae

responsible for the massive, watery diarrhea of Cholera infection in the small intestine.[51, 52] CT belongs to the larger family of AB toxins, is comprised of a 27 kDa A subunit and five copies of B subunit each weighing 11.5 kDa (Figure 3.1C).[53] Cholera is a highly infectious disease that spread mostly by unsafe water and contaminated food. Natural disasters and poor sanitation are major players in the spread of cholera without proper management of patients and their waste.[54]

Our results demonstrated a sensitive detection of CT in undiluted blood serum that is uncompromised when compared to buffer samples. Further sensitivity was achieved with enhanced detection with AuNPs enables detection in ultralow concentrations. Given the universal nature of protein A, it can be envisioned that this surface could be translated to a variety of other clinical sensing applications using SPR and adjacent biosensing technologies.

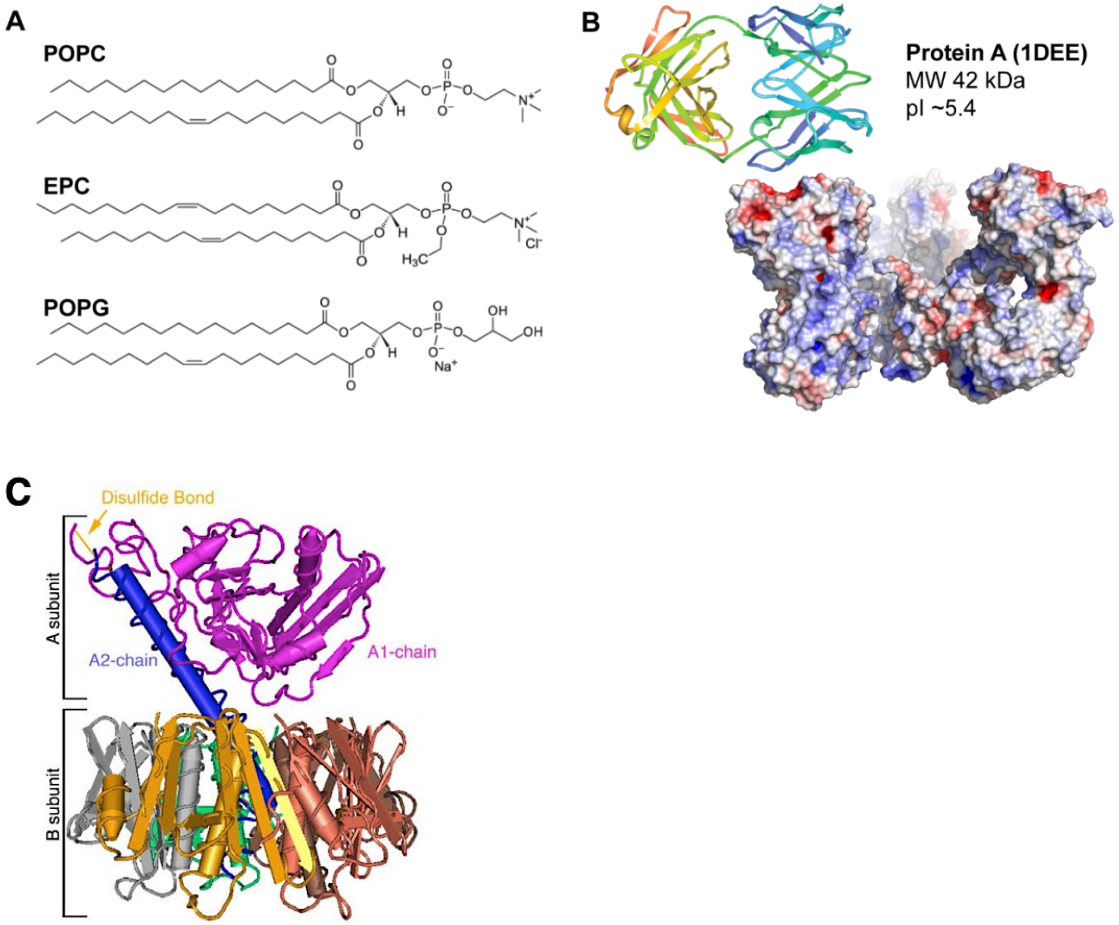

Figure 3.1 (A) Structures of the lipids investigated based on varied charges. (B) Crystal structure and electrostatic potential map of protein A. Blue is indicative of negatively charged areas, while red is indicative of positively charged areas. (C) Cholera toxin (CT) crystal structure showing the A and B subunits (Edited from ref. 53)

3.2 Experimental Section

3.2.1 Materials and reagents

1-palmitoyl-2-oleoyl-*sn*-glycero-3-phosphocholine (POPC), 1-palmitoyl-2-oleoyl-*sn*-glycero-3-ethylphosphocholine (EPC), 1-palmitoyl-2-oleoyl-*sn*-glycero-3-phospho-(1'-*rac*-glycerol) (POPG), and 1,2-dipalmitoyl-*sn*-glycero-3-phosphoethanolamine-N-(7-nitro-2-1,3-benzoxadiazol-4-yl) (NBD-PE) were obtained from Avanti Polar Lipids (Alabaster, AL). Silane-PEG-Maleimide was obtained from Nanocs (New York, NY). Thiolated recombinant protein A was obtained from Protein Mods (Madison, WI). Functionalized oligonucleotides were obtained from Integrated DNA Technologies (Coralville, IA). Anti-Mouse IgG (rabbit polyclonal purified IgG) was obtained from EMD Millipore (Temecula, CA). Biotinylated antibodies were conjugated in house using the EZ-Link™ Sulfo-NHS-Biotin labeling kit obtained from Thermo Fischer Scientific (Waltham, MA). All other reagents were obtained from Millipore-Sigma (St. Louis, MO).

3.2.2 Lipid vesicle preparation

Stocks POPC (5 mg / mL), EPC^+ (5 mg / mL), and $POPG^-$ (10 mg / mL^-) were diluted in chloroform to the designated concentrations, and stored at -80 °C. Appropriate amounts of these stock solutions were aliquoted into glass vials and dried under nitrogen to form thin lipid films, which were then stored in a vacuum desiccator overnight to remove any residual solvent. The dried lipids were resuspended in 1× PBS (10 mM Na_2HPO_4, 1.8 mM KH_2PO_4, 137 mM NaCl, 2.7 mM KCL, pH 7.4) to a final concentration of 1 mg / mL followed by vigorous vortexing and bath sonication for 30 min. This solution was extruded

through a polycarbonate filter (Whatman, 100 nm) to produce small, unilamellar vesicles of uniform size. All lipid vesicle suspensions were stored at 4 °C and used within one week of preparation. The final centration of 1 mg / mL is above the critical micelle concentration (CMC) of the lipids and high enough to form bilayer vesicles.

3.2.3 Preparation of gold surrogate and gold surface for fluorescence microscopy

Glass coverslips were cleaned with boiling Piranha solution (3:1 H_2SO_4 / 30% H_2O_2) for 2 h then thoroughly cleaned with water and ethanol before drying with compressed air. The coverslips were then submerged in a 1 mg / mL solution of Silane-PEG-Maleimide in ethanol overnight at room temperature. After cleaning with ethanol and drying with compressed air, a 10 μg / mL solution of thiolated protein A in 10 mM PBS was added to the surface for 2 h at room temperature. Coverslips were then washed with distilled water and dried under a stream of N_2 before being coated with a 1 mM solution of 3-mercapto-1-propanol (MPO) in 10 mM PBS for 1 h at room temperature. After washing with distilled water and drying with N_2, lipid vesicles at 1 mg / mL were added to the surface in PDMS wells for 1 h and protected from ambient lighting. Lipids were prepared according to a standard protocol and consisted of either EPC, POPC, or a 1:1 mixture of EPC / POPC with 2% (w/w) NBD-PE, as specified in the main text. The coverslips were then rinsed thoroughly with distilled water, taking care not to expose the lipid surfaces to air, and then mounted onto glass slides. For fluorescent measurements of lipids not formed over a protein A surface, the lipids were directly added to the piranha treated glass coverslips. Fluorescence microscopy images were taken using an inverted Leica TCS SP5

II (Leica Microsystems, Buffalo Point, IL) using the 488 nm Argon laser line and a 40× objective, and FRAP analysis was carried out by photobleaching for 500 ms and monitoring the recovery using the FRAP wizard on the LAS AF software (Leica Microsystems, Buffalo Point, IL). The mobile fractions (ß) and diffusion coefficients (D) were obtained using a previously reported protocol.[55] Briefly, these coefficients provide information about the mobility of a fluorescent molecule in a defined compartment, in practical the fluidity of a membrane formed naturally on a surface, and how fast the molecule is moving due to active transport in diffusion.[56]

For fluorescent measurements of EPC lipids with human serum, the preparation was carried out in a sample reservoir made of PDMS mold placed on a cleaned glass slide deposited with a thin layer (~ 4 nm) of gold. Following the same procedures in preparing Protein A, MCH and EPC with 2% (w/w) NBD-PE coatings as described above, an additional step is carried out following the rinse after lipid incubation. The surface was coated with undiluted serum for 1 hour before the final rinse and then the surface was covered with a cover slip to prevent drying.

3.2.4 Gold nanoparticle conjugation

Gold nanoparticles were prepared using a standard citrate reduction. Briefly, a 12.5 mM solution of $HAuCl_4$ was dissolved in 500 mL of distilled water in glassware previously cleaned with aqua regia (3:1 HCl to HNO_3). This solution was heated until boiling with vigorous stirring, then a 30 mM solution of sodium citrate tribasic dihydrate was added, and the solution boiled for another 15 min before being allowed to cool to room

temperature. The size of gold nanoparticles was determined from UV-Vis method and is the core diameter of the gold nanoparticles prior to functionalization.[57] These nanoparticles were functionalized with thiolated oligonucleotides consisting of poly-thymine and biotinylated poly-thymine in a 1:1 ratio according to a protocol previously reported in our group.[58] The as-synthesized gold nanoparticles were concentrated by a factor of 3 before the addition of 2.5 nmol DNA (100 μM, H_2O) to 1 mL of concentrated gold nanoparticles. Immediately, 20 μL of citrate-HCL (500 mM, pH 3.0) was added and the solution vortexed before the addition of 10 μL of 10% (v/v) Tween 20. Finally, the NaCl concentration was increased to 1 M and the nanoparticles were incubated overnight at 4 °C. Excess reagents were removed from the nanoparticle solution by centrifugal filtration (Amicon, MWCO 50 kDa), and the resulting conjugates were stored at 4 °C.

3.2.5 Gold sensor fabrication and functionalization

BK-7 glass microscope slides (Corning, Painted Post, NY) were cleaned with a boiling piranha solution (3:1 H_2SO_4 and 30% H_2O_2) for 2 h then subsequently rinsed with water and absolute ethanol before drying under compressed air. A 2 nm layer of chromium (0.5 Å s^{-1}) followed by a 50 nm layer of gold (1.0 Å s^{-1}) was deposited onto the glass slides using electron-beam evaporation (Temescal, Berkeley, CA) at 5×10^{-6} Torr in a Class 1000 cleanroom facility (UCR Center for Nanoscale Science & Engineering). These gold sensor chips were rinsed with ethanol and dried under compressed air before being coated with 10 μg / mL thiolated protein A (Protein Mods, Madison, WI) in 1× PBS for 2 h at room temperature (*ca.* 23 °C), followed by a 1 mM solution of 3-mercapto-1-propanol (MPO,

Millipore-Sigma, St. Louis, MO) in 1× PBS for 1 h at room temperature. The sensor chips were rinsed with nanopure water (≥18 MΩ·cm, Barnstead E-Pure) and dried under a nitrogen stream after each step before final storage at 4 °C. Nanoglassified gold sensor chips were prepared by depositing a thin layer of silica (*ca.* 2-4 nm) via plasma-enhanced chemical vapor deposition using a Unaxis Plasmatherm 790 (Santa Clara, CA) directly after electron-beam evaporation of gold, and these chips were not subject to any further functionalization.[43]

3.2.6 SPR analysis of lipid deposition and fouling

Surface plasmon resonance (SPR) spectroscopy was conducted at room temperature on a NanoSPR5-321 (NanoSPR, Addison, IL) using 1× PBS as the running buffer set to a flow rate of 5 mL h^{-1} (*ca.* 83 μL min^{-1}) unless otherwise noted. Lipid deposition was carried out by injection of 1 mg / mL lipid vesicles into the instrument and the minimum angle was tracked over 1 h under zero flow conditions. After a 10 min rinse with 1× PBS, undiluted human serum (male from AB plasma, Millipore-Sigma) or plasma (pooled, Millipore-Sigma) was injected and allowed to interact with the surface under zero flow for 30 min, before a final 15 min rinse with PBS.

For analysis of mouse immunoglobulin (IgG) and cholera toxin (CT) within spiked human serum and plasma, 100 μg / mL of capture antibody (rabbit anti-mouse IgG or rabbit anti-CT, Millipore-Sigma, St. Louis, MO) was incubated for 1 h. This was followed by lipid vesicle deposition as described above, and the surface was subsequently interacted with human serum or plasma spiked with the target antigen, mouse IgG or CT. All steps

were separated by a 10 min PBS rinse with the exception of the post-sample rinse, which was extended to 30 min. Detection antibodies were introduced at a concentration of 10 μM for 1 h. For the nanoparticle enhanced detection, the same protocol was followed, with the addition of 100 μg / mL streptavidin, followed by 1 nM of 30 nm biotinylated gold nanoparticles (bT_{20}/AuNPs).[58]

3.2.7 Fluorescence microscopy and fluorescence recovery after photobleaching (FRAP)

Fluorescence microscopy images were generated on an inverted Leica TCS SP5 II (Leica Microsystems, Buffalo Point, IL) using the 488 nm Argon laser line in conjunction with a 40× objective (N.A. 1.1). Photobleaching for 500 ms and monitoring of fluorescence recovery within defined regions of interest were performed using the LAS AF software package (Leica Microsystems, Buffalo Point, IL). Mobile fractions (ß) and diffusion coefficients (*D*) were determined using the methods of Axelrod and Soumpasis as previously reported.[41, 59, 60]

3.2.8 SPR analysis of human serum and plasma on lipid bilayers

BK-7 glass microscope slides were cleaned with boiling Piranha solution (3:1 H_2SO_4 / 30% H_2O_2) for 2 h then thoroughly cleaned with water and ethanol and dried with compressed air. A 2 nm layer of chromium followed by a 50 nm layer of gold was deposited onto the glass slides using e-beam evaporation. These gold chips were washed with ethanol and dried under compressed air before being coated with 10 μg / mL thiolated protein A in 1 x PBS for 2 h at room temperature (ca. 23°C), followed by a 1 mM solution

of 3-mercapto-1-propanol (MPO) in 1 x PBS for 1 h at room temperature. The chips were washed with distilled water and dried under a stream of N_2 between the protein A and MPO conjugation and before storage at 4 °C. Alternatively, nanoglassified gold chips were prepared by depositing a thin layer of SiO_2 using plasma-enhanced chemical vapor deposition (PECVD), and these chips were not subject to any further functionalization before analysis by SPR. For both protein A / MPO coated and nanoglassified gold chips, lipid formation was carried out by the injection of 1 mg / mL lipid vesicles into the SPR instrument and the minimum angle tracked over 1 hour under stopped flow conditions. After a 10 min wash with 1 x PBS undiluted human serum or plasma was injected and reacted with the bilayers under stopped flow for 30 min, before a final 15 min wash step with PBS.

3.2.9 Analysis of analytes spiked human serum and plasma

Gold chips were functionalized with 10 μg / mL thiolated protein A and 1 mM MPO solution according to the protocol previously described. In this experiment all biological components were diluted to concentration with 1 x PBS (10 mM Na_2HPO_4, 1.8 mM KH_2PO_4, 137 mM NaCl, 2.7 mM KCL, pH 7.4) and was carried out at room temperature (c.a 23°C). 100 μg / mL of anti-CT was first incubated on the protein A surface for 1 hour. Following washing step with 1 x PBS, 1 mg / mL EPC lipid vesicles, human serum spiked with 10 μg / mL CT and 1μM anti-CT were injected and incubated for 1 hour. After the final washing step, the binding was monitored and quantified to obtain the angle shift. For the nanoparticle enhanced detection of CT, 1 μM biotinylated anti-CT was added instead

of anti-CT after the washing step following serum spiked with 0.05 μg / mL CT. The injection steps were continued with 100 μg / mL streptavidin, followed by 1 nM of 25 nm biotinylated AuNPs. The steps were repeated with different concentration of CT for constructing calibration curves without AuNPs and with AuNPs enhancement.

For analysis on IgG, 100 μg / mL of Anti-mouse IgG diluted in was incubated on the protein A surface for 1 hour and the binding monitored using SPR. This was followed by the injection and incubation of 1 mg / mL EPC lipid vesicles (1 hour), human serum or plasma spiked with 10 μg / mL mouse IgG (1 hour) and 1 μM biotinylated anti-mouse IgG (1 hour). All steps were separated by a 10 min PBS wash with the exception of the wash after the human serum which was extended to 30 min. For the nanoparticle enhanced detection of IgG in human serum, the same protocol was observed, with the exception of the Anti-IgG being added to the surface offline before analysis, and the addition of 100 μg / mL streptavidin, followed by 1 nM of 30 nm biotinylated AuNPs.

3.2.10 Comparison to the traditional SAM surface

This was carried out following a basic protocol previously reported by our group,[61] with necessary changes made for the detection of the antibodies within this paper. Gold chips were fabricated with a 2 nm layer of chromium and 50 nm layer of gold via electrodepostion, washed with ethanol, and dried under compressed air. Next the chips were soaked in 1 mM of 1-mercaptoundecanoic acid (MUA) (in ethanol) solution overnight to form a self-assembled monolayer with carboxyl functional groups on the surface. The chips were washed with deionized water and dried under a stream of N_2. In the SPR

instrument, a mixture of 0.4 M EDC and 0.1 M NHS was injected into the flow cell and incubated for 30 min. After a 15 min wash with PBS, 100 μg / mL anti-cholera toxin (anti-CT) was injected and incubated for 30 min to allow formation of covalent amide linkages. Following this, passivation of the unused activated carboxyl groups was carried out by injecting a 4 mM PEG-amine and incubated for 20 min. Next 25 μg / mL of CT was injected and incubated for 30 min to allow binding with the capture anti-CT. Finally, 100 μg / mL of anti-CT was injected to amplify the detection signal, then incubated for 30 min before a 30 min washing step. All injection steps were separated by a 15 min washing with PBS unless different washing time is specified.

3.3 Results and Discussions

3.3.1 Formation of an antifouling lipid membrane over Protein A

The use of protein A in immunoassay design carries the distinct advantage of being able to provide a site for optimal orientation-controlled attachment of antibodies, with the Fc (fragment crystallizable) region bound by protein A and directed toward the sensor surface, and the Fab (fragment antigen-binding) region extending into the sample matrix.[46] Leveraging this capability for the analysis of crude samples would present a powerful tool, provided that levels of nonspecific binding are controlled. We previously developed a lipid membrane interface for antibody-based detection in undiluted animal serum, which was formed over a gold surface functionalized with a mixed self-assembled monolayer (SAM) of cysteamine and 3-mercapto-1-propanol (MPO).[45] Building upon this design, initial studies retained use of MPO as a spacer molecule while the cysteamine constituent was

substituted with protein A. Protein A was first deposited onto the gold surface at a concentration of 10 μg / mL for 2 h, and the interstitial area was backfilled with MPO. Introduction of undiluted human serum to this interface resulted in massive angular resonance shifts ($\Delta\theta$ = 0.73 °), indicative of high levels of nonspecific binding that could not be rinsed away by buffer or surfactant (Figure 3.2A), thereby necessitating the use of a blocking agent or barrier. A membrane of zwitterionic phosphocholine (POPC) was naturally favored for this task due to the molecule's well-characterized antifouling properties and demonstrated increases in bioanalytical sensor performance.[37, 62] However, when a suspension of POPC vesicles was introduced to the protein A/MPO surface, followed by serum, nonspecific binding remained unaffected compared to the surface without lipids (Figure 3.2B). As the angular resonance shift from lipid introduction appeared low ($\Delta\theta$ < 0.1 °) compared to previous SPR investigations of supported lipid bilayer formation ($\Delta\theta$ > 0.45 ° over silica/silicate nanofilms on gold),[41, 43, 58] a low surface coverage of POPC was suspected to be the issue here, thus requiring confirmatory studies using a complementary analytical technique.

Confocal fluorescence microscopy was employed to investigate the spatial distribution of fluorophore-tagged phospholipids over the protein A/MPO interface. A surrogate material was used in place of the gold SPR substrates, which consisted of a glass coverslip functionalized with a SAM of silane-PEG-maleimide (see Supporting Information for fabrication details). This surface provided an even monolayer of thiol-reactive sites, analogous to gold, though circumvented the issue of fluorescent quenching by nonradiative energy transfer to the gold surface. Once protein A, MPO, and a suspension

of POPC vesicles containing a fluorophore-labeled constituent (2% wt NBD-PC) were applied as described above, the surface was kept submerged in an aqueous environment and imaged. From the image in Figure 3.2B, the distribution of fluorescence appears patchy and uneven, indicating that POPC vesicle adsorption was inefficient, thereby leaving large areas of the protein A/MPO surface exposed to incoming contaminants from the sample matrix. Utilization of these lipid membranes to combat nonspecific binding would require a more targeted approach in which lipid interactions with the underlying surface were discreetly considered.

Although the formation of supported lipid bilayers via the fusion of small unilamellar vesicles (SUVs) is conventionally carried out over smooth, rigid, and hydrophilic surfaces,[41, 43, 63] lipid membranes have also been formed over a variety of SAMs in which interactions with lipid headgroups were electrostatically favored.[64, 65] Given that the theoretical isoelectric point (pI) of protein A is *ca.* 5.4,[66] the protein A/MPO sensor surface is expected to carry a net negative charge within our running buffer at pH 7.4. Therefore, it was hypothesized that lipid vesicles exhibiting a net positive charge would be required for greater surface interaction strength toward forming a contiguous barrier. Indeed, when a new vesicle suspension consisting solely of a positively charged lipid, ethylphosphocholine (EPC^+), was introduced to the protein A/MPO surface, resonance angular shifts increased by *ca.* 0.7 ° compared to POPC, suggesting that the surface was more completely coated with lipids (Figure 3.2C). This was confirmed by fluorescence microscopy of labeled (2% wt NBD-PC) EPC^+ vesicles deposited on protein A/MPO, revealing a more complete and even distribution of fluorescence (Figure 3.2C).

Interestingly, upon introduction of human serum to the EPC^+ laden surface, a lower angular shift was observed ($\Delta\theta = 0.5$ °) compared to the untreated and POPC modified surfaces ($\Delta\theta = 0.73$ °). This signal remarkably returned to the baseline EPC^+ value post-incubation (1 h) and a buffer rinse (10 min), suggesting that all serum contaminants can easily be removed without also having to strip away the membrane. The EPC^+ lipids remain stably bound to the surface after this time, exhibiting no decrease in angular shift, which would be indicative of detachment or deterioration of the interface, even after an extended (2 h) rinse under a constant flow of buffer (Figure 3.3). The use of a mixed lipid vesicle suspension consisting of 50 % POPC and EPC^+ was also investigated in an attempt to see if the overall charge could be reduced (Figure 3.4), though while the results were better than POPC alone, a fair amount of serum material remained on the surface after the buffer wash ($\Delta\theta = 0.34$°). In an effort to more completely validate the idea that charge-matching between these lipids and the underlying surface is necessary for complete coverage, negatively charged $POPG^-$ vesicles were investigated for their antifouling properties. However, much like the POPC vesicles, a low ($\Delta\theta < 0.1$ °) angular resonance shift was observed upon introduction of lipids to the surface, as well as a high ($\Delta\theta = 0.59$ °) level of nonspecific binding from serum that could not be rinsed away under flow of buffer (Figure 3.5). Therefore, tailoring the charge of these lipid vesicles to their underlying surface chemistry appears critical for enabling successful formation of a supported lipid membrane over protein A, in turn rendering it resistant to biofouling from human serum.

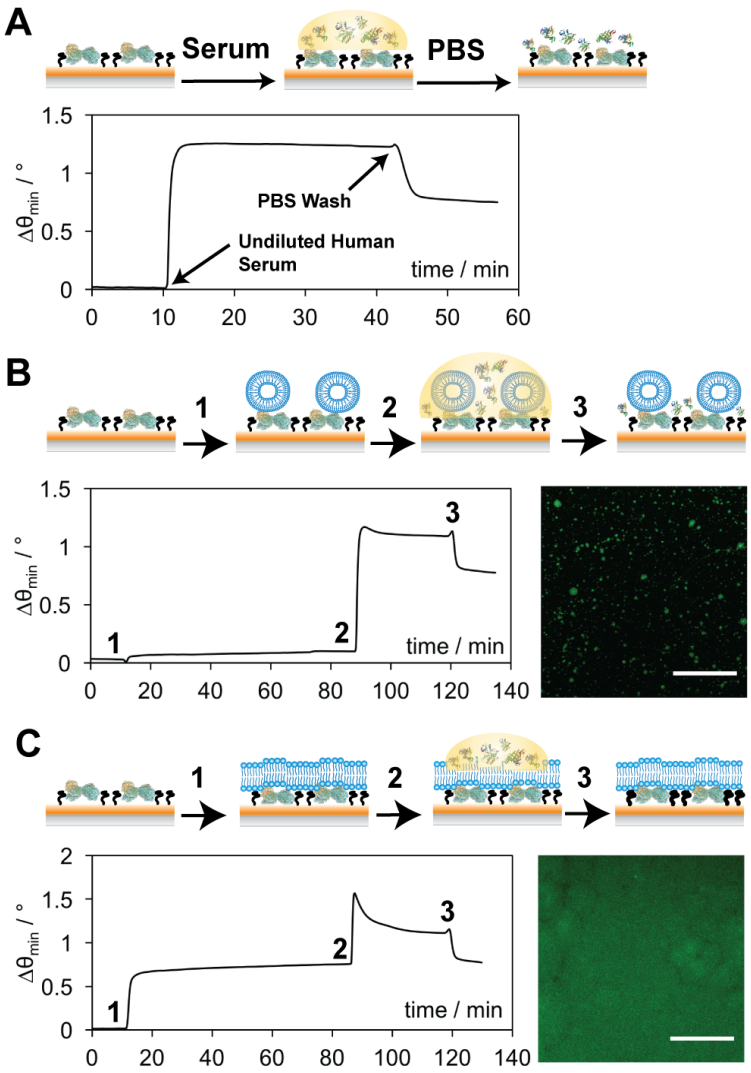

Figure 3.2 Schematic representations and corresponding data for the addition of undiluted human serum to a protein A/MPO surface (A), POPC over protein A/MPO (B) and EPC^+ over protein A/MPO (C). Lipid vesicles (B and C) were injected (1) and incubated for 1 h, before the addition of undiluted human serum (2) for 30 min, followed by a PBS rinse (3) to remove any unbound components. Corresponding fluorescence micrographs depict distribution of POPC (B) and EPC^+ (C), respectively, over protein A/MPO. Scale bars represent 30 μm.

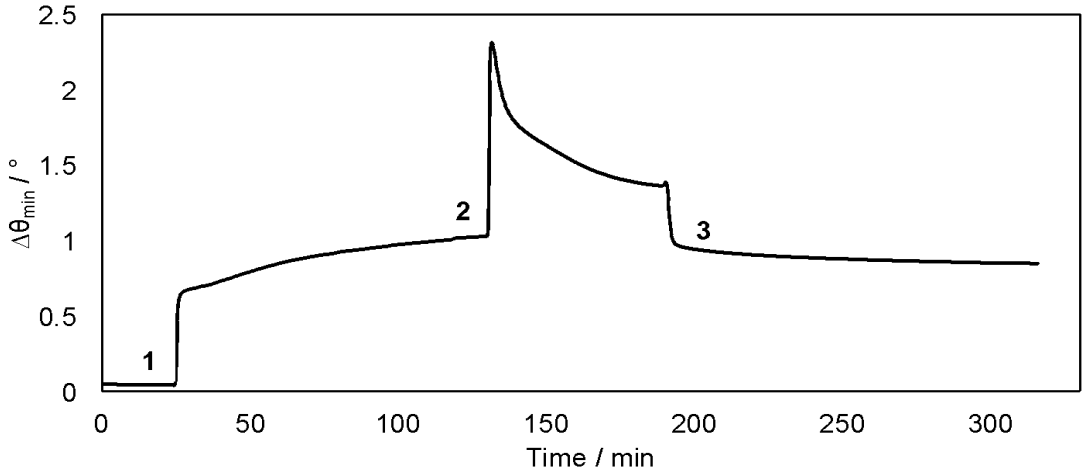

Figure 3.3 Sensorgram depicting an extended wash step on an antifouling lipid bilayer formed over the protein A/MPO gold surface. EPC was injected over the surface (1) and incubated for 1 h, followed by the injection of undiluted human serum (2) for 30 min, and finally a 2 h PBS wash (3) was carried out to assess stability of the membrane over time.

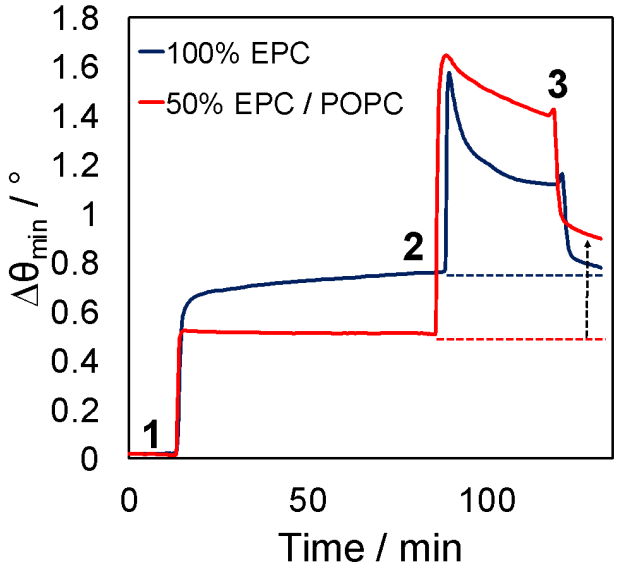

Figure 3.4 Sensorgram depicting the extent of non-specific binding from human serum components onto lipid bilayers when the overall charge is reduced. Gold chips were coated with protein A and MPO according to the standard protocol. A solution of EPC lipid vesicle (black) or a 50% mixture of EPC and POPC were injected for 1 h (1), followed by undiluted human serum for 30 min (2), and a PBS wash (3).

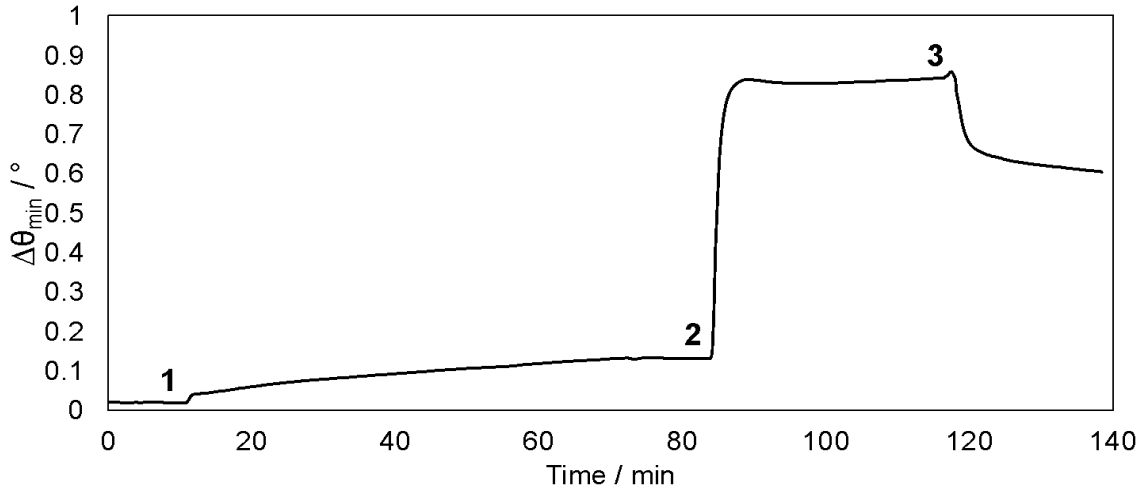

Figure 3.5 Sensorgram depicting the extent of non-specific binding from human serum onto a gold chip modified with protein A, MPO and POPG. POPG was injected over the surface (1) and incubated for 1 h, followed by the injection of undiluted human serum (2) for 30 min, and finally a PBS wash (3) was used to remove unbound serum components.

3.3.2 Extension to undiluted human plasma

Blood plasma is generally prepared by introducing anticoagulants to whole blood and centrifuging to collect the supernatant, requiring less technical expertise and considered less time consuming to separate than serum. Although it is a more complex medium, containing fibrinogen and other clotting factors that are absent from serum, a high interest in plasma profiling exists due to its comparatively facile preparation and higher reproducibility in the characterization of select metabolites and proteins.[67-69] Given that the EPC^+ lipid membrane over protein A/MPO demonstrated high antifouling activity against human serum, translatability to other crude fluids such as plasma presented a tantalizing possibility and was therefore investigated (Figure 3.6). High levels of non-specific interactions over the protein A/MPO surface were once again observed ($\Delta\theta = 0.72$ °) when

undiluted human plasma was incubated over the surface in the absence of any lipids (Figure 3.6A). This observation reiterates that although protein A is ideal for antibody orientation and ease of attachment, it does represent one of the more universally difficult surface chemistries to work with for clinical sample analysis. However, once EPC^+ lipids have been deposited over this surface, non-specifically bound components from plasma can be completely removed under a buffer flow, in an identical manner to that of the serum samples (Figure 3.6B). Therefore, either matrix should be compatible for immunosensing over this protein A/MPO surface chemistry in conjunction with the EPC^+ lipid barrier.

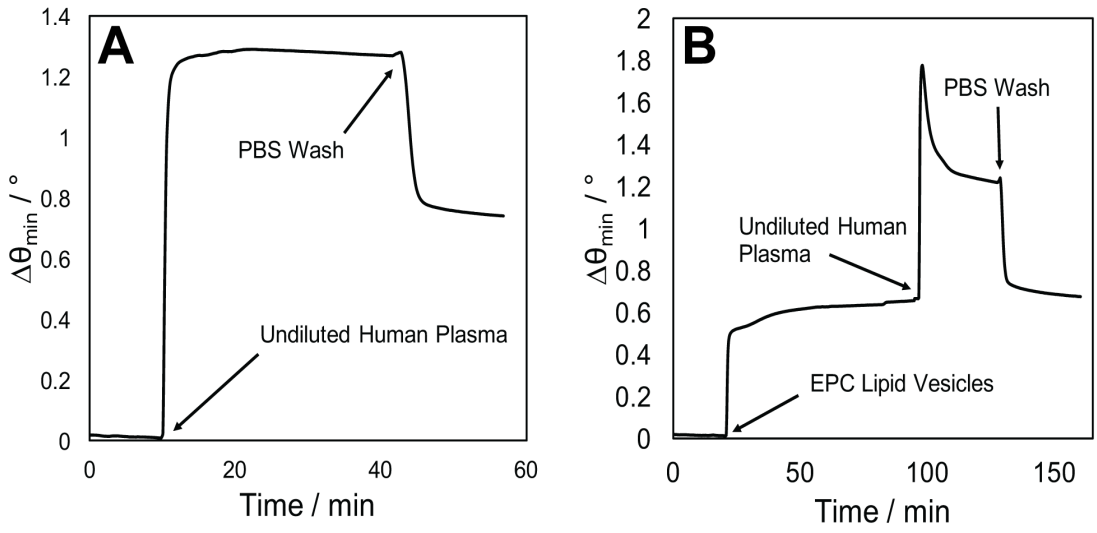

Figure 3.6 Surface plasmon resonance sensorgrams demonstrating the extent of non-specific binding from undiluted human plasma injected over a protein A/MPO coated gold surface (A) and a protein/MPO surface coated with an EPC+ lipid barrier (B).

3.3.3 Performance-affecting considerations

With successful EPC^+ deposition and antifouling activity, we sought to define other parameters that could affect the performance of this interface; that is, whether certain experimental variables are robust enough to be altered without any notable decrease in performance, or whether a delicate balance exists between these variables. Injection of POPC or EPC^+ vesicle suspensions over a planar, silica surface resulted in altered deposition and antifouling effectiveness compared to the protein A/MPO surface, which we suspected to be attributed to differences in hydrophilicity and adsorbed surface features (e.g., from protein A and SAMs) (Figure 3.7). The effect of increasing the density of protein A deposited on the gold surface was investigated, which consisted of raising the incubation concentration from 10 μg mL^{-1} to 100 μg mL^{-1}. MPO was retained for backfilling of interstitial space, and EPC^+ injection and serum effects were analyzed by SPR. Effects of raising this concentration were deleterious, however, with a lower resonance angle shift ($\Delta\theta$ = 0.6 °) for the lipids, and increased nonspecific binding ($\Delta\theta$ = 0.4 °) from undiluted serum (Figure 3.8). Conversely, the effects of holding the 10 μg / mL of protein A constant while replacing MPO with other selected SAMs was tested. 3-mercaptopropionic acid (MPA) was selected for its similar length to MPO, though functionalized with a different end terminal (*i.e.*, carboxylic acid) and charge, while 11-mercapto-1-undecanol (MUO) was selected for its identical end terminal functionalization (*i.e.*, hydroxyl) and longer length. A protein A surface without any backfilling SAM was also included in this investigation. While the EPC^+ lipids were successfully deposited on all surfaces at a similar level as protein A/MPO ($\Delta\theta \sim 0.8$ °), nonspecific interactions with serum were notably

different (Figure 3.9). Both the protein A surface with no SAM and MPA-backfilled surfaces exhibited a higher level of nonspecific binding than protein A/MPO ($\Delta\theta$ = 0.1 °), though this was still minimal in comparison to a surface in which serum was introduced without EPC^+ ($\Delta\theta$ = 0.73 °, Figure 3.2A). MUO faired the least successful of the SAMs studied, with an angular shift of *ca.* 0.25 ° after serum was introduced and rinsed with buffer. From these data, the packing density of protein A on the gold surface at 10 µg mL^{-1} provides sufficient interstitial space for backfilling by an appropriate SAM. While MPO has proven to be the most efficient backfilling agent chosen, it can be inferred that the length of this SAM is the most critical parameter to balance against protein A surface chemistry, with the end terminal functionality playing a comparatively more minor role.

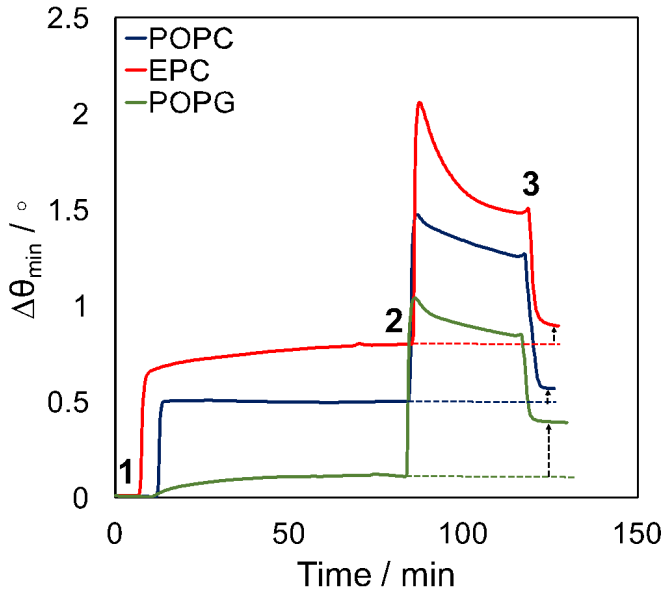

Figure 3.7 Sensorgram depicting the extent of non-specific binding from human serum onto various lipids formed over silica coated gold chips. POPC (blue), EPC (red), and POPG (green) were injected onto the surface (1) and incubated for 1 h, followed by the inject ion of undiluted human serum (2) for 30 min, and finally a PBS wash (3) was used to remove unbound serum components.

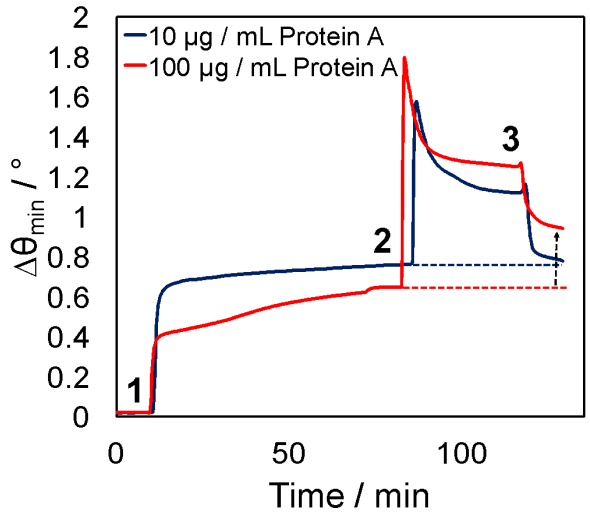

Figure 3.8 Sensorgram depicting the formation of EPC lipid vesicles over an increased concentration of protein A. Gold chips were coated with protein A at a concentration of either 10 µg / mL (black) or 100 µg / mL (red), and 1 mM MPO. A 1 mg / mL solution of EPC lipid vesicles were injected for 1 h (1), followed by undiluted human serum for 30 min (2), and a PBS wash (3)

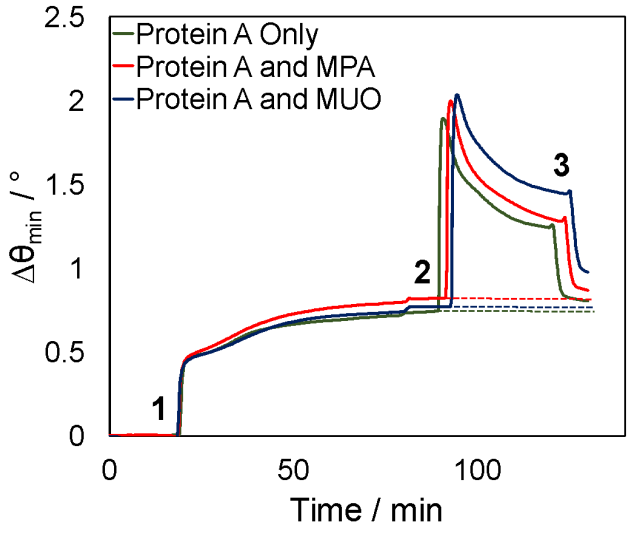

Figure 3.9 Sensorgram depicting the extent of non-specific binding from human serum components onto a protein A surface functionalized surface with varying spacers. Gold chips were coated with 10 µg / mL protein A only (green), protein A and 1 mM mercaptopropionic acid (blue), or protein A and 1 mM mercapto-un-decanol. EPC lipid vesicles were injected for 1 h (1), followed by undiluted human serum for 30 min (2), and a PBS wash (3).

3.3.4 Lipid-surface interactions and lateral mobility

In light of this specific amalgam (*i.e.*, protein A, MPO, and 100% EPC^+) giving rise to such high antifouling efficacy, in contrast with the convention of using zwitterionic/neutral SAMs and brush networks for this purpose,[36, 70] we sought a better understanding of how EPC^+ assembles and interacts with the underlying protein A/MPO surface. Fluorescence recovery after photobleaching (FRAP) was employed to shed light on these interactions and glean information on the architecture of surface-adsorbed EPC^+ structures. FRAP has been used to measure the lateral mobility of fluorescent molecules within liquids,[71] hydrogels,[71, 72] and lipid bilayers.[41, 43] In principle, mobility kinetics may be assessed by bleaching a selected two-dimensional area under high laser intensity and monitoring the recovery of fluorescence within the bleached region as non-bleached molecules laterally diffuse and redistribute. Applied toward the study of lipid membranes supported by solid surfaces, only lipids within a contiguous lipid bilayer formed by fusion of adsorbed vesicles will exhibit measurable diffusivities (*i.e.*, measure of the speed at which lipids are diffusing). If the diffusivity is low or the lipids are completely immobile, strong interactions with the surface or lack of vesicle fusion, both of which prevent long-range mobility, could be inferred.[41, 63] When EPC^+ vesicles are applied to a glass support, a supported lipid bilayer is formed similar to POPC membranes on glass (Figure 3.10A).[41, 43] The lipids embedded within the EPC^+ membrane are fluid and mobile, exhibiting a diffusivity (D) of 1.87 ± 0.12 μm^2 s^{-1} and a mobile fraction (β) of 97 % ($R^2 = 0.97$), with β serving as an indicator of the percentage of lipids that are freely diffusing. In contrast, EPC^+ vesicles deposited over protein A/MPO behave far differently, exhibiting no redistribution

of fluorescence within the region of interest after photobleaching (Figure 3.10A). Attempting to extract diffusivity and mobile fractions from this data result in near negligible values that do not fit the model for lateral lipid diffusion (R^2 = 0.23), suggesting that these lipids, while appearing continuous and uniform, are tightly bound via strong electrostatic interactions to the underlying protein A/MPO surface. For reference, 50 % POPC/EPC^+ vesicles exhibited a similar pattern in mobility, albeit with the FRAP results suggesting that the membrane is not as tightly bound to protein A/MPO with D = 0.42 ± 0.35 $\mu m^2\ s^{-1}$ and β = 44 % (R^2 = 0.99) (Figure 3.11). The FRAP results confirm that EPC^+ vesicles are tightly bound to the protein A/MPO surface after their introduction, and that the diffusional characteristics of embedded lipids are far different than conventional phosphocholine-based supported lipid bilayers on glass. Taken together with the antifouling characteristics unique to this identified set of constituents, the strong adsorption and self-assembled architecture of EPC^+ on protein A/MPO appear to play critical roles for reduction of nonspecific binding. This architecture may consist of a tightly packed monolayer of adsorbed vesicles, or an immobile bilayer of EPC supported by protein A/MPO. As the vesicle diameter (ca. 100 nm), is below the diffraction limit of our microscope, neither could be confirmed by the fluorescence microscopy/FRAP studies.

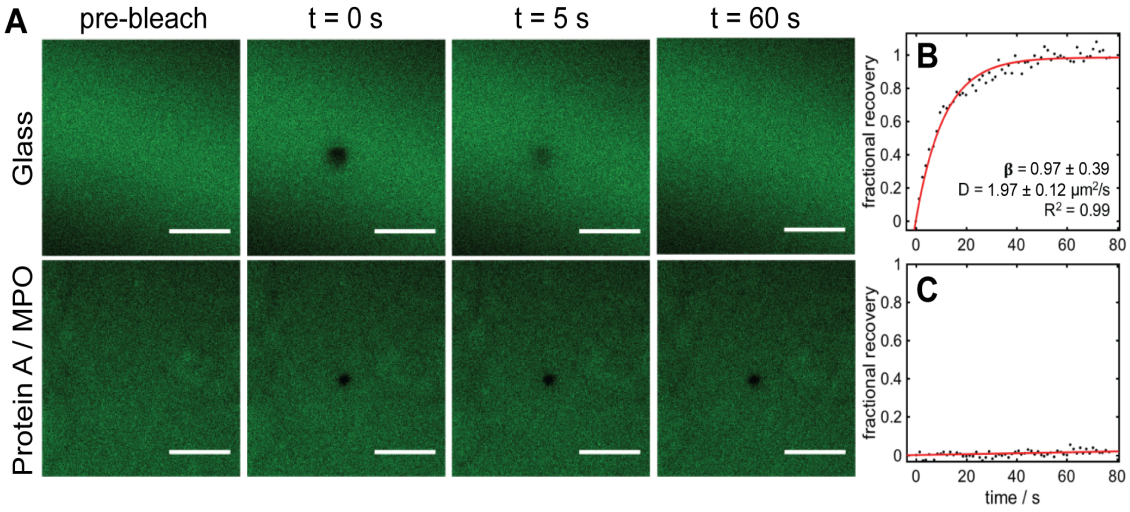

Figure 3.10 Images depicting FRAP analysis of EPC+ lipids formed over a glass coverslip and a protein A/MPO coated coverslip. (A) Fluorescence micrographs of photobleaching and recovery. Scale bars represent 30 μm. (B-C) Corresponding recovery data for EPC+ over glass (B) and protein A/MPO surface (C). Error bars represent standard deviations from three replicate experiments.

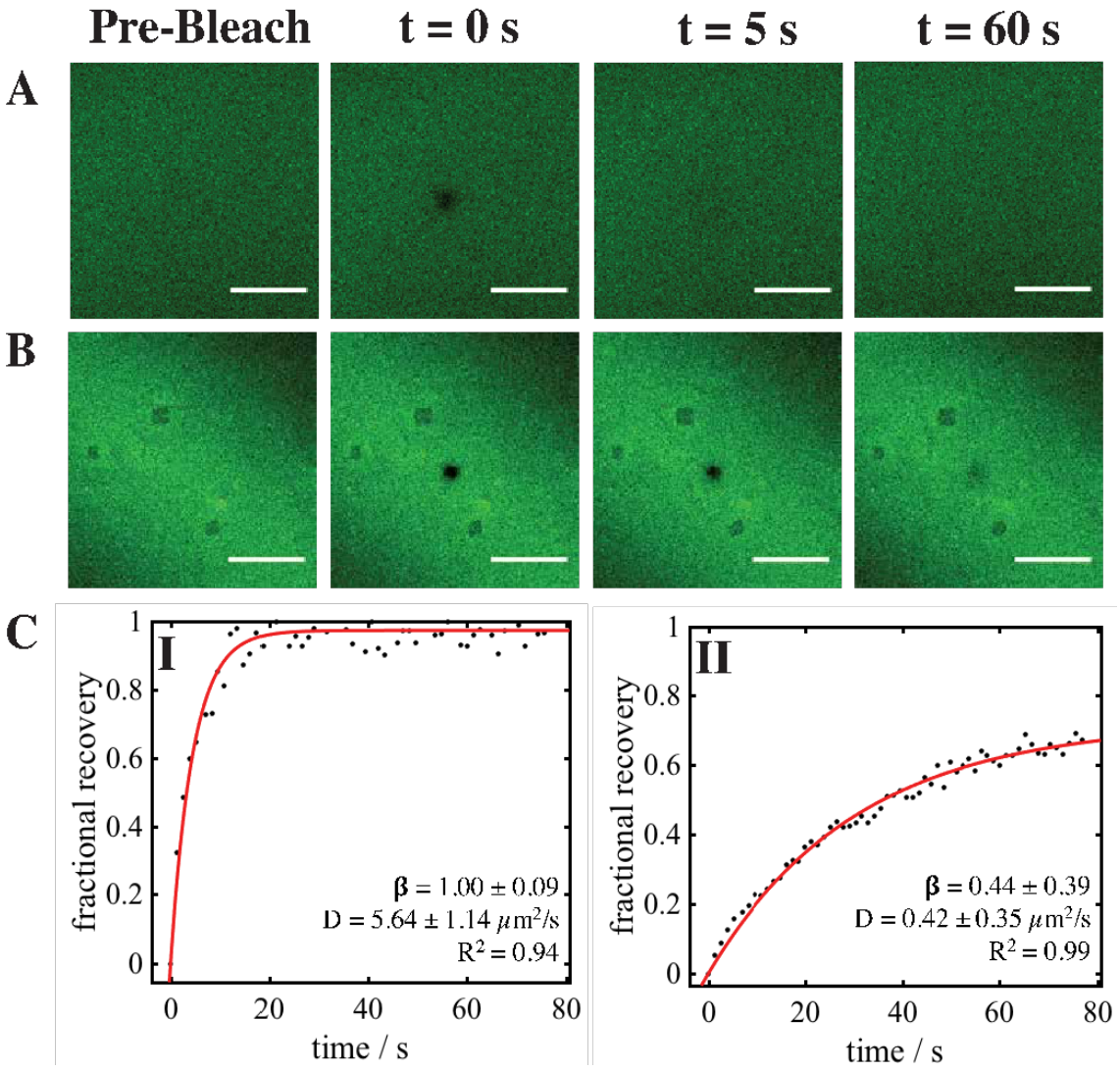

Figure 3.11 Images depicting FRAP analysis of a 50% EPC / POPC lipid mixture formed over (A) a glass coverslip and (B) a protein A coated glass chip, and the corresponding recovery data (C) for the glass (I) and protein A surface (II). Standard deviations represent 3 replicate experiments, and scale bars represent 30 μm.

3.3.5 Characterization of Protein A surface for detection of antibodies in complex biofluids

In order to confirm that this lipid membrane could be used in an immunosensing application and retain its high antifouling properties, a biosensor for IgG was constructed through incubation of a capture antibody, anti-IgG, over protein A/MPO prior to the introduction of IgG spiked serum. For this proof of concept experiment the selected capture antibody was raised against mouse, from which the target antigen was also procured, so that human antibodies present in serum or plasma would not be recognized. The binding of this capture antibody (100 µg / mL) to protein A was confirmed by SPR ($\Delta\theta$ = 0.17 °, Figure 3.12A), as was the deposition of EPC^+ ($\Delta\theta$ = 0.55 °). The reduction of angular shift during EPC^+ introduction compared to when no capture antibody is present ($\Delta\theta$ = 0.8 °, Figure 3.2C) is attributed to IgG being bound by protein A on the surface, thus reducing available deposition area. Blood plasma (Figure 3.12A) or serum (Figure 3.13) spiked with IgG (10 µg / mL) was then incubated over the surface for 1 h. While the majority of non-specific components from plasma or serum can still be removed using a buffer rinse, no significant change in angular shift is observed between the samples with and without IgG. This is common in the detection of lowly abundant analytes in complex matrices, and the issue was overcome by simple addition of a detection antibody (*i.e.*, anti-IgG) for indirect measurement.[73, 74] Once introduced, angular shifts from the detection antibody were only observed for samples spiked with IgG ($\Delta\theta$ = 0.25 °), confirming specificity. This detection signal exhibits very little variation whether the matrix is plasma, serum, or PBS, and moreover, the EPC^+ lipids appear to provide no deleterious effects on sensitivity, with a relative standard deviation (RSD) of only 9.7 % between all experimental conditions

(Figure 3.14). The use of protein A in place of a traditional coupling scheme (*i.e.*, EDC/NHS coupling over a mercaptoundecanoic acid surface) also proves advantageous, with higher detection antibody signal observed when protein A is used (Figure 3.15), which is likely due to optimal capture antibody orientation.

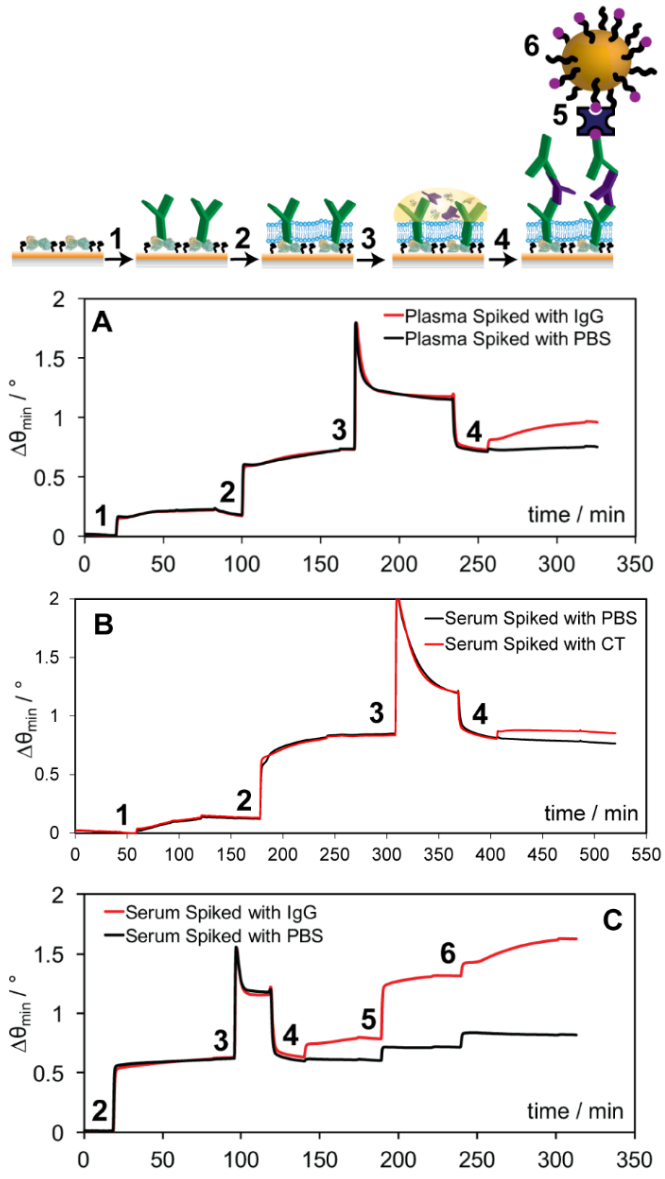

Figure 3.12 Schematic and (A) sensorgram representing the detection of mouse IgG (red) in undiluted human plasma where the capture antibody is injected (1), followed by the EPC lipid vesicles (2), the plasma spiked with mouse IgG (3), and finally a detection antibody for enhancement (4). (B) Sensorgram representing the detection of CT (red) in undiluted human serum using the similar surface chemistry to the IgG, and the addition of serum spiked with CT (3), and finally a detection anti-CT for enhancement (4). (C) Sensorgram representing the detection of mouse IgG (red) in undiluted human serum where the capture antibody is injected was applied offline and the EPC lipid vesicles injected online (2), followed by the serum spiked with mouse IgG (3), a biotinylated detection antibody (4), streptavidin bridge (5) and biotin labelled gold nanoparticles (6) for enhancement.

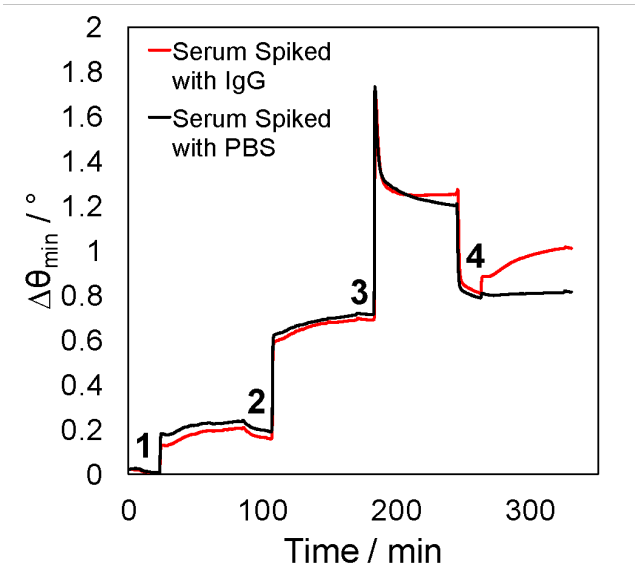

Figure 3.13 Sensorgrams representing the detection of mouse IgG (red) in undiluted human serum where the capture antibody is injected (1), followed by the EPC lipid vesicles (2), the plasma spiked with mouse IgG (3), and finally a detection antibody for enhancement (4). A 10 min PBS wash was included in between each step and a control sample was carried out by spiking the plasma with PBS only (black).

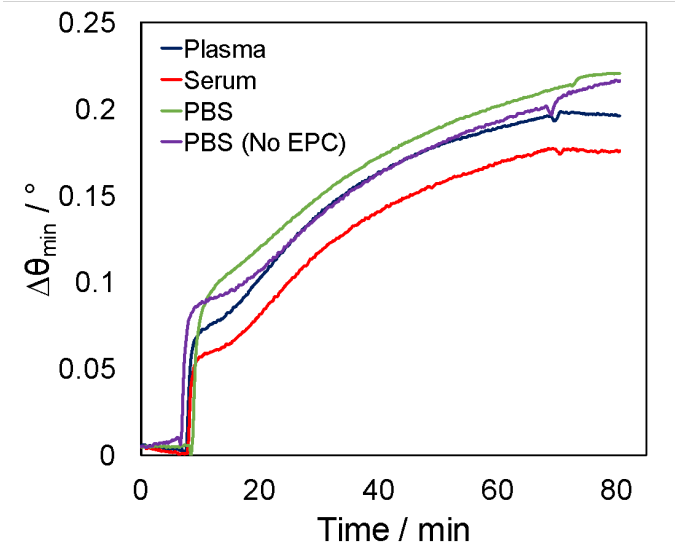

Figure 3.14 Comparison of the antibody enhancement step for IgG detection in various matrices including plasma (blue), serum (red), and PBS (green), along with a no EPC analysis in PBS (purple).

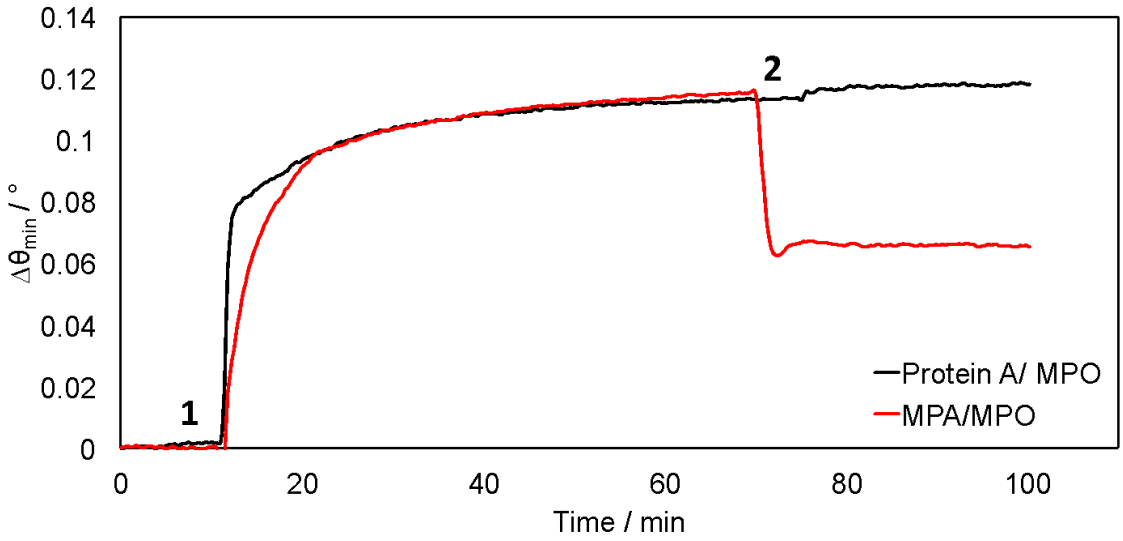

Figure 3.15 Comparison of the capture antibody attachment method, where anti-CT was conjugated to the surface via protein A (black) or via EDC/NHS coupling chemistry to 11-mercaptoundecanoic acid (red). Sensorgrams depict the addition of a secondary antibody after the detection of CT (1) and a PBS wash (2).

3.3.6 Analysis of Cholera Toxin (CT) detection in undiluted serum

To demonstrate the use of this interface for biosensing, specific recognition of cholera toxin (CT) in undiluted human serum was also performed. Though it targets the small intestine and is primarily diagnosed from stool, transport to the bloodstream though the jejunum has been documented,[75] which may provide an additional vantage point in the characterization of disease progression.[76] Once anti-CT (100 µg / mL) was immobilized on protein A/MPO, the antifouling capabilities of the EPC^+ lipids are still observed, as demonstrated by the angular shift returning to baseline after the buffer rinse (Figure 3.12B). Similar to IgG, no direct measurement of CT (10 µg / mL) was noted, though specific binding of CT was readily confirmed using a detection antibody (*i.e.*, anti-CT)

enhancement step, yielding an angular shift of 0.05 °. While this signal is lower than that for indirect IgG measurement, it is anticipated that a stringent screening for matching capture and detection antibody pairs will improve results.[77] Nonetheless, this angular shift was proven to be concentration dependent, demonstrating the promise of this platform for targeted quantitation of biomarkers in crude samples (Figure 3.16) and confirming the results obtained for IgG measurement.

While the above sensitivities should prove sufficient for many applications, there are a plethora of biomarkers that require more sensitive detection strategies for accurate clinical diagnoses and decisions to be made. Ultrasensitive SPR analysis can be achieved through electromagnetic coupling of metallic nanoparticles with the sensor chip, substantially lowering limits of detection.[58, 73, 78] We therefore included additional enhancement steps to each of our model assays with the goal of targeted gold nanoparticle binding. Detection antibodies were conjugated with biotin, and introduced at a concentration of 1 μM. Using a streptavidin bridge (100 μg mL^{-1}), the interaction of biotin-labelled gold nanoparticles (bT_{20}/AuNPs) was quantified and used to investigate the interaction specificity in the presence of the EPC^{+} barrier (Figure 3.12B). Although we do see some background binding from streptavidin, and hence, the bT_{20}/AuNPs, we can still easily discriminate between when IgG (10 μg / mL) is present in serum ($\Delta\theta$ = 0.30 °) and when it is not ($\Delta\theta$ = 0.10 °). Similar results were obtained for nanoparticle-enhanced CT (0.05 μg mL^{-1}) detection (Figure 3.17), where background signal ($\Delta\theta$ = 0.08 °) was lower than target-specific signal ($\Delta\theta$ = 0.21 °). Given that these bT_{20}/AuNPs have been designed to carry a high density of negative charge through DNA spacers for maximum colloidal

stability,[58] it is impressive that specific recognition is retained over EPC^+ carrying a net positive charge, from which excessively high background would be expected. While the antifouling membrane formed over protein A/MPO is resistant to fouling from common blood derivatives, it could also be used in conjunction with other materials, organic or inorganic, for sensitive and specific recognition of clinically relevant targets. The limit of detection of cholera toxin achieved is 5 μg / mL with secondary antibody detection (Figure 3.16) and 0.05 μg / mL with gold nanoparticle enhancement (Figure 3.17). The limit of detection is also reported in terms of number of molecules, which is summarized in Table 3.1.

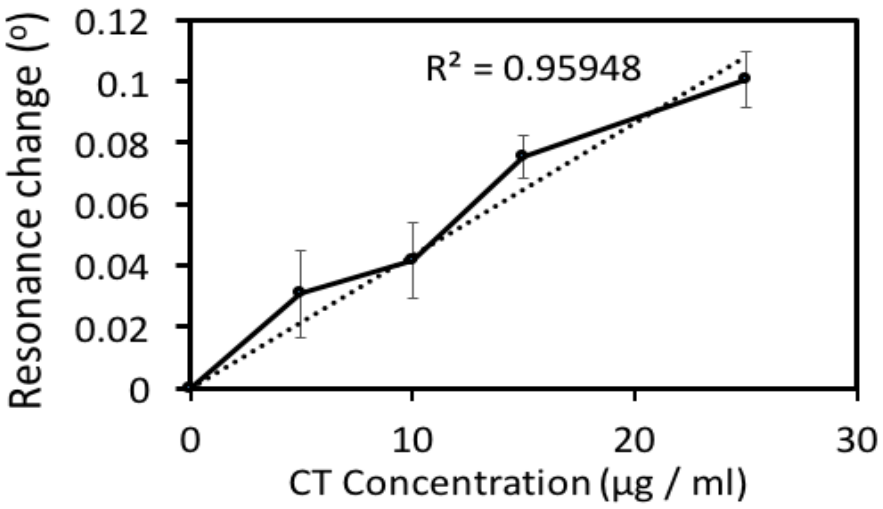

Figure 3.16 Calibration curve for detection of Cholera Toxin (CT) using an anti-CT enhancement step

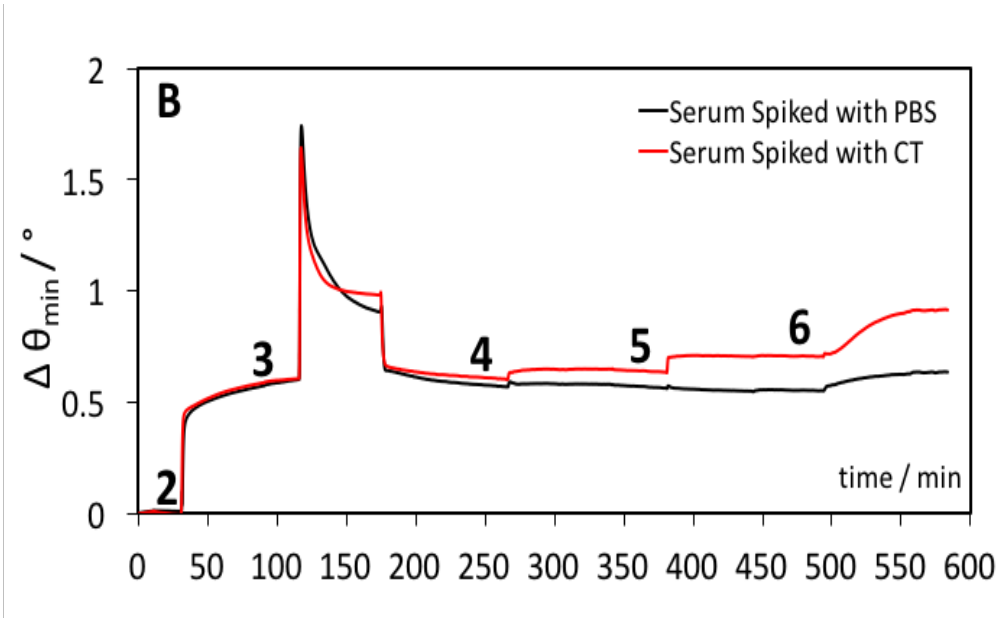

Figure 3.17 Sensorgram representing the detection of 0.05 µg / mL CT (red) in undiluted human serum where the capture anti-CT is injected offline and the EPC lipid vesicles injected online (2), followed by the serum spiked with CT (3), a biotinylated detection anti-CT (4), streptavidin bridge (5) and biotin labelled gold nanoparticles (6) for enhancement. A 15-minute PBS wash was included in between each step and a control sample was carried out by spiking the serum with PBS only (black).

Table 3.2 Summary of SPR data for both IgG and CT in different test medium, detection mode (e.g., via detection antibody, AuNPs) and their angle shifts.

Medium	IgG (µg / mL)	IgG (No. of molecules)	Δθ (anti-IgG)	Δθ (AuNPs)	Figure
Blood plasma	10	4.4×10^{12}	0.25°		3.12A
Human Serum	10	4.4×10^{12}	0.25 °		3.13
Human Serum	10	4.4×10^{12}		0.20 °	3.12C

Medium	CT (µg / mL)	CT (No. of molecules)	Δθ (anti-CT)	Δθ (AuNPs)	Figure
Human Serum	10	7.9×10^{12}	0.05°		3.12B
Human Serum	0.05	4.0×10^{10}		0.13 °	3.17

To calculate concentration in number of molecules, the µg/mL was converted to Molar (M) then multiplied by injection volume (110µL) to obtain number of mol. The number of molecules were then determined by Avogadro's number. Molecular weight of IgG and CT is 150 kDa and 83 kDa, respectively.

3.3.7 Detection of CT with AuNPs amplification

In addition to the results above, additional experiments and data were gathered during the course of CT analysis. The absorbance of synthesized 25 nm AuNPs and conjugated bT_{20}/AuNPs were characterized with UV-Vis, not only to find the size but to confirm the conjugation result. By comparing the spectra of both AuNPs states, the bT_{20}/AuNPs showed a red shift of the maximum peak indicates the increase of diameter in presence of biotin and the DNA spacer (Figure 3.18). The schematic and sensorgrams of CT detection with and without AuNPs enhancement are as showed in Figure 3.19 and Figure 3.20.

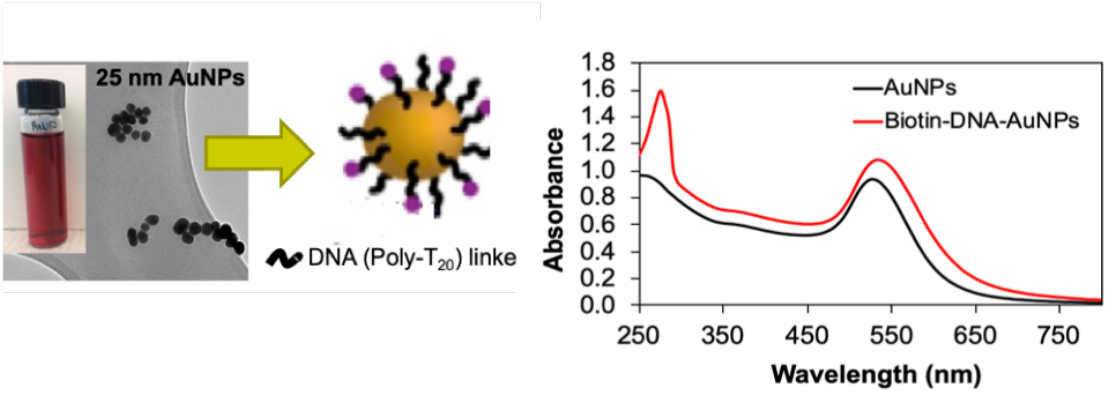

Figure 3.18 SEM image of the 26 nm AuNPs used for the bioconjugation of biotin using DNA linkers.[58] UV-Vis spectra showing the red-shift of the maximum peak indicates the increase of diameter in presence of biotin.

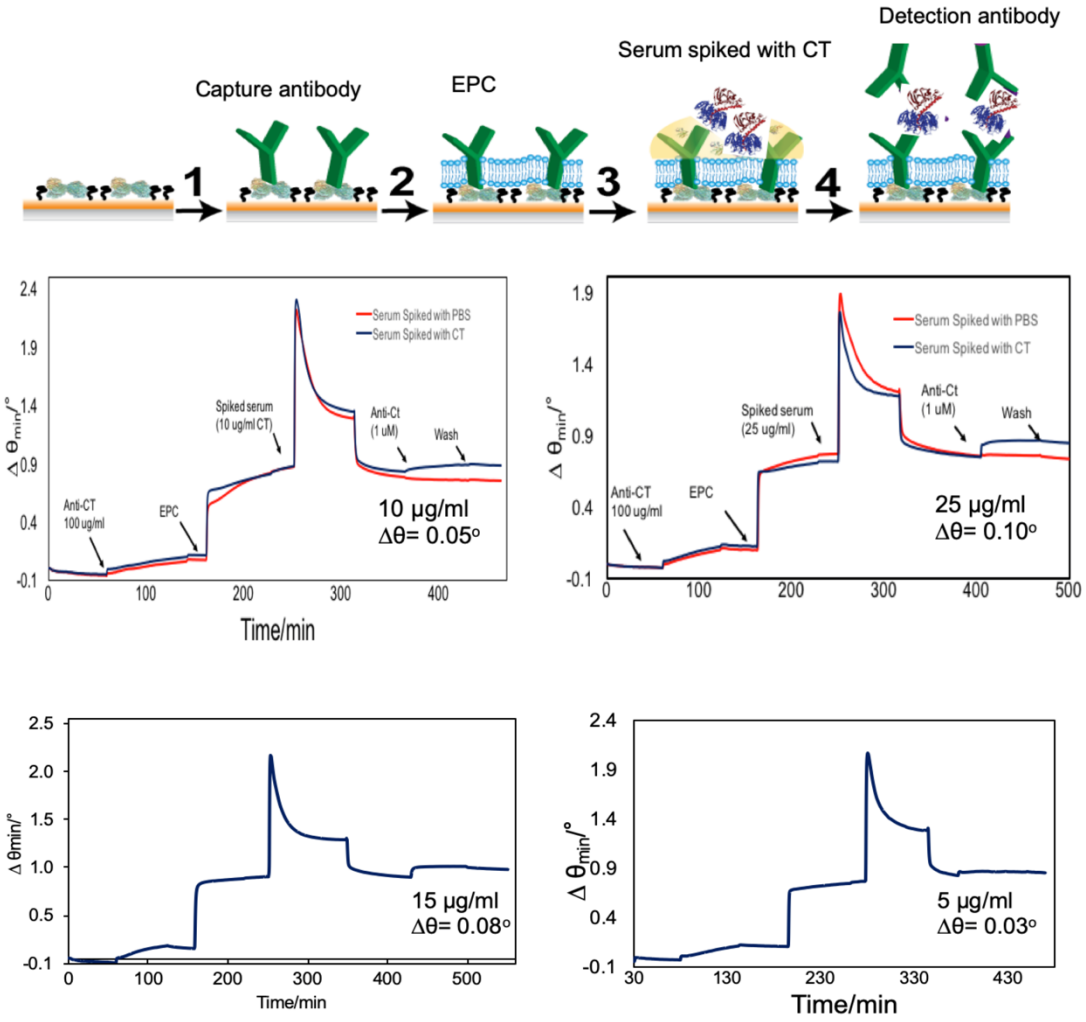

Figure 3.19 Schematic and (A) sensorgram representing the detection of cholera toxin (CT) (blue) in undiluted human serum where the capture antibody is injected (1), followed by the EPC lipid vesicles (2), the plasma spiked with CT (3), and finally a detection antibody (4)

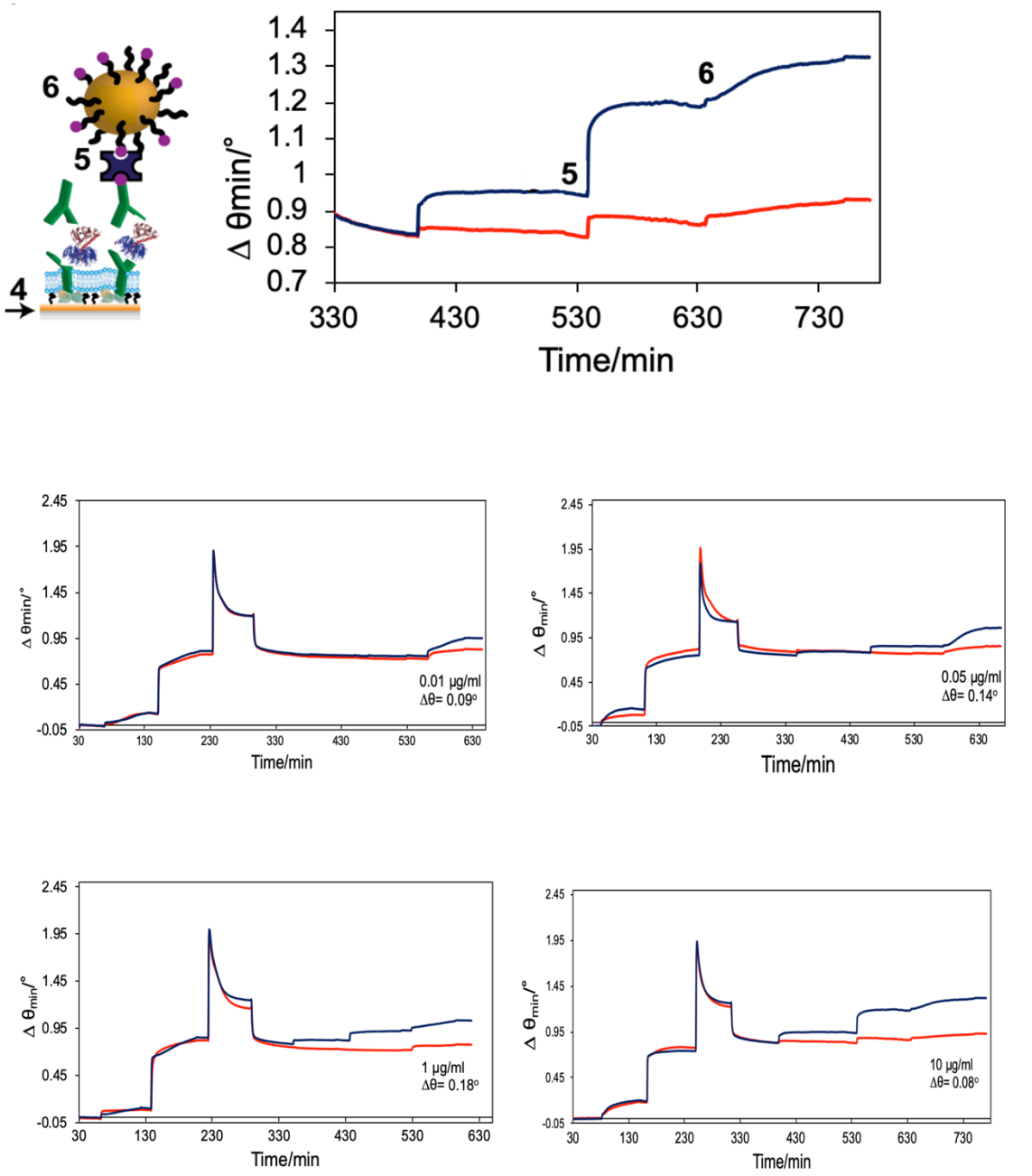

Figure 3.20 Schematic and sensorgram representing the detection of cholera toxin (CT) (blue) in undiluted human serum with AuNPs amplification steps where the following injection was applied after step (3); biotinylated antibody (4), streptavidin bridge (5) and **bT$_{20}$**/AuNPs (6) for enhancement

3.3.8 Comparing sensitivity of CT detection with and without AuNPs enhancement

The SPR measurements were repeated for different concentration of CT for at least three times per concentration, a calibration curve of the resonance change as the function of CT concentration was plotted (Figure 3.21), showing the linear range of the detection sensitivity. It is worth to mention that saturation (a plateau) occurred after 25 µg / ml and 0.05 µg / ml of CT for the detection without and with AuNPs, respectively. Possible reason is because of the saturation at the analyte-antibody binding sites which makes further enhancement not significant. The calibration curves show that the linear range without AuNPs is 0 - 25 ug / ml, while after AuNPs enhancement a higher signal was obtained which enabled the lower detection range of 0 - 0.05 ug / ml. The angle shift ($\Delta\theta$) was calculated by subtracting the angle shift of the non-specific binding (control channel) from the shift of the specific binding (experiment channel).

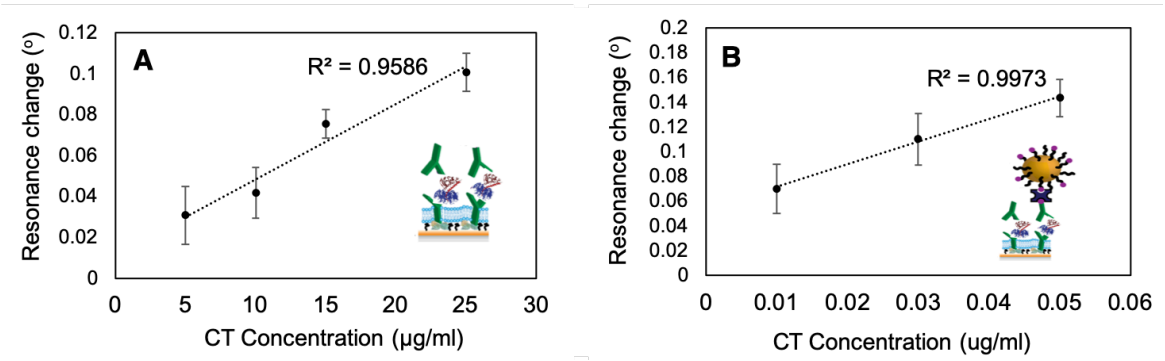

Figure 3.21 Calibration curves of the detection of CT (A) with and (B) without AuNPs enhancement.

3.3.9 Performance compared to the traditional self-assembled monolayer (SAM)

We compared the detection system of using bilayer membranes to the traditional SAM. For this purpose, the golds chip was incubated with 11-mercapdoundecanoic acid (MUA) to form self-assembled monolayer with carboxyl group on the surface. Then, the anti-CT was immobilized onto the surface via EDC/NHS coupling chemistry to MUA. We showed that this surface chemistry can be successfully applied to undiluted human serum with minimal sacrifice in SPR signal when compared to buffered analysis. Using Protein A, lipid membrane and serum does not compromise detection of CT at same concentration 25 µg/ml ($\Delta\theta$=0.10+ 0.01°) (Figure 3.22).

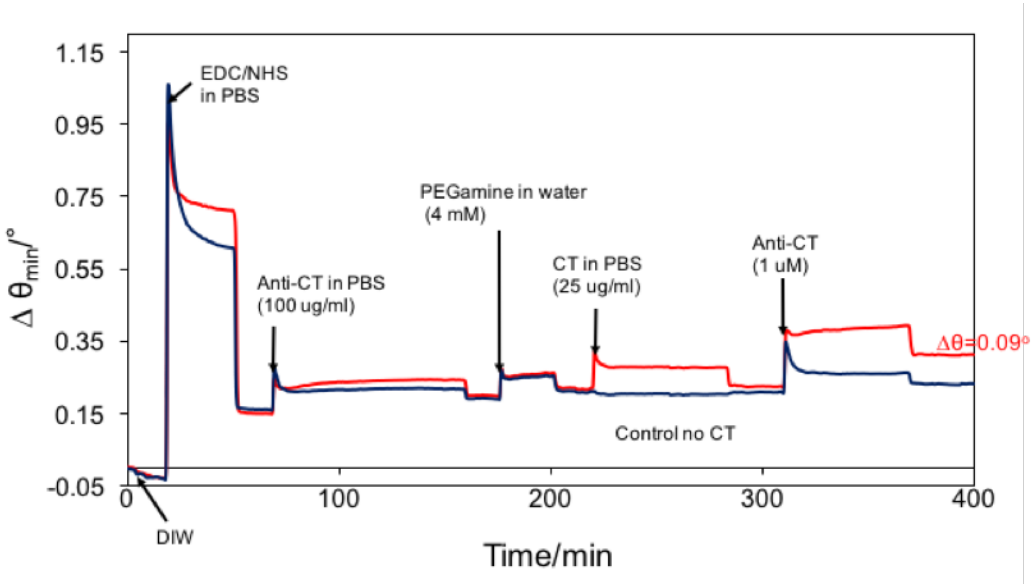

Figure 3.22 Sensorgram showing detection of CT on self-assembled monolayer in buffered analysis

3.3.10 Effect of serum incubation on protein A-lipid interface

Our results showed that all non-specifically bound serum components were completely removed from the surface, as verified by the SPR signal when it returned to the level before serum injection after rinsing. However, it was unclear from this method, whether the EPC^+ lipid bilayer was disrupted structurally by the serum. To address this question, we utilized fluorescence microscopy and FRAP analysis of the lipid on the Protein A/ MPO/ EPC^+ in additional to serum incubation that mimics the SPR surface (a collaborative work with Daniel Stuart). First, the images verified that the fluorescence signal came from the fluorescent-tagged lipid, when no fluorescent was observed just on the protein A surface (Figure 3.23A). Although the fluorescent intensity of the protein A surface was lower on average without the serum (Figure 3.23B), we can still observe good coverage of fluorescent lipids and when compared against the control it clearly indicates that we have lipids remaining on the surface. The FRAP images in Figure 3.24A suggesting that there is a strong adsorption and self-assembled architecture of EPC^+ on protein A/ MPO surface as no redistribution of fluorescence within the region of interest after photobleaching. The same finding was observed after incubation of serum, indicating the EPC^+ structure remain strongly adsorbed on the protein A/ MPO surface even after rinsing (Figure 3.24B and Figure 3.25).

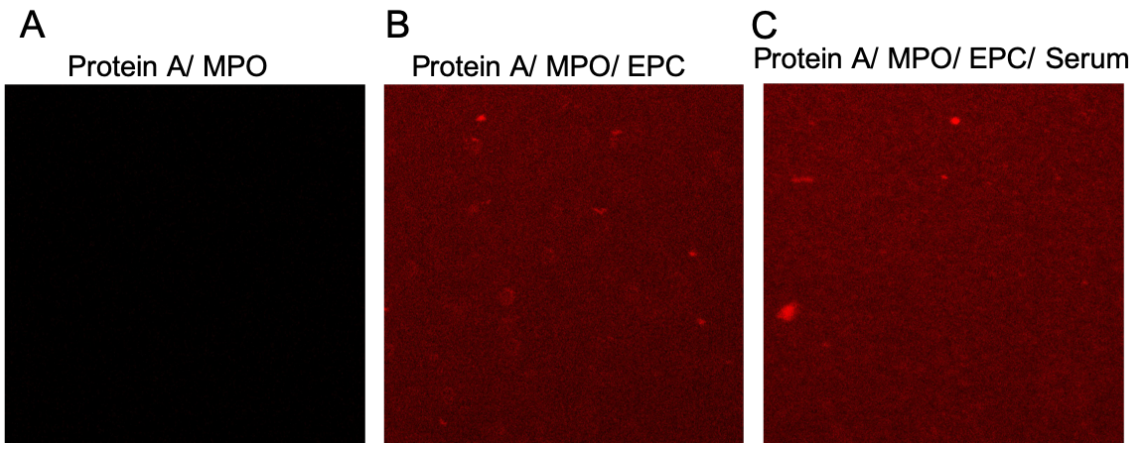

Figure 3.23 Images depicting fluorescence analysis of EPC^+ lipids formed over a protein A/MPO coated gold slide. (A) Fluorescence micrographs of just the Protein A surface showing no fluorescence. Corresponding fluorescence micrographs for EPC^+ on Protein A/ MPO surface (B) without and (C) with serum incubation

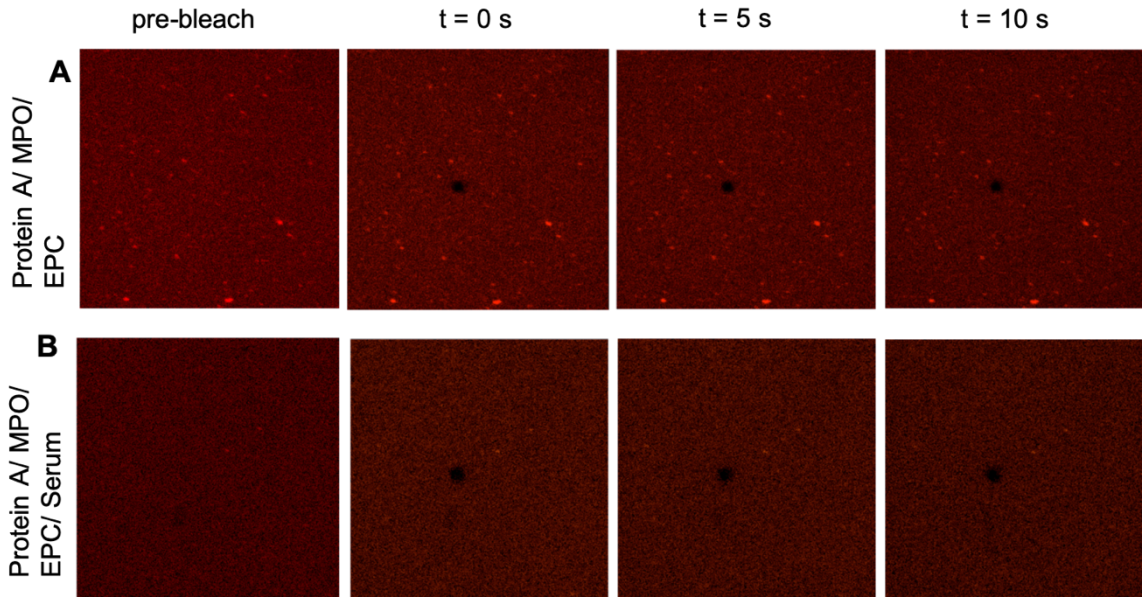

Figure 3.24 Images depicting FRAP analysis of EPC^+ lipids formed over a protein A/MPO coated gold slide. Fluorescence micrographs of photobleaching and recovery for the surface (A) Without serum. (B) With serum, from pre-bleach to t = 10s after bleaching

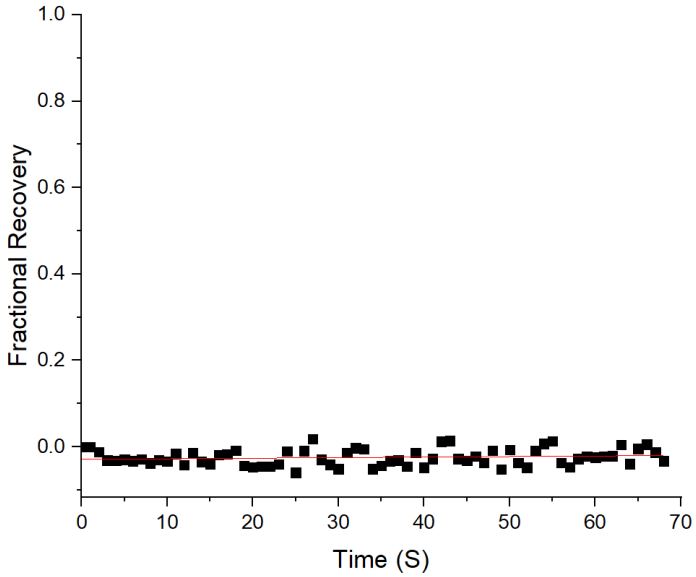

Figure 3.25 Corresponding recovery data for EPC+ over protein A/MPO surface, representative of both of the FRAP images for serum and without serum

3.4 Conclusion

We have reported the use of charge-matched lipid membranes as an antifouling surface capable of carrying out analysis in undiluted human serum and plasma. By tailoring the charge of the lipid vesicles used, as well as selection of an appropriate backfilling SAM, the membrane successfully formed over a protein A surface, additionally allowing for orientation controlled immunosensing. We have shown that the addition of this membrane caused no reduction in SPR signal for bacterial toxin and antibody detection, and that analysis in complex matrices could be carried out with similar results to those seen for buffered samples. The sensitivity performance in CT detection was further improve by AuNPs amplification step.

Moving forward and given the universal nature of protein A, this surface chemistry could potentially be used in a range of surface based biosensing platforms. Current techniques aside from SPR, including ELISA, fluorescent microarrays, and electrochemical based methods of analysis, which also suffer from non-ideal antibody orientation and ineffective surface blocking, could benefit from this novel surface chemistry, allowing for the sensing of clinically relevant targets within a range of complex biological matrices.

3.5 References

1. Bauer, M.; Reinhart, K., Molecular diagnostics of sepsis—Where are we today? *International Journal of Medical Microbiology* **2010,** *300* (6), 411-413.

2. Schmiemann, G.; Kniehl, E.; Gebhardt, K.; Matejczyk, M. M.; Hummers-Pradier, E., The diagnosis of urinary tract infection: a systematic review. *Deutsches Arzteblatt international* **2010,** *107* (21), 361-367.

3. Graseck, A. S.; Shih, S. L.; Peipert, J. F., Home versus clinic-based specimen collection for Chlamydia trachomatis and Neisseria gonorrhoeae. *Expert review of anti-infective therapy* **2011,** *9* (2), 183-194.

4. Al-Zamel, F. A., Detection and diagnosis of Mycobacterium tuberculosis. *Expert Review of Anti-infective Therapy* **2009,** *7* (9), 1099-1108.

5. Ryan, C.; Kinghorn, G., Clinical assessment of assays for diagnosis of herpes simplex infection. *Expert Review of Molecular Diagnostics* **2006,** *6* (5), 767-775.

6. Bourlet, T.; Memmi, M.; Saoudin, H.; Pozzetto, B., Molecular HIV screening. *Expert Review of Molecular Diagnostics* **2013,** *13* (7), 693-705.

7. Pemán, J.; Zaragoza, R., Combined use of nonculture-based lab techniques in the diagnosis and management of critically ill patients with invasive fungal infections. *Expert Review of Anti-infective Therapy* **2012,** *10* (11), 1321-1330.

8. Cowman, A. F.; Healer, J.; Marapana, D.; Marsh, K., Malaria: Biology and Disease. *Cell* **2016,** *167* (3), 610-624.

9. Grodzinski, P.; Silver, M.; Molnar, L. K., Nanotechnology for cancer diagnostics: promises and challenges. *Expert Review of Molecular Diagnostics* **2006,** *6* (3), 307-318.

10. Ludwig, J. A.; Weinstein, J. N., Biomarkers in Cancer Staging, Prognosis and Treatment Selection. *Nature Reviews Cancer* **2005,** *5* (11), 845-856.

11. Mayeux, R., Biomarkers: potential uses and limitations. *NeuroRx : the journal of the American Society for Experimental NeuroTherapeutics* **2004,** *1* (2), 182-188.

12. Mueller, W. H., Biological markers in epidemiology. Edited by B. S. Hulka, T. C. Wilcosky, and J. D. Griffith. xi + 236 pp. New York: Oxford University Press, 1990, $40.00 (cloth). *American Journal of Human Biology* **1991,** *3* (2), 218-219.

13. McKeating, K. S.; Aube, A.; Masson, J.-F., Biosensors and nanobiosensors for therapeutic drug and response monitoring. *Analyst* **2016,** *141* (2), 429-449.

14. Zhao, S. S.; Bukar, N.; Toulouse, J. L.; Pelechacz, D.; Robitaille, R.; Pelletier, J. N.; Masson, J.-F., Miniature multi-channel SPR instrument for methotrexate monitoring in clinical samples. *Biosens. Bioelectron.* **2015,** *64*, 664-670.

15. Masson, J.-F., Surface plasmon resonance clinical biosensors for medical diagnostics. *ACS Sens.* **2017,** *2* (1), 16-30.

16. Aubé, A.; Charbonneau, D. M.; Pelletier, J. N.; Masson, J.-F. o., Response Monitoring of Acute Lymphoblastic Leukemia Patients Undergoing l-Asparaginase Therapy: Successes and Challenges Associated with Clinical Sample Analysis in Plasmonic Sensing. *ACS Sens.* **2016,** *1* (11), 1358-1365.

17. Yang, C.-T.; Pourhassan-Moghaddam, M.; Wu, L.; Bai, P.; Thierry, B., Ultrasensitive Detection of Cancer Prognostic miRNA Biomarkers Based on Surface Plasmon Enhanced Light Scattering. *ACS Sens.* **2017,** *2* (5), 635-640.

18. Aubé, A.; Campbell, S.; Schmitzer, A. R.; Claing, A.; Masson, J.-F., Ultra-low fouling methylimidazolium modified surfaces for the detection of HER2 in breast cancer cell lysates. *Analyst* **2017**.

19. Jayanthi, V. S. P. K. Sankara A.; Das, A. B.; Saxena, U., Recent advances in biosensor development for the detection of cancer biomarkers. *Biosens. Bioelectron.* **2017,** *91*, 15-23.

20. Kim, S.; Wark, A. W.; Lee, H. J., Femtomolar Detection of Tau Proteins in Undiluted Plasma Using Surface Plasmon Resonance. *Anal. Chem.* **2016,** *88* (15), 7793-7799.

21. Bellassai, N.; D'Agata, R.; Jungbluth, V.; Spoto, G., Surface Plasmon Resonance for Biomarker Detection: Advances in Non-invasive Cancer Diagnosis. *Frontiers in chemistry* **2019,** *7*, 570-570.

22. Yockell-Lelievre, H.; Bukar, N.; McKeating, K.; Arnaud, M.; Cosin, P.; Guo, Y.; Dupret-Carruel, J.; Mougin, B.; Masson, J.-F., Plasmonic sensors for the competitive detection of testosterone. *Analyst* **2015,** *140* (15), 5105-5111.

23. McKeating, K. S.; Aubé, A.; Masson, J.-F., Biosensors and nanobiosensors for therapeutic drug and response monitoring. *Analyst* **2016,** *141* (2), 429-449.

24. Lu, J.; Spasic, D.; Delport, F.; Van Stappen, T.; Detrez, I.; Daems, D.; Vermeire, S.; Gils, A.; Lammertyn, J., Immunoassay for Detection of Infliximab in Whole Blood Using a Fiber-Optic Surface Plasmon Resonance Biosensor. *Anal. Chem.* **2017,** *89* (6), 3664-3671.

25. Blaszykowski, C.; S., S.; Thompson, M., A survey of state-of-the-art surface chemistries to minimize fouling from human and animal biofluids. *Biomater. Sci.* **2015,** *3* (10), 1335-1370.

26. Liu, B.; Liu, X.; Shi, S.; Huang, R.; Su, R.; Qi, W.; He, Z., Design and mechanisms of antifouling materials for surface plasmon resonance sensors. *Acta Biomater.* **2016,** *40*, 100-118.

27. Bakker, E., So, You Have a Great New Sensor. How Will You Validate It? *ACS Sens.* **2018,** *3* (8), 1431-1431.

28. Wade, J. H.; Alsop, A. T.; Vertin, N. R.; Yang, H. W.; Johnson, M. D.; Bailey, R. C., Rapid, Multiplexed Phosphoprotein Profiling Using Silicon Photonic Sensor Arrays. *ACS Cent. Sci.* **2015,** *1* (7), 374-382.

29. Washburn, A. L.; Shia, W. W.; Lenkeit, K. A.; Lee, S. H.; Bailey, R. C., Multiplexed cancer biomarker detection using chip-integrated silicon photonic sensor arrays. *Analyst* **2016,** *141* (18), 5358-5365.

30. Cristina Pelaez, E.; Estevez, M. C.; Portela, A.; Salvador, J. P.; Marco, M. P.; Lechuga, L. M., Nanoplasmonic biosensor device for the monitoring of acenocoumarol therapeutic drug in plasma. *Biosens. Bioelectron.* **2018,** *119*, 149-155.

31. Ramirez-Priego, P.; Martens, D.; Elamin, A. A.; Soetaert, P.; Van Roy, W.; Vos, R.; Anton, B.; Bockstaele, R.; Becker, H.; Singh, M.; Bienstman, P.; Lechuga, L. M.,

Label-Free and Real-Time Detection of Tuberculosis in Human Urine Samples Using a Nanophotonic Point-of-Care Platform. *ACS Sens.* **2018**.

32. Ng, A. H. C.; Fobel, R.; Fobel, C.; Lamanna, J.; Rackus, D. G.; Summers, A.; Dixon, C.; Dryden, M. D. M.; Lam, C.; Ho, M.; Mufti, N. S.; Lee, V.; Asri, M. A. M.; Sykes, E. A.; Chamberlain, M. D.; Joseph, R.; Ope, M.; Scobie, H. M.; Knipes, A.; Rota, P. A.; Marano, N.; Chege, P. M.; Njuguna, M.; Nzunza, R.; Kisangau, N.; Kiogora, J.; Karuingi, M.; Burton, J. W.; Borus, P.; Lam, E.; Wheeler, A. R., A digital microfluidic system for serological immunoassays in remote settings. *Sci. Transl. Med.* **2018,** *10* (438).

33. Peungthum, P.; Sudprasert, K.; Amarit, R.; Somboonkaew, A.; Sutapun, B.; Vongsakulyanon, A.; Seedacoon, W.; Kitpoka, P.; Kunakorn, M.; Srikhirin, T., Surface plasmon resonance imaging for ABH antigen detection on red blood cells and in saliva: secretor status-related ABO subgroup identification. *Analyst* **2017,** *142* (9), 1471-1481.

34. Aube, A.; Breault-Turcot, J.; Chaurand, P.; Pelletier, J. N.; Masson, J. F., Non-specific Adsorption of Crude Cell Lysate on Surface Plasmon Resonance Sensors. *Langmuir* **2013,** *29* (32), 10141-10148.

35. Aube, A.; Campbell, S.; Schmitzer, A. R.; Claing, A.; Masson, J.-F., Ultra-low fouling methylimidazolium modified surfaces for the detection of HER2 in breast cancer cell lysates. *Analyst* **2017,** *142* (13), 2343-2353.

36. Lísalová, H.; Brynda, E.; Houska, M.; Víšová, I.; Mrkvová, K.; Song, X. C.; Gedeonová, E.; Surman, F.; Riedel, T.; Pop-Georgievski, O.; Homola, J., Ultralow-Fouling Behavior of Biorecognition Coatings Based on Carboxy-Functional Brushes of Zwitterionic Homo- and Copolymers in Blood Plasma: Functionalization Matters. *Anal. Chem.* **2017,** *89* (6), 3524-3531.

37. Li, H.; Dauphin-Ducharme, P.; Arroyo-Curras, N.; Tran, C. H.; Vieira, P. A.; Li, S.; Shin, C.; Somerson, J.; Kippin, T. E.; Plaxco, K. W., A Biomimetic Phosphatidylcholine-Terminated Monolayer Greatly Improves the In Vivo Performance of Electrochemical Aptamer-Based Sensors. *Angew. Chem. Int. Ed. Engl.* **2017,** *56* (26), 7492-7495.

38. Goda, T.; Tabata, M.; Sanjoh, M.; Uchimura, M.; Iwasaki, Y.; Miyahara, Y., Thiolated 2-methacryloyloxyethyl phosphorylcholine for an antifouling biosensor platform. *Chem. Commun.* **2013,** *49* (77), 8683-8685.

39. Akkahat, P.; Kiatkamjornwong, S.; Yusa, S.-i.; Hoven, V. P.; Iwasaki, Y., Development of a Novel Antifouling Platform for Biosensing Probe Immobilization from Methacryloyloxyethyl Phosphorylcholine-Containing Copolymer Brushes. *Langmuir* **2012,** *28* (13), 5872-5881.

40. Gong, Y. K.; Liu, L. P.; Messersmith, P. B., Doubly biomimetic catecholic phosphorylcholine copolymer: a platform strategy for fabricating antifouling surfaces. *Macromol. Biosci.* **2012,** *12* (7), 979-985.

41. Hinman, S. S.; Ruiz, C. J.; Cao, Y.; Ma, M. C.; Tang, J. J.; Laurini, E.; Posocco, P.; Giorgio, S.; Pricl, S.; Peng, L.; Cheng, Q., Mix and Match: Coassembly of Amphiphilic Dendrimers and Phospholipids Creates Robust, Modular, and Controllable Interfaces. *ACS Appl. Mater. Interfaces* **2017,** *9* (1), 1029-1035.

42. Perez, L.; Mettry, M.; Hinman, S. S.; Byers, S. R.; McKeating, K. S.; Caulkins, B. G.; Cheng, Q.; Hooley, R. J., Selective protein recognition in supported lipid bilayer arrays by tailored, dual-mode deep cavitand hosts. *Soft Matter* **2017,** *13*, 3966-3974.

43. Hinman, S. S.; Ruiz, C. J.; Drakakaki, G.; Wilkop, T. E.; Cheng, Q., On-Demand Formation of Supported Lipid Membrane Arrays by Trehalose-Assisted Vesicle Delivery for SPR Imaging. *ACS Appl Mater Interfaces* **2015,** *7* (31), 17122-17130.

44. Liu, Y.; Cheng, Q., Detection of Membrane-Binding Proteins by Surface Plasmon Resonance with an All-Aqueous Amplification Scheme. *Anal. Chem.* **2012,** *84* (7), 3179-3186.

45. Phillips, K. S.; Han, J. H.; Cheng, Q., Development of a "membrane cloaking" method for amperometric enzyme immunoassay and surface plasmon resonance analysis of proteins in serum samples. *Anal. Chem.* **2007,** *79* (3), 899-907.

46. Valsecchi, C.; Jones, T.; Wang, C.; Lochbihler, H.; Menezes, J. W.; Brolo, A. G., Low-Cost Leukemic Serum Marker Screening Using Large Area Nanohole Arrays on Plastic Substrates. *ACS Sens.* **2016,** *1* (9), 1103-1109.

47. Iijima, M.; Kuroda, S. i., Scaffolds for oriented and close-packed immobilization of immunoglobulins. *Biosens. Bioelectron.* **2017,** *89*, 810-821.

48. Taheri, R. A.; Rezayan, A. H.; Rahimi, F.; Mohammadnejad, J.; Kamali, M., Development of an immunosensor using oriented immobilized anti-OmpW for sensitive detection of Vibrio cholerae by surface plasmon resonance. *Biosens. Bioelectron.* **2016,** *86*, 484-488.

49. Lee, T. H.; Hirst, D. J.; Kulkarni, K.; Del Borgo, M. P.; Aguilar, M. I., Exploring Molecular-Biomembrane Interactions with Surface Plasmon Resonance and Dual Polarization Interferometry Technology: Expanding the Spotlight onto Biomembrane Structure. *Chem. Rev.* **2018,** *118* (11), 5392-5487.

50. Hinman, S. S.; McKeating, K. S.; Cheng, Q., Surface Plasmon Resonance: Material and Interface Design for Universal Accessibility. *Anal. Chem.* **2018,** *90* (1), 19-39.

51. Baldauf, J. K.; Royal, M. J.; Hamorsky, T. K.; Matoba, N., Cholera Toxin B: One Subunit with Many Pharmaceutical Applications. *Toxins* **2015,** *7* (3).

52. Sanchez, J.; Holmgren, J., Cholera toxin - a foe & a friend. *The Indian journal of medical research* **2011,** *133* (2), 153-163.

53. Wernick, N. L. B.; Chinnapen, D. J. F.; Cho, J. A.; Lencer, W. I., Cholera toxin: an intracellular journey into the cytosol by way of the endoplasmic reticulum. *Toxins* **2010,** *2* (3), 310-325.

54. Stine, O. C.; Morris, J. G., Jr., Circulation and transmission of clones of Vibrio cholerae during cholera outbreaks. *Current topics in microbiology and immunology* **2014,** *379*, 181-193.

55. Hinman, S. S.; Ruiz, C. J.; Drakakaki, G.; Wilkop, T. E.; Cheng, Q., On-Demand Formation of Supported Lipid Membrane Arrays by Trehalose-Assisted Vesicle Delivery for SPR Imaging. *ACS Applied Materials & Interfaces* **2015,** *7* (31), 17122-17130.

56. Reits, E. A. J.; Neefjes, J. J., From fixed to FRAP: measuring protein mobility and activity in living cells. *Nature Cell Biology* **2001,** *3* (6), E145-E147.

57. Haiss, W.; Thanh, N. T. K.; Aveyard, J.; Fernig, D. G., Determination of Size and Concentration of Gold Nanoparticles from UV−Vis Spectra. *Analytical Chemistry* **2007,** *79* (11), 4215-4221.

58. Hinman, S. S.; McKeating, K. S.; Cheng, Q., DNA Linkers and Diluents for Ultrastable Gold Nanoparticle Bioconjugates in Multiplexed Assay Development. *Anal. Chem.* **2017,** *89* (7), 4272-4279.

59. Axelrod, D.; Koppel, D. E.; Schlessinger, J.; Elson, E.; Webb, W. W., Mobility Measurement by Analysis of Fluorescence Photobleaching Recovery Kinetics. *Biophys. J.* **1976,** *16* (9), 1055-1069.

60. Soumpasis, D. M., Theoretical-Analysis of Fluorescence Photobleaching Recovery Experiments. *Biophys. J.* **1983,** *41* (1), 95-97.

61. Liu, Y.; Dong, Y.; Jauw, J.; Linman, M. J.; Cheng, Q., Highly Sensitive Detection of Protein Toxins by Surface Plasmon Resonance with Biotinylation-Based Inline Atom Transfer Radical Polymerization Amplification. *Analytical Chemistry* **2010,** *82* (9), 3679-3685.

62. Phillips, K. S.; Han, J. H.; Martinez, M.; Wang, Z. Z.; Carter, D.; Cheng, Q., Nanoscale glassification of gold substrates for surface plasmon resonance analysis of protein toxins with supported lipid membranes. *Anal. Chem.* **2006,** *78* (2), 596-603.

63. Hinman, S. S.; Nguyen, R. C. T.; Cheng, Q., Plasmonic nanodisc arrays on calcinated titania for multimodal analysis of phosphorylated peptides. *RSC Adv.* **2017,** *7* (76), 48068-48076.

64. Wang, Z. Z.; Wilkop, T.; Han, J. H.; Dong, Y.; Linman, M. J.; Cheng, Q., Development of air-stable, supported membrane arrays with photolithography for study of phosphoinositide - Protein interactions using surface plasmon resonance imaging. *Anal. Chem.* **2008,** *80* (16), 6397-6404.

65. Hinman, S. S.; McKeating, K. S.; Cheng, Q., Plasmonic Sensing with 3D Printed Optics. *Anal. Chem.* **2017,** *89* (23), 12626-12630.

66. Kozlowski, L. P., IPC - Isoelectric Point Calculator. *Biol. Direct* **2016,** *11* (1), 55.

67. Yu, Z. H.; Kastenmuller, G.; He, Y.; Belcredi, P.; Moller, G.; Prehn, C.; Mendes, J.; Wahl, S.; Roemisch-Margl, W.; Ceglarek, U.; Polonikov, A.; Dahmen, N.; Prokisch, H.; Xie, L.; Li, Y. X.; Wichmann, H. E.; Peters, A.; Kronenberg, F.; Suhre, K.; Adamski, J.; Illig, T.; Wang-Sattler, R., Differences between Human Plasma and Serum Metabolite Profiles. *PLoS One* **2011,** *6* (7).

68. Oddoze, C.; Lombard, E.; Portugal, H., Stability study of 81 analytes in human whole blood, in serum and in plasma. *Clin. Biochem.* **2012,** *45* (6), 464-469.

69. Geyer, P. E.; Kulak, N. A.; Pichler, G.; Holdt, L. M.; Teupser, D.; Mann, M., Plasma Proteome Profiling to Assess Human Health and Disease. *Cell Syst* **2016,** *2* (3), 185-195.

70. Zhang, Z.; Chao, T.; Chen, S. F.; Jiang, S. Y., Superlow fouling sulfobetaine and carboxybetaine polymers on glass slides. *Langmuir* **2006,** *22* (24), 10072-10077.

71. Deschout, H.; Hagman, J.; Fransson, S.; Jonasson, J.; Rudemo, M.; Loren, N.; Braeckmans, K., Straightforward FRAP for quantitative diffusion measurements with a laser scanning microscope. *Opt. Express* **2010,** *18* (22), 22886-22905.

72. Ramanujan, S.; Pluen, A.; McKee, T. D.; Brown, E. B.; Boucher, Y.; Jain, R. K., Diffusion and convection in collagen gels: Implications for transport in the tumor interstitium. *Biophys. J.* **2002,** *83* (3), 1650-1660.

73. Masson, J. F., Surface Plasmon Resonance Clinical Biosensors for Medical Diagnostics. *ACS Sens.* **2017,** *2* (1), 16-30.

74. Aubé, A.; Charbonneau, D. M.; Pelletier, J. N.; Masson, J.-F., Response Monitoring of Acute Lymphoblastic Leukemia Patients Undergoing l-Asparaginase Therapy: Successes and Challenges Associated with Clinical Sample Analysis in Plasmonic Sensing. *ACS Sens.* **2016,** *1* (11), 1358-1365.

75. Vaughan Williams, E. M.; Dohadwalla, A. N., Absorption of Cholera Toxin into Blood from a Separated Jejunal Segment. *Nature* **1967,** *215*, 552.

76. Harris, J. B.; Khan, A. I.; LaRocque, R. C.; Dorer, D. J.; Chowdhury, F.; Faruque, A. S.; Sack, D. A.; Ryan, E. T.; Qadri, F.; Calderwood, S. B., Blood group, immunity, and risk of infection with Vibrio cholerae in an area of endemicity. *Infect. Immun.* **2005,** *73* (11), 7422-7.

77. Couture, M.; Ray, K. K.; Poirier-Richard, H.-P.; Crofton, A.; Masson, J.-F., 96-Well Plasmonic Sensing with Nanohole Arrays. *ACS Sens.* **2016,** *1* (3), 287-294.

78. Yockell-Lelievre, H.; Bukar, N.; McKeating, K. S.; Arnaud, M.; Cosin, P.; Guo, Y.; Dupret-Carruel, J.; Mougin, B.; Masson, J. F., Plasmonic sensors for the competitive detection of testosterone. *Analyst* **2015,** *140* (15), 5105-5111.

CHAPTER 4 : SPR Study of Cancer Cell Toxicology Based on Morphological and Refractive Index Changes

ABSTRACT

Morphological changes of cancer cells are often used in the studies of efficiency of anticancer drugs. Morphological cell analysis on cell size and shape distribution are typically performed by microscopic methods, which are time consuming and require skilled personnel. Recently, more advanced image processing and pattern recognition has enabled identification and quantitative analysis of the cells abnormality and classification in an automated way[1]. However, these methods usually involve multiple staining steps. In addition to computational complexity, the processes greatly compromise real-time applications of the system. Therefore, a non-invasive, real-time method allowing assessment of living cells' reactions to a death inducer is very much needed. Here we have developed an SPR biosensor that measures the changes in cancer cells' size and detachment, relating the cell confluency with the changes of the refractive index on the cell-substrate interface. As a proof-of-concept, we chose HeLa cell and hydrogen peroxide (H_2O_2) induced apoptosis as the model system to study the morphological changes of the cell. The results show that the SPR response to the cell apoptosis agreed with the cellular morphology changes observed by microscopy. Interestingly, we observed simultaneous apoptosis and necrosis when the concentration of H_2O_2 was high enough. The simultaneous occurrence was verified using a mathematical model, and other factors such as cell

thickness and intercellular refractive index were incorporated into the model, which helped resolve the disagreement between SPR signal and cell confluency at high H_2O_2 concentrations. Our results show the potential of SPR as a label free and real time monitoring method for morphology changes and surface detachment of cancer cells. This method can be fully expanded to other cell-based sensing applications.

4.1 Introduction

SPR has been applied to the label-free, non-invasive and real-time monitoring of living cells' conditions and functions for life science research and clinical diagnosis purposes.[2] The cell-based SPR sensors are desirable due to intrinsic property of the sensors and many exciting potentials for exploration towards new biomedical fronts. Because SPR is a surface sensitive method, it is usually useful for the studies quantified by cell-substrate interaction of adhered cells. For example, SPR response to cell attaching and spreading processes, and cell attachment area as the result of the cells responses to biological and chemical stimuli.[3-5] However, the actual mechanism of how the physical alterations of the cells affect influence SPR signal still remains elusive. There is limited literature on SPR detection of whole cells. One study relates the change of density on the sensor chip to the increase after the stimulation.[6] SPR was also used to study morphological changes of cells in response to stimulation agents or cell death inducers.[4, 7]

In more recent studies, the cell-based SPR began to include the influence of cell refractive index in explaining the SPR responses. A study showed that the intercellular

cell components such as the membrane and nucleus possess a different refractive index.[8] It was also found that cellular refractive index is distributed throughout the cell body and values vary at different stages of cell death.[9] The influence of refractive index in cell bodies to SPR signal was demonstrated in a study where the SPR signal increases when the volume of the cell decreases as the cytoplasmic concentration increases leading to increase in the refractive index.[10] The same conclusion was made by a study of exocytosis of cells , where the shift of resonance angle was observed due to elevated concentration of secretory vesicles close to the cell membrane.[11]

In this study, we systematically investigated the SPR response to cell size, deformity and detachment, by relating SPR signal to the percentage of the surface of a substrate that is covered by adherent cells, known as cell confluency. Conventionally, the changes in cells after activation by molecular stimuli are often evaluated through changes in cellular morphology such as cell spreading, contraction, shrinkage and swelling, which are observed through a simple confocal and/or fluorescence microscopy, or through more sophisticated and quantitative microscopy techniques.[12,13] However, microscopy techniques are limited by the resolution and are therefore unable to observe changes on the cell-substrate interface of adhered cells without being destructive to the cells. Therefore, a surface sensitive method, such as SPR, is a good alternative approach for quantifying cell confluency because it is sensitive enough to measure changes around the cell membrane adhered on the substrate. To further investigate this technique and to potentially improve the current status of cervical cancer therapeutic treatment, we choose to apply SPR analysis

to the morphological features of HeLa cells during cell death and the mechanism of cell death induced by hydrogen peroxide (H_2O_2).

In 2018, a total of 570,000 cases and 311, 000 deaths were estimated for cervical cancer, making this disease the fourth most frequently diagnosed and leading cause of cancer death in women.[14] Current treatments for cervical cancer include surgery, radiation and chemotherapy, and follow-ups after treatment are required to check for recurrences and to screen for possible complications.[15] Most clinical trials for patients with cervical cancer involve development of drugs that induce apoptosis, a type of cells death.[16] Thus, recent advances in cervical cancer studies have mainly focused on identifying agents that can selectively induce cytotoxicity and stimulation of apoptosis caused by anticancer agents. In laboratory practices, cell-based assays are used as indicators of therapeutic efficiency, which is determined by measuring cell viability, cell proliferation, cytotoxicity, induction of apoptosis, and cell cycle arrest, and these methods are essential in early stages of anti-cancer drug development.[17] The most commonly used assays include MTT assay,[18] TUNEL assay, [19] and LDH Cytotoxicity assay,[20] which measure cell metabolism, DNA fragmentation and cell cytotoxicity, respectively. A study using SPR was reported to predict the efficacy of cancer drugs on human pancreatic cancer cells. The results showed a decrease of SPR signal as the percentage of cell viability increases.[21] They hypothesized that the change of SPR signal was a result of decreased inner mitochondrial membrane potential. However, no relationships between the results and the biophysical cell-substrate interaction were determined.

The process of apoptosis has a unique biophysical cell-substrate interaction and therefore offers an alternative detection method other than the cell-based assays. Cells can undergo apoptosis through two apoptotic pathways; the death receptor pathway or mitochondrial pathway.[22] This process of programmed cell death is characterized by distinct morphological characteristics such as cell shrinkage, cell rounding, membrane blebbing, chromatin condensation and nucleus fragmentation. With cell shrinkage, the cells are smaller in size and the apoptotic cell appear round. For adhered cells, the size change is a direct measurement to surface area or confluency. Other than cells size, the shapes and thickness of apoptotic cells can be observed by light and electron microscopy[23] and recently by atomic force microscopy (AFM).[24] However these methods require pre-treatment and destructive to the cells.

Our cell model system, HeLa, was derived from cervical cancer cells taken from a patient who died of cervical cancer. It was initially used for cancer research, but more discoveries on the cell have led to many important researches in biological science due to its immortality when given nutrients and a suitable environment.[25] Hydrogen peroxide, as a reactive oxygen species (ROS), induces apoptosis in HeLa cell through the intrinsic mitochondrial pathway by several proposed mechanisms. Studies suggested apoptosis induced by H_2O_2 is mediated by decreased superoxide (O_2^-) concentration[26] and by activation of p73 pro-apoptotic genes, which triggers apoptosis in response to DNA damaging agents.[27]

The morphological analysis of HeLa cells under the growth phase and apoptosis have been examined by SEM, phase contrast, and fluorescence microscopy, showing that

control interphase HeLa cells have a polygonal shape while mitotic cells are spherical in shape and have a smooth surface (Figure 4.1).[28]

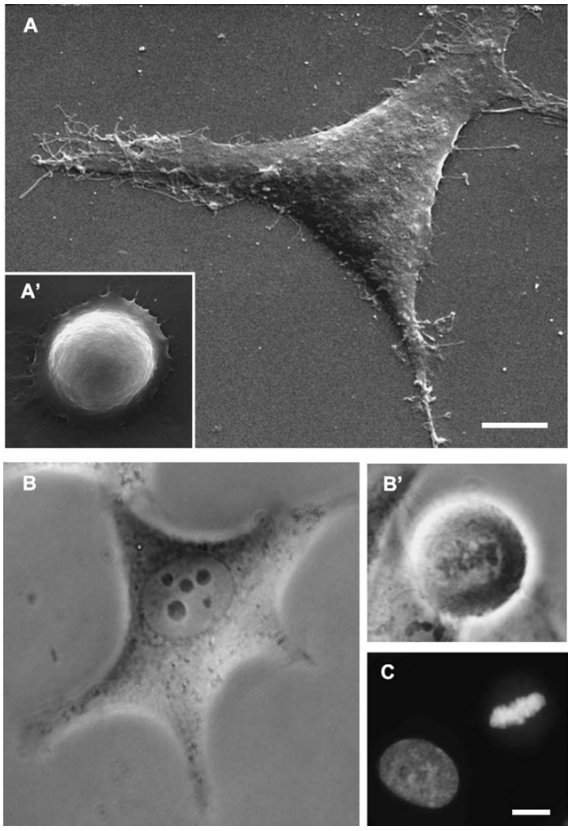

Figure 4.1 Different morphologies of HeLa cells observed either by SEM (A, A′), phase contrast microscopy (B, B′); or fluorescence microscopy (C). Reprinted from Ref. 27, Copyright 2005, with permission from Springer

In contrast, apoptotic HeLa cells exhibited rounding, shrinkage, and severe blebbing of the plasma membrane.[28] As shown in Figure 4.2, early apoptotic cells lose plasma membrane connection with neighbor cells before the detaching process, and

eventually, detached cells appear to float in the culture medium. Apoptotic HeLa cells also demonstrated a reduction in cell density and rounded shrunken cells.[29]

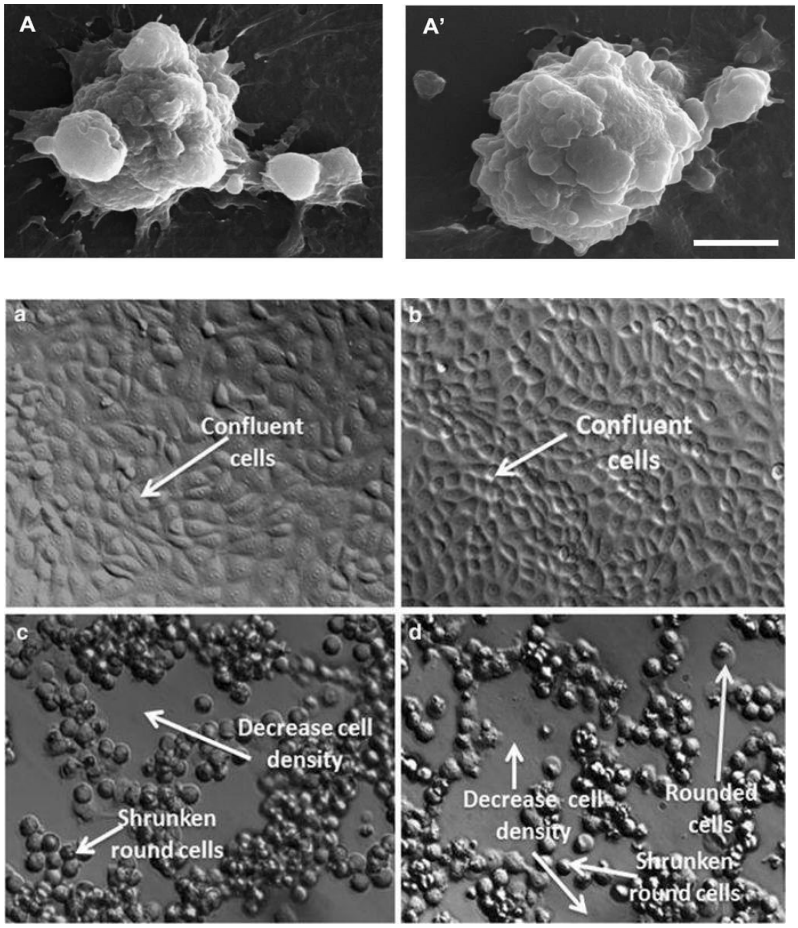

Figure 4.2 Top: SEM images of apoptotic HeLa cells. Edited from Ref. 27, Copyright 2005, with permission from Springer (top) and Ref 28 (bottom)

The ability of SPR to detect and quantify morphological characteristic of cells is very useful for diagnosing cancer and in studying the efficiency of anticancer drugs. For the diagnosis, cancer cells can be detected and classified by the specific features including the shape and size, and the distribution of the cells.[30] This is useful when comparing the

normal, pre-cancer and malignant cells, as demonstrated in studies of breast cancer[31, 32] and cervical cancer[33]. Moreover, SPR does not require the cells to be fixed to preserve the cells, compare to other microscopic methods. However, the physical features more related to SPR capability are the cell-cell and cell-substrate interactions. For example, cancer cells often become disordered, and less adherent to the other cells and to the extracellular matrix, [34] which cause the changes in confluency and optical properties on the interface, both are measurable by SPR.

In this work, the change of SPR response towards HeLa cell morphological changes on the sensor chips was studied (Figure 4.3). Experimentally, HeLa cells were cultured on SPR chips until 80% to 100% confluent monolayer was achieved. SPR measurements were then carried out with injection of different concentrations of H_2O_2 where the signals changes were observed until stabilized. Another set of chips were prepared in a six wells culture plate where the same H_2O_2 treatments were performed and the cells images were taken using a microscope. The SPR sensorgram results were then compared with cell confluency data after the images were processed with Image J.

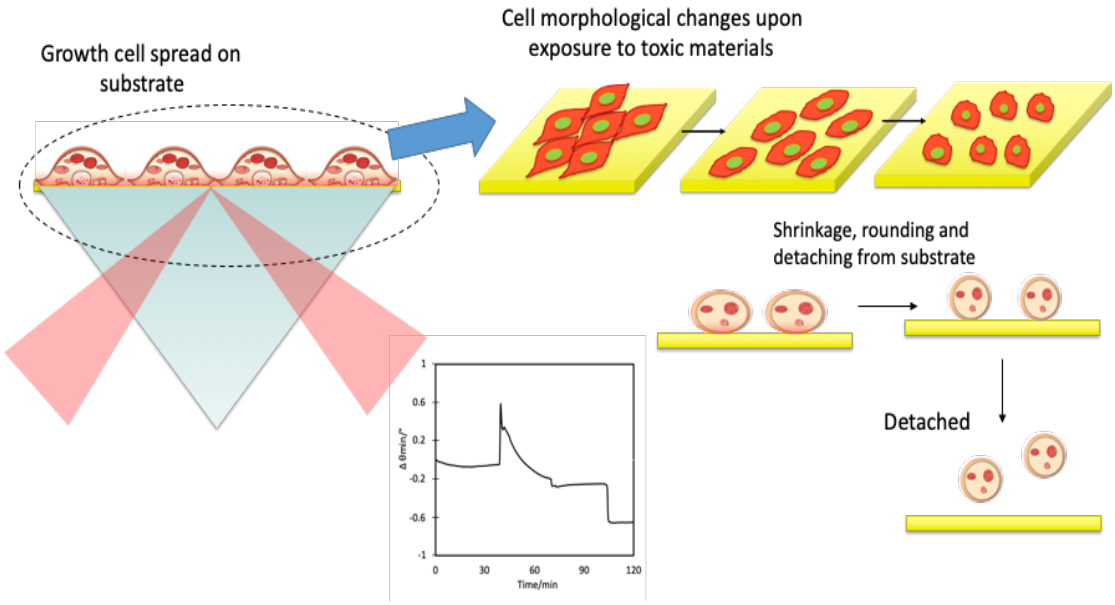

Figure 4.3 SPR measurement to measure resonance angle towards cell morphological changes on sensor chip

4.2 Experiment Section

4.2.1 Materials and Solutions

The human cervical cancer HeLa cell line was purchased from American Type Culture Collection (ATCC) and cryopreserved in a liquid nitrogen storage until use. The cells were grown in Dulbecco's Modified Eagle Medium (DMEM) (1X) supplemented with 10% fetal bovine serum (FBS) from Gibco. Cells were cultured at 37°C, 5% CO_2 in a humidified incubator. Cells were harvested every 2 days by standard trypsinization (0.05% Trypsin-EDTA (1X) from Gibco) to suspend the cells. To prepare the running buffer for SPR, the HEPES-buffered salt solution (HBSS) was chosen, as this buffer is recommended

to keep the cells viable for longer time at room temperature without CO_2 supply. The buffer contains 10 mM HEPES, 150 mM NaCl, 5 mM KCl, 1.2 mM $MgCl_2$, 2 mM $CaCl_2$ and 10 mM D-glucose, pH 7.4 adjusted with NaOH [11]. The buffer was filtered, degassed and autoclaved before use. For cell culture and SPR, the sanitization was done using 70% ethanol spray.

4.2.2 Apparatus

For cell culture, a Class II A/B3 biological safety cabinet, Fisher Scientific ISOTEMP 205 water bath, Pelton & Crane Validator 8 autoclave, CF-80-1 electronic centrifuge, Fisher Scientific CO_2 incubator and Kenmore lab refrigerator were used. Microscopic imaging was done with Omano microscope with AmScope digital camera. The refractive index of various liquid solutions was measured with American Optical ABBE refractometer. SPR data was measured with NanoSPR 3 (Addison, IL) with 650 nm GaAs semiconductor laser light source and Orion Sage syringe pump. Nanopure water ($\geq$ 18 MΩ.com), purified through a Barnstead E-Pure filtration system (Thermo Scientific, Rockford, IL) was used for all reagent preparations and rinsing.

4.2.3 HeLa cells reactivation and seeding

A vial of cryopreserved cells from liquid nitrogen storage was thawed in a 37°C water bath, just until ice is no longer visible. The entire content was transferred into a 15-mL conical centrifuge tube with 3 mL growth medium (DMEM supplemented with 10% FBS). Then, 1 mL of the medium was added into the cell vial, rinsed and added into the centrifuge tube. This step was repeated several times to make sure all content from the cell

vial was transferred into the centrifuge tube. Once transferred, the cells were centrifuged at 4000 rpm for 10 min. After that, remove supernatant was carefully removed from the centrifuge and disposed accordingly. The cell pellets were resuspended in a culture flask filled with 7 mL growth medium, added into culture flask (Figure 4.4) and the suspension was checked under microscope to ensure the cells were uniformly distributed. Finally, the cells were kept in a 37^{o}C, 5% CO_2 humidified incubator.

4.2.4 Culturing of HeLa cells

HeLa cells, pre-incubated in a culture dish, were harvested at about 80% confluence. A buffer exchange was performed by first discarding the growth medium from the culture flask. Cells were detached from the culture flask by a standard trypsinization protocol. For this purpose, 2 ml of 0.05% trypsin was added into the culture flask and placed in incubator to allow the trypsin to work. The flask was inspected microscopically every minute until the cell is slightly detached from the wall and appeared rounded. Once the cells appeared detached, the trypsin was removed from the flask. Then, the flask was rinsed by pipetting 5 ml medium over the cell layer surface with several times to ensure sure the cells is transferred and dispersed into the solution. Then, 2 ml of the cell suspension was transferred into a new culture flask and then resuspended in a 5 ml of fresh medium. The cells were kept in incubator and subcultures of confluent cells were performed every 1-2 days.

4.2.5 Culturing of HeLa cells on SPR chips

Gold chips from glass slides were fabricated with layers of e-beam deposited 4 nm Chromium and 50 nm gold, using the cleanroom facility at the UCR. Prior to use, the chips were rinsed with the Nanopure water, pure ethanol and air dried. gold chips with DIW, pure ethanol and air dry. Next, the chips were sterilized by UV radiation overnight. For cell culture, the chips were immersed in 8 ml of culture medium using 6 well cell culture plate (Figure 4.4). For cell suspension preparation, HeLa cells were removed from culture flasks by trypsinization, suspended in 8 mL of culture medium. A 2 mL of this cell suspension was transferred into a new culture flask, followed by adding 5 mL of culture medium. One mL of the suspension and 3 mL of culture medium were added into each well. The wells content was inspected under microscope for uniform distribution of cells. The chips were kept in the incubator for 1-2 days until their surfaces were covered with ~80-100% layer of cells, prior to use for SPR.

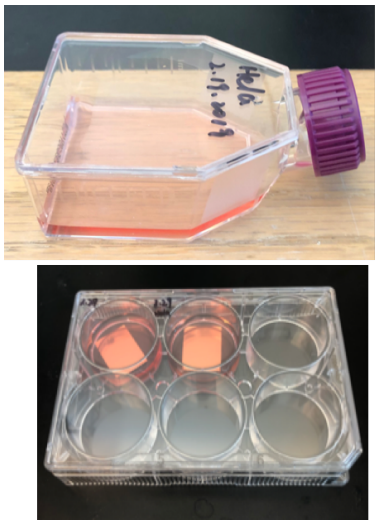

Figure 4.4 Culture flask and 6 well culture plate for cell culture

4.2.6 SPR measurements

The measurements of SPR signal response to HeLa cells death were performed on the NanoSPR instrument equipped with a PlasmonSerial software that provides the reflectivity curve and sensorgrams of the real-time minimum angle. The running buffer in which the chips were immersed when are not exposed to H_2O_2 solution, in this study being the HBSS, also functioned to rinse the solution off the surface before the next solution is introduced. The syringe pump controlled the buffer flow speed and was used to set the pump on pause for incubation purpose. All SPR measurements were done at room temperature. Prior to measurements, the microfluidic systems consist of the chambers and inlet/outlet tubing, the injection ports and the device accessories were sterilized by flowing 70% (v/v) ethanol for 30 min and then rinsed with HBSS. The cell coated chips were transferred immediately from the incubator to the SPR using a pre-sterilized tweezers. The back side of the chips were cleaned with 70% ethanol and water, followed by applying a thin layer of refractive index matching liquid (n = 1.517, Cargille Laboratories New Jersey), before the chips were placed on top of a BK7 prism. The flow cell consists of two 30 μL flow channels (Figure 4.5) was attached afterwards, and the buffer flow were run for 30 min to obtain stable baseline, before injection of H_2O_2 at a flow rate of 5.0 mL/h. The signal was monitored until no further increase or decrease for at least 40 min before the flow pump was turned on for rinsing. After the measurement was completed, the outlet was disposed in a biological container and the instrument parts were cleaned with 70% ethanol.

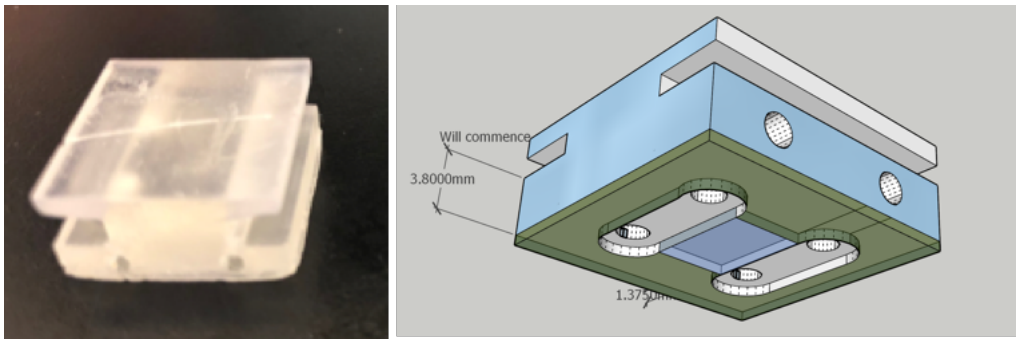

Figure 4.5. SPR flow cell in actual image and schematic drawing showing the bottom structure

4.2.7 Microscope examination of the cell covered SPR chips

For relating SPR response to cell confluency, the microscope imaging was performed at the conditions and procedure replicating SPR experiments. All cells covered chips were examined for cell viability and confluency using microscopy prior to SPR measurement and when the cells were exposed to different concentrations of H_2O_2. The chips were removed from incubator and were placed in a 6 well plate staged on the microscope platform. A 5 mL of HBSS buffer was added into the wells and was left for 30 min. The cell images were taken at specific time intervals using the digital microscope camera before and after exposure to H_2O_2 at 25x magnification. To ensure accuracy, the images were taken at the same location on the chips.

4.2.8 Cell confluency measurement

The cell coverage on the chip was measured by Image-J. A calibration was performed using a stage micrometer prior to measurements. To quantify the fraction of covered areas, the cells boundaries were traced manually using the freehand selection tool to enable the image threshold function. Then, the particle analysis tool was used to calculate the percentage of covered area, which also represents the cell confluency. This method can also be used to determine cell number, cell density and cell shapes, which are another useful parameter in call-based assay and in estimation of adherent cell culture characteristics.

4.3 Results and Discussions

4.3.1 Characterization of the SPR system for monitoring living cells

To show that our SPR system can be applied to monitoring cell-surface interactions, we first investigated the SPR response of HeLa cells detachment form the gold surface using trypsin. In this preliminary study, 10 mM PBS (137 mM NaCl, 2.7 mM KCl, 10 mM Na_2HPO_4 and 1.8 mM KH_2PO_4) was used as the running buffer. From the sensorgram (Figure 4.6), the experiment channel where 0.05% trypsin (in PBS) was injected showed the signal rapidly decreases after 4 min into incubation. For comparison purposes, a time-lapse microscopic image was also captured on a separate setup that represents the timing procedure conducted on SPR. From the inserted image, at 4 min exposure to trypsin, the cell confluency decreases because the cells become smaller in size, as trypsinization

induces rounding up of HeLa cells that leads to detachment from the gold surface. [35, 36] The signal continued to decrease at a fast rate ($\Delta\theta = 1.0^{o}$) and then plateaued after the cells completely detached from the surface during the rinsing step, , as shown by the inserted image. In comparison, the control channel where PBS was injected instead of trypsin, the rate of decrease was smaller, even after rinsing; the cells maintained their shape and the signal decrease was caused by the change of refractive index from culture medium to PBS (Figure 4.7). After 20 min incubation with trypsin, the channels were rinsed with PBS. This result demonstrates that our SPR system is sensitive to changes in cell confluency and attachment, and the observed trends are in agreement with the results from the literature, where it was also demonstrated that the effective refractive index decrease as cells detach from their initial surface.[3, 11]

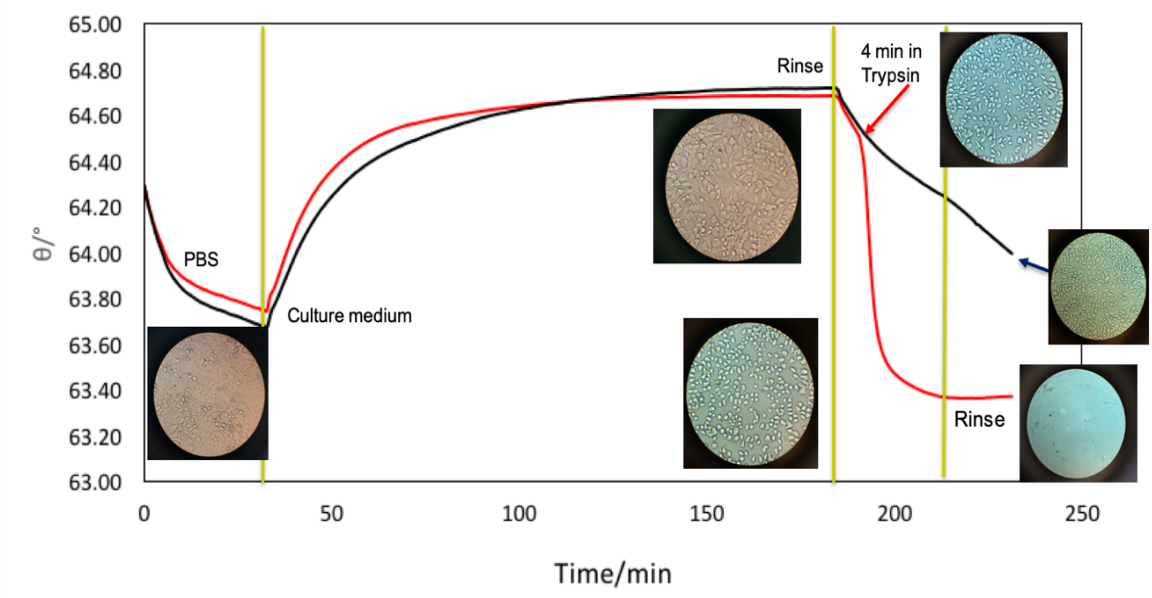

Figure 4.6 HeLa cell detachment progress monitored using SPR by the injection of Trypsin. After 30 min baseline, the culture medium was injected and incubated for 2.5 hrs. The 5 min wash was followed by Trypsin incubation for 20 min (red channel). After 4 min the cells started to shrink. Final wash with PBS removed the cells from the surface.

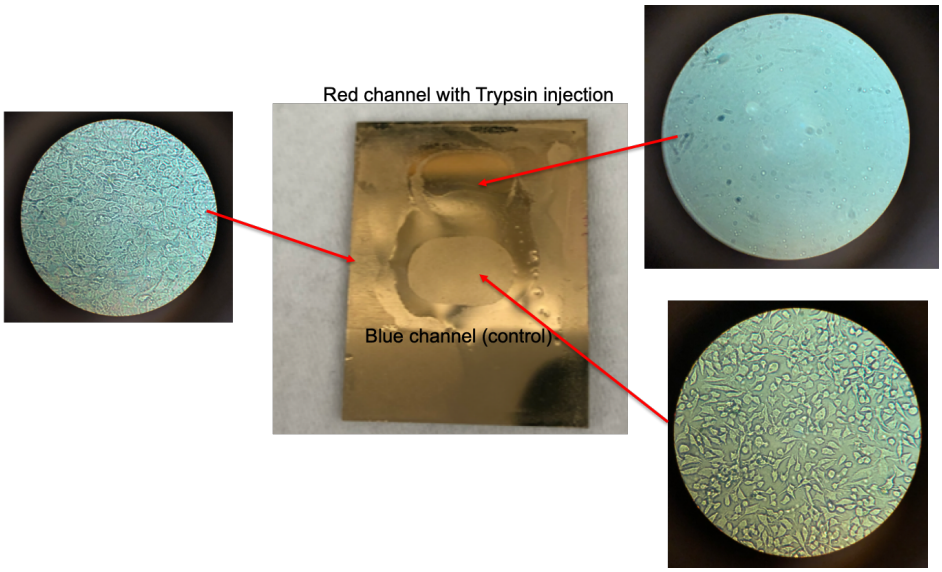

Figure 4.7. Analysis of sensor chip after SPR measurement showing the cells were removed from surface treated with Trypsin (top channel). The non-treated cells remained on the surface (bottom channel)

4.3.2 Microscopic images of cell morphology changes after exposure to H_2O_2

To quantify the cell confluency and to compare the microscopic images with our SPR signal, time-lapse imaging was collected for 0.1 M, 0.5 M, 1.0 M, 2.5 M and 5.0 M of H_2O_2 (Figure 4.8). The images show a decrease in the cell size and an increase in the amount of the intercellular space, due to apoptosis. The images were processed by Image J to calculate the total cell attachment area. For example, the cell confluencies extracted from the images of 1.0 M H_2O_2 were 82%, 60%, 50%, 45% and 40%, at 0 min, 30 min, 60 min, 90 min and 120 min, respectively (Figure 4.9). It can be seen that the confluency decreases with incubation time at the 1.0 M concentration.

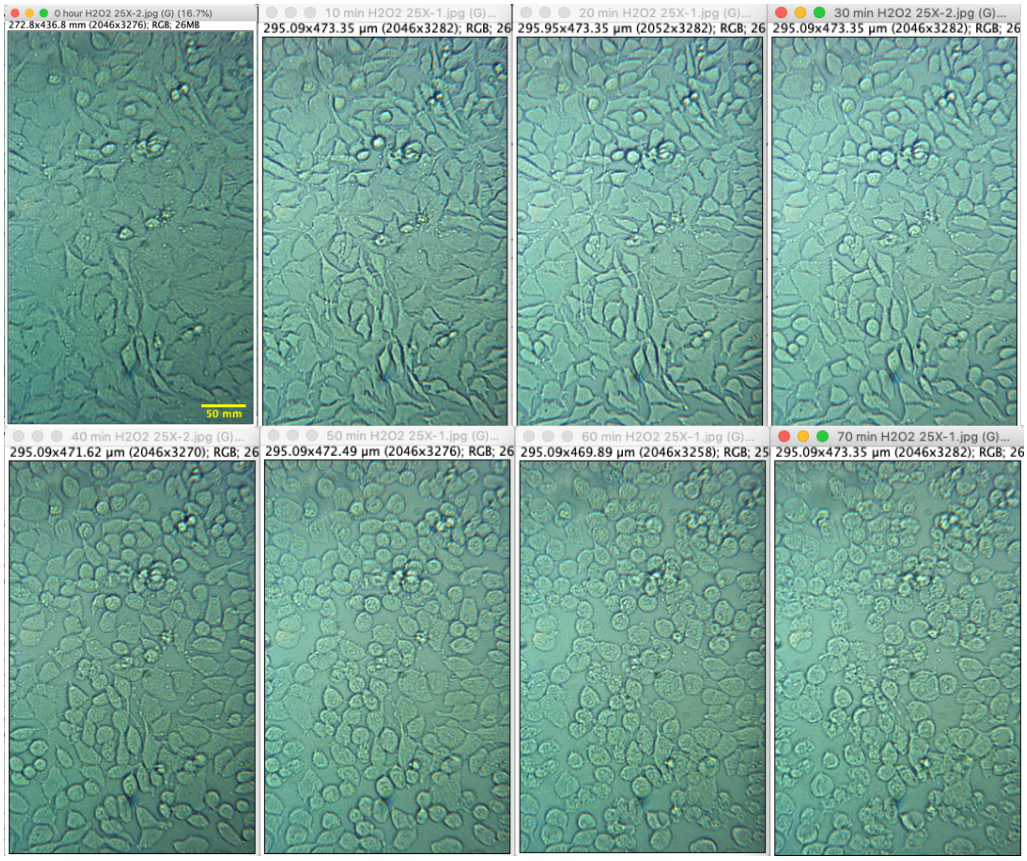

Figure 4.8 Time-lapse microscopic imaging (25x) of HeLa cells after exposure to 2.5 M H2O2. From the images, our HeLa cells grown to 30 – 40 µm in length at confluent.

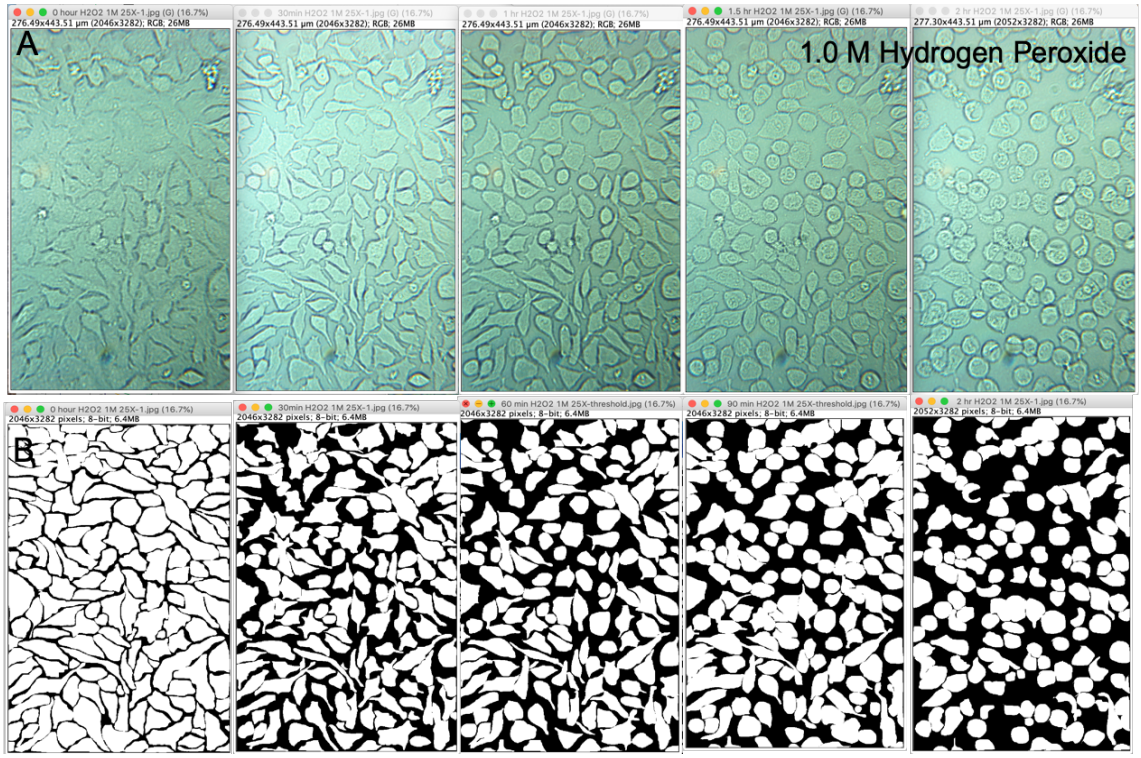

Figure 4.9. Images of HeLa cell after exposure to 1.0 M Hydrogen Peroxide (H2O2) and percentage confluency determination (A) Microscopy 25X and (B) Threshold analysis by Image J, the white spots represent the cells. 0 min (85%), 30 min (60%), 60 min (50%), 90 min (45%) and 120 min (40%)

4.3.3 SPR monitoring of cell morphological changes after exposure to H_2O_2

The cell morphology changes especially the reduced size due to shrinkage is a distinguishing feature of HeLa cell death induced by apoptosis. Therefore, cell confluency measurement could be used to evaluate the relationship between SPR response and HeLa cell toxicity. For the SPR measurements, one channel was dedicated as the experiment channel where the H_2O_2 was injected, which the other channel was the negative control channel that is without H_2O_2. The negative control is needed to confirm that the observed

changes were cause by direct stimulation by H_2O_2 and not by other factors such as temperature or the buffer flow shear. As shown on Figure 4.10 (top), after 50 min baseline, 1 M of H_2O_2 was injected into the experiment channel while HBSS was injected into the control channel. The change in SPR response after exposure to H_2O_2 was then monitored by SPR until 120 min after injection, when the flow pump was turned on for the rinsing step. From the sensorgram, a decrease in SPR response ($\Delta\theta = 0.3^o$) was observed for the H_2O_2 channel while the control channel remained steady.

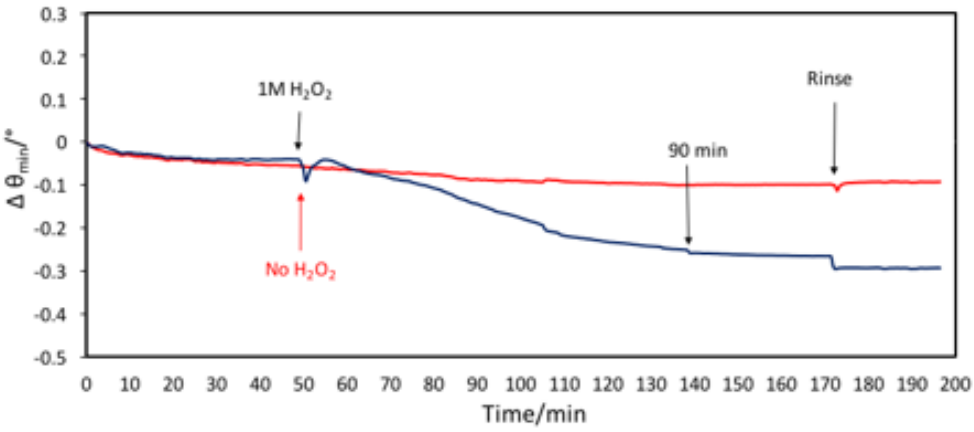

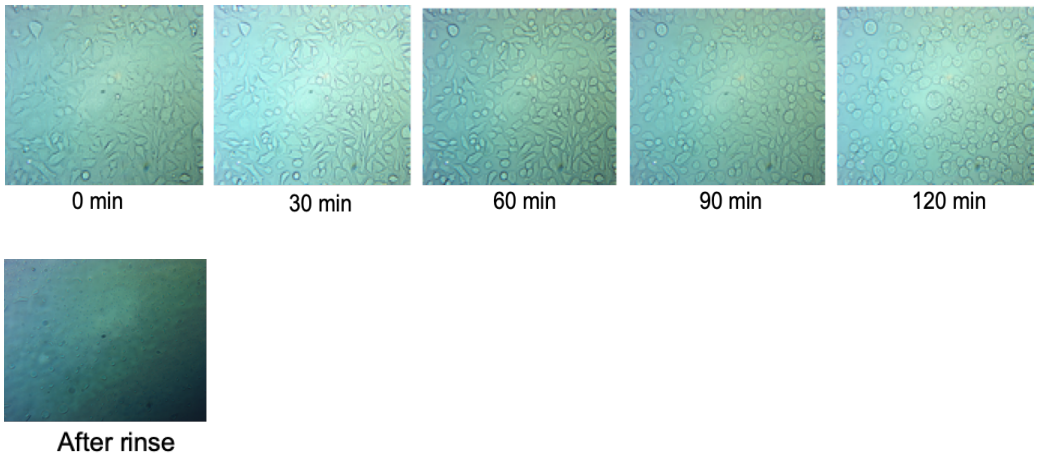

Figure 4.10. SPR sensorgram showing SPR response after injection of 1 M H_2O_2 (top) and microscopy images taken at corresponding times showing the progression of cell size after the stimulation (bottom)

Throughout the experiments, another chip with confluent HeLa cells was placed on a petri dish on the microscope platform. A picture was taken before 1 M of H_2O_2 was injected into the petri dish. Microscopic images were taken every 30 min and rinsed at the end point, for the 1 M concentration, as in Figure 4.10 (bottom). The images were analyzed using Image J to calculate confluency and were used for the next analysis. However, even without additional analysis the decreased confluency over time can be visually observed. Next, the experiments were repeated for different concentrations of H_2O_2, the results were summarized in the same plot (Figure 4.11). From the results, 0.1 M of H_2O_2 has the least effect on HeLa apoptosis as the signal is nearly unchanged after injection. For other concentrations, a significant decrease in SPR angle shift was observed; 0.2^o, 0.3^o, 0.5^o and 0.9^o for 0.5 M, 1.0 M, 2.5 M and 0.5M, respectively. Higher concentration of H_2O_2, starting from 2.5 M caused formation of air bubbles inside the channel, which were removed by tapping the flow chamber, as depicted on the plot by a sharp drop at 20 min and 30 min for 2.5 M and 5.0 M, respectively. At the 5.0 M concentration, the SPR response decreased at

a fast rate and achieved a steady signal after 25 min. After 60 min, the flow pump was turned on causing drastic signal drop when all cells were detached from the surface. These results confirm that higher concentration of H_2O_2 lead to a stronger toxicity effect to HeLa cells and that the system is sensitive to the concentrations.

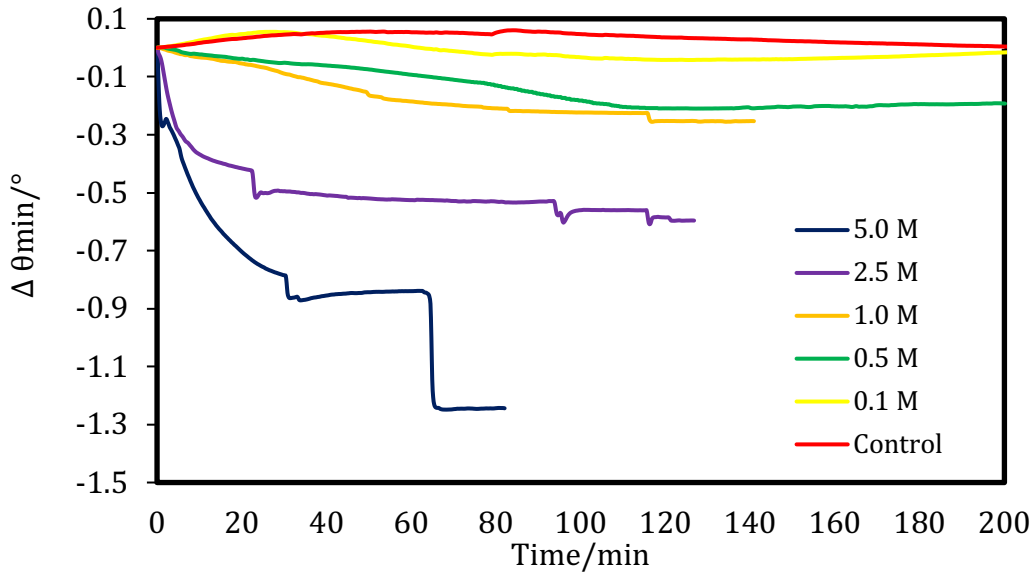

Figure 4.11. SPR sensorgram showing signal change when HeLa cells were exposed to different concentration of H_2O_2

4.3.4 Relationship between SPR signal and cell confluency

To evaluate the correlation between SPR response with the changes in cell confluency, the data of each H_2O_2 concentration were plotted on a same graph (Figure 4.12). The results show that a decrease in cell confluency leads to a decrease in SPR angle shift, $\Delta\theta$. The magnitude of the changes increase as the concentration of H_2O_2 increases, as expected. We also observed the slope of the line, representing the rate of the changes,

were higher at the beginning of the measurements for all concentrations. The shape of the curves for SPR response and cell confluency closely match at lower concentrations, which means that the correlation becomes weaker at higher concentrations. A possible reason could be SPR is a more sensitive method than microscopy, taking into consideration the change of the effective refractive index on the substrate surface.

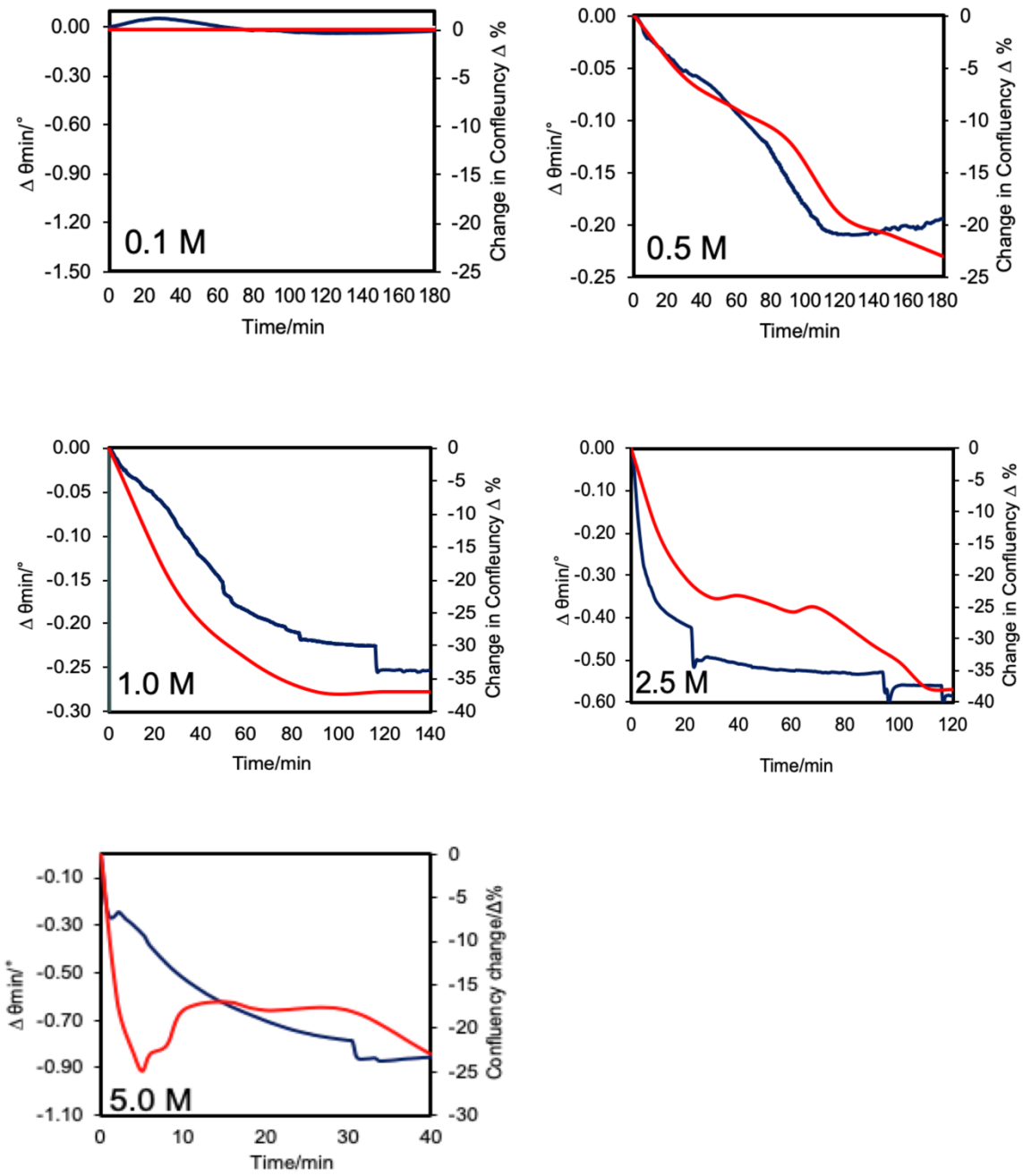

Figure 4.12 Correlation between SPR response (blue line) and cell confluency (red line)

The same observation was reported in a study of cell confluency during HeLa cell attachment and spreading,[3] where the SPR results were much lower than cell confluency by microscopic imaging, although the overall trends were similar. They postulated it was because cells attached to the substrate with gaps in the cell-substrate contact, therefore the effective attachment area detected by SPR was less than the imaging attachment contour area. Nevertheless, our SPR results shows very good correlation with cell confluency at very low concentrations (0.1 M to 1.0 M), while the change of cell confluency was not as drastic at higher concentrations.

4.3.5 Explaining the abnormal behavior at high concentration of H_2O_2

From the results, HeLa cells exposed to 5.0 M H_2O_2 exhibits different behavior between SPR signal and cell confluency compared to the lower concentrations. At 5 min exposure time, the SPR signal keep decreasing while the confluency increases then decreases again at 30 min. The microscopy images of HeLa cells induced with 5.0 M H_2O_2 (Figure 4.13, top) where the confluency data extracted using Image J (Figure 4.13, bottom), showed the confluency decreased from 90% to 34% in 5 min, then increased and stabilized around 43% before decreasing to 37%. This indicated cell shrinkage occurred in the first 5 min before the cells underwent swelling that increases confluency and then reducing in size again. This trend can be explained by cell death mechanism induced by H_2O_2, according to literatures that high concentration of H_2O_2 induces necrosis, whereas low concentration induces apoptosis.[28, 37, 38] For HeLa cells, it was reported that 0.1 M of H_2O_2 induced

necrosis[28] and 125 μM induced apoptosis.[27] For our study, cell death by necrosis was achieved at 5.0 M and we did not have data to show whether necrosis happened at lower concentrations than 5.0 M. Necrosis, refers to the degradative processes that occur after cell death and does not follow the apoptotic signal transduction pathway.[22] Necrosis usually happens following apoptosis but can also occur simultaneously depending on factors such as the intensity an duration of the stimulus.[39] Necrosis is distinguished from apoptosis by the different in morphological changes, as observed by cell swelling, loss of membrane integrity and possible release of the cytoplasmic contents into the surrounding.[40, 41] Our results indicate that apoptotic cells during 2 min exposure to H_2O_2 exhibited cell rounding, shrinkage and detaching. In 4 min, the cell membrane started to disintegrate, and the cell inner body began ruptured, indicating early necrosis, while some cells remain apoptotic. After 6 min we observed cell swelling and the number of necrotic cells increased (Figure 4.14).

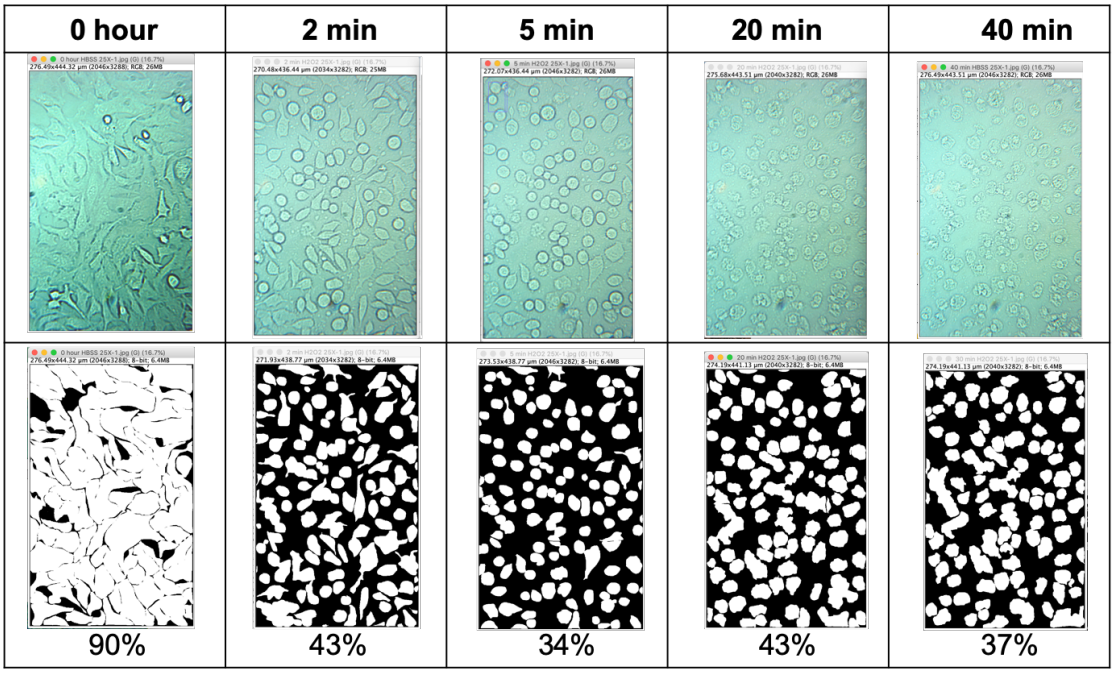

Figure 4.13. HeLa cells exposed to 5.0 M H_2O_2 over time. The upper images are the original images and the lower show processed threshold images by Image J with the respective percentage confluency

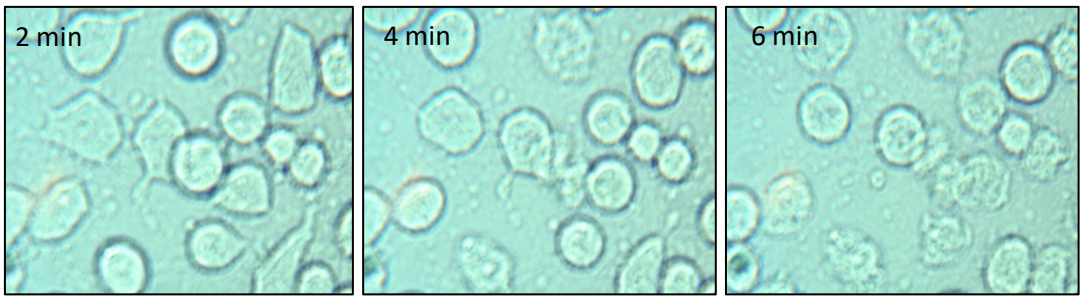

Figure 4.14. Analysis of HeLa cells apoptotic and necrotic features induced by 5.0 M H_2O_2

This observation was in agreement with results reported in a study that distinguished cell death induces by apoptotic and necrotic treatment of HeLa cells.[28] In the study, necrotic cells were characterized by loss of membrane integrity, as well as cytoplasmic damage during early necrosis, followed by uniform condensation and fragmentation of the

chromatin (Figure 4.15). In the late stage of necrosis, cell flattening occurred and eventually the cell body completely detached while some debris remained on the surface. The complete detachment of the cell bodies may be the reason for decreased cell size at the end of necrosis, leading to decreased confluency. Even though we were able to validate the trend in cell confluency induced by 5.0 M H_2O_2, the reason why SPR does not respond with the same trend remained unexplained. Clearly, the combination of different morphological features of apoptosis and necrosis are affecting SPR response, which provoked us to reexamine the biophysical changes on the cell-substrate interface, as these contribute more toward changes of SPR signal than the cell morphology.

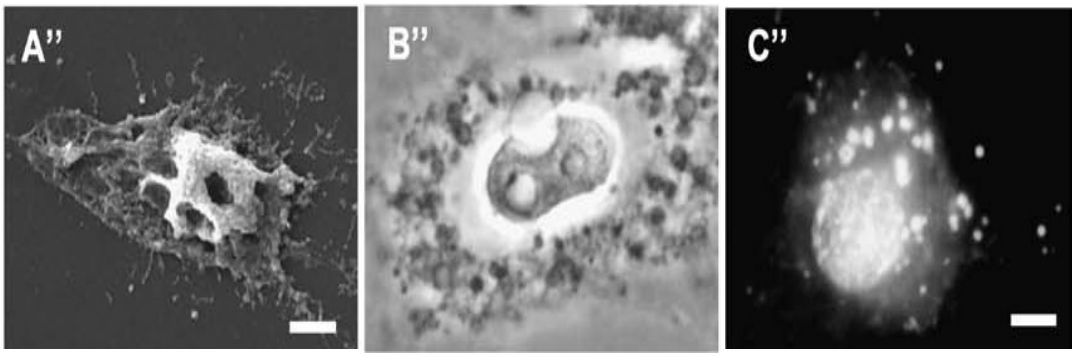

Figure 4.15. Microphotographs of HeLa cells showing that characterize the cell death in early (A", B") and late (C") necrosis. Edited from Ref. 27, Copyright 2005, with permission from Springer

4.3.6 Mathematical modelling of SPR response

A mathematical relationship between the SPR signal and the adsorbed film thickness and coverage was previously established based on the effective refractive index model.[42] This model allows quantitative analysis to predict the response of an SPR sensor when molecular or adsorbate (for example thiolate, protein and cell monolayer) binds on

an SPR surface and the adsorbate has a different refractive index from the bulk solution. The theoretical description for the SPR signal response to a bulk solution and a uniform layer of adsorbate**,** is shown in Figure 4.16, where R is the SPR response as the shift in angle ($\Delta\theta$), $\Delta\eta$ is the change in the refractive index, m is the slope of the calibration curve, which is also the sensitivity factor for SPR, η_s and η_a is the refractive index for the bulk solution and the film layer, d is the thickness of film and l_d is the characteristic decay length, which is 20 to 50% of the wavelength of light source used in SPR. The slope of the calibration curve was obtained by sequentially injecting 0.5 M, 1.0 M, 1.5 M, 2.5 M, 3.0 M and 5.0 M NaCl solutions, and each injection was separated by a buffer wash. A graph of SPR response vs. bulk refractive index of the solutions was plotted to determine the dynamic range of the SPR system, allowing the m value to be obtained by fitting into the model equation. It can be seen from Equation 2 that the SPR response is determined by the refractive index of HeLa cell intracellular fluid and the bulk solution, and the thickness of the cell layer.

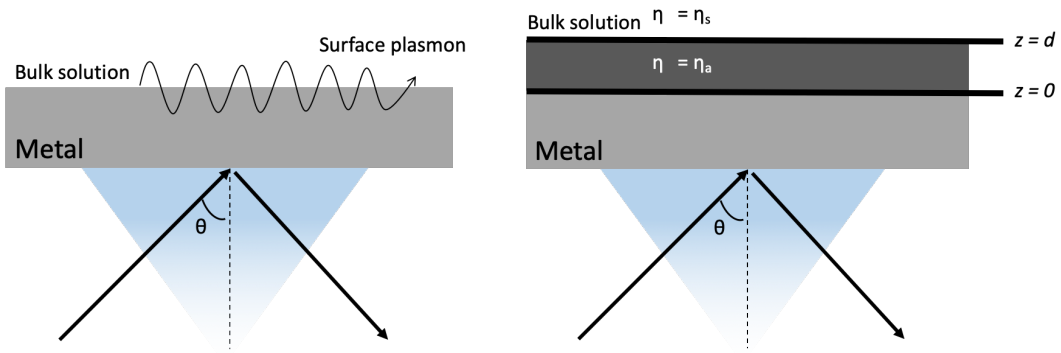

(a) (b)

$$R = m\,\Delta\eta = m\left[\eta_{final} - \eta_{initial}\right] \quad \text{Eqn. 1} \qquad R = m(\eta_a - \eta_s)[1 - exp(-2d/l_d)] \quad \text{Eqn. 2}$$

Figure 4.16. Schematic diagrams and corresponding equation of the working interface of a thin metal film in contact with (a) bulk solution *s* and (b) a bilayer structure consisting of a uniform layer adsorbate *a* and bulk solution *s* (edited from [42])

The accuracy and stability of our SPR measurements were verified by comparing the SPR angle measured for different buffers with the calculated values from the equation obtained from the calibration curve. The data were compiled in Table 4.1, showing good agreement between SPR angles obtained from experimental and calculated data, for different types of buffer solutions.

Table 4.1. Comparison of experimental and calculated SPR angle shift for different buffers

Bulk solution	**RI**	**$\theta_{calculated}$**	**$\theta_{experimental}$**
DIW	1.334	62.4°	62.3°
PBS	1.338	62.5°	62.6°
HBSS	1.338	62.5 °	62.8°
5.0 M H_2O_2	1.345	62.7 °	63.0°

4.3.7 The SPR response to a single adlayer of uniform thickness

For such structures as shown in Figure 4.16b, a thin film of uniform thickness *d* and refractive index of η_a is adsorbed to the metal surface of SPR chip, with a bulk liquid solution with refractive index η_s is above the layer, and the SPR response in angle shift ($\Delta\theta$) can be calculated using Equation 2. This equation was simplified from the estimation that the effective refractive index of the bilayer, η_{eff}, is the properly weighted average of η_a plus η_s. Other assumptions made in this model are that the evanescent electromagnetic field decays exponentially into this medium with a characteristic decay length, l_d, ~25-50% of the wavelength of the incident light, and the intensity of light is the field strength squared, so it decays with height z above the metal surface as $[\exp(-z/ l_d)]$.[2] The above assumption is valid for an SPR response that is linearly proportional to the change of refractive index over the range η_a plus η_s. For a nonlinear response, this relation is no longer valid and must be replaced with a different equation.

We then plot the curve of SPR response in $\Delta\theta$ as a function of adlayer thickness (of a confluent HeLa cells on a 50 nm gold chip in HBSS buffer) as predicted in Equation 2, for a particular value of *m*, η_a , η_s and l_d (Figure 4.17a) and plot the curve in SPR angle θ taking 62.8^o as initial angle when there is no cell layer on the surface (Figure 4.17b). From these plots, we can estimate the thickness of the cell layer from the measured and calculated SPR response. Based on our data, the measurable thickness of HeLa cells is less than 300 nm. In addition, we can see that after 400 nm the SPR response is no longer sensitive to the changes of the cell-substrate interface.

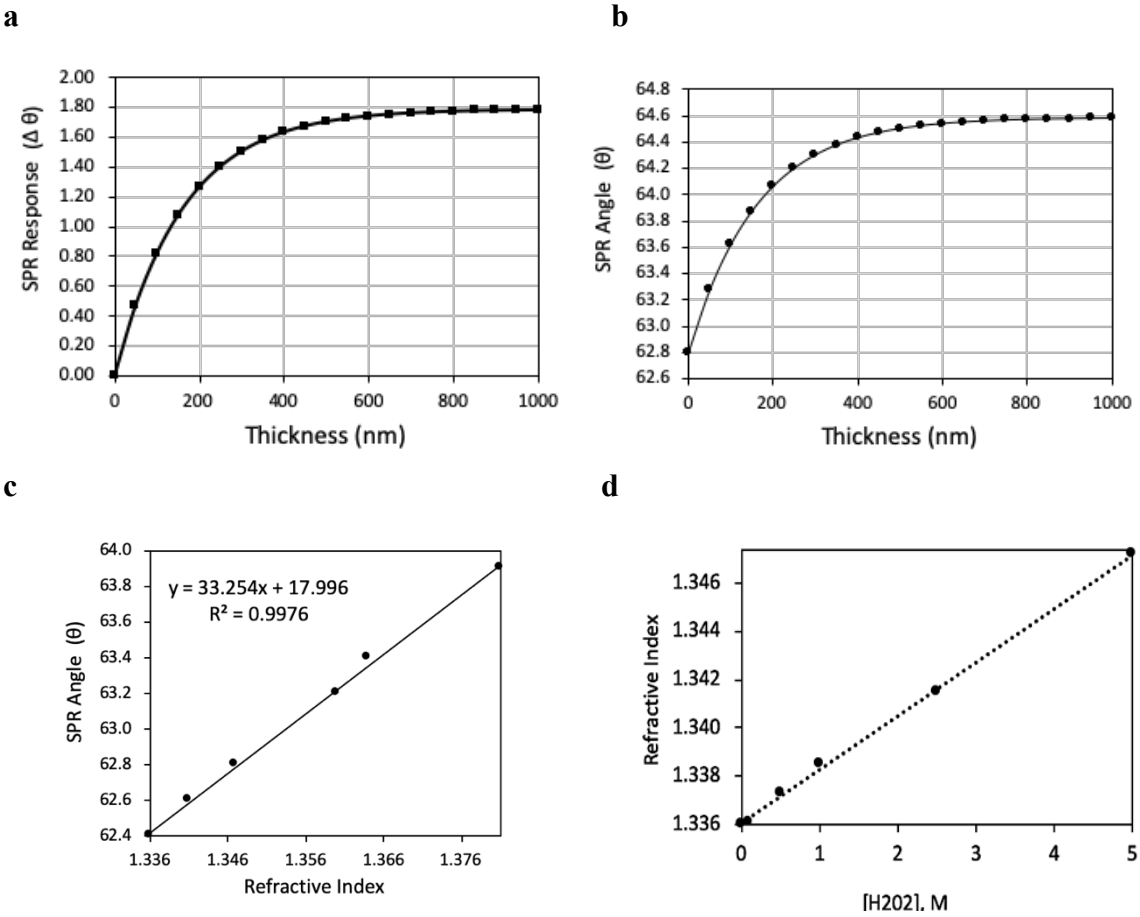

Figure 4.17. Calculated SPR response to thickness *d*, in angle shift (a) and in angle (b), for a bilayer of HeLa cells on gold chip in HBSS solution, as represented on Figure 18b, where η_a = 1.392, η_s = 1.338, λ= 650 nm, *l*d = 325 nm (50% of λ). The curve fitting is calculated using Equation 2 with *m* =33° per RIU as obtained from the linear calibration plot (c) using a bulk NaCl solution from η = 1.336 to η = 1.381 (0.5 M to 5.0 M). (d) Refractive Index of H_2O_2 (η_s) at different concentrations used in the calculations

4.3.8 Corrections for SPR response to include nonuniform coverage

Other than the calculation for uniform adlayer, our model also considers nonuniform coverage like the structure in Figure 4.18, where the adsorbate covers a fraction (*f*) of the metal surface with thickness of *d*. In this case, the SPR response is just *f*

times the response when $f = 1$, which is the response for uniform coverage calculated using Equation 2. We then used the correlation to calculate the SPR response as a function of percentage cell confluency (f). This assumption is valid for when the thickness, d, is less or about the same as l_d, which is true in our case. For a very small thickness, the response of nonuniform structure would be the same as uniform structure, while for a very large thickness it would give a complex SPR with a double minimum reflectivity curve, where any material further away from the metal surface does not contribute strongly to the SPR response.

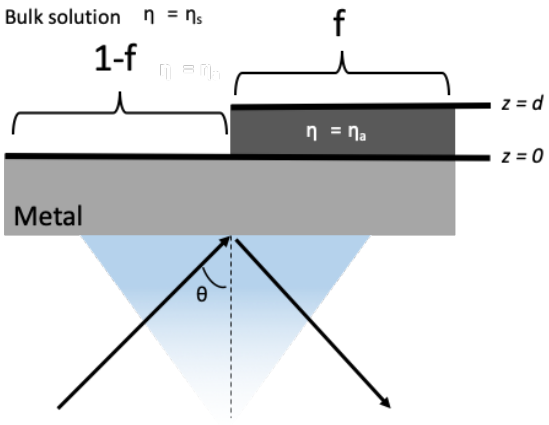

$$R_{\text{non-uniform}} = f \times R_{\text{uniform}} \quad \text{Eqn. 3}$$

Figure 4.18. Schematic diagram of a bilayer structure with a nonuniform coverage, adapted from ref 42

4.3.9 Comparison between measured and calculated SPR response to cell confluency

For this purpose, we calculated the SPR response over time for each H_2O_2 concentration, based on the confluency data plotted in Figure 4.12, and the combined sensorgrams are shown in Figure 4.19. The thickness of the uniform cell layer was determined from the SPR angle at baseline before H_2O_2 was injected and by using the angle-thickness data in Figure 4.17C. After the thickness was obtained, we were able to calculate the SPR response by Equation 2, which is the $\Delta\theta$ when $f = 1$. The data of $R_{non\text{-}uniform}$ are the response of $R_{uniform}$ times the percentage confluency, as indicated in Equation 3. Because the calculations are highly dependent on percentage confluency, the trend observed for the calculated response is the same as the confluency data, where the correlations are better at lower concentrations. An abnormal behavior was observed for 5.0 M H_2O_2, where the calculated response does not follow the experimental data after 5 min of exposure, with the signal increasing instead of decreasing.

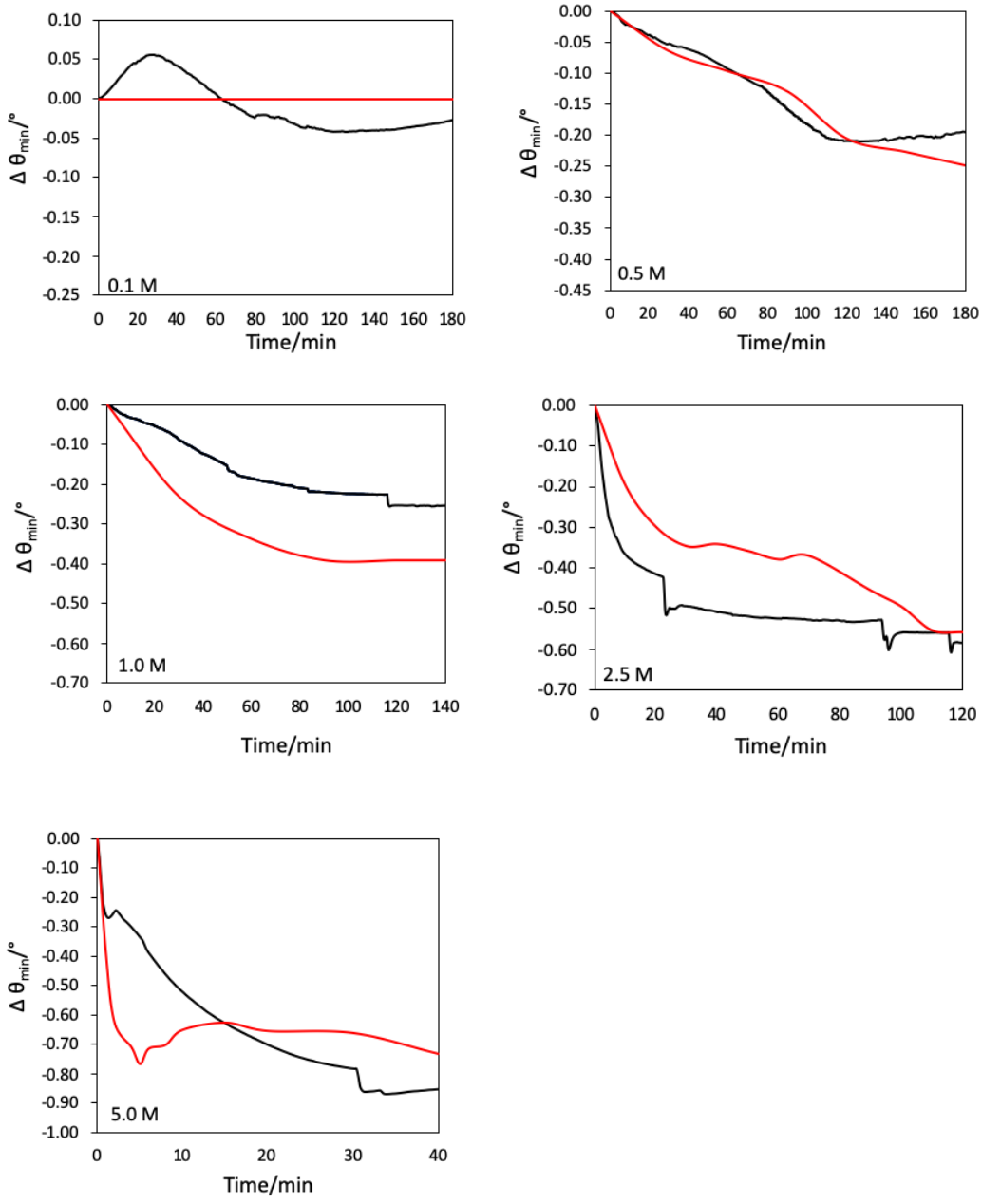

Figure 4.19 SPR experiment (black) and calculated (red). For the calculated SPR response, the refractive index of H_2O_2 solution used as following η_s of 1.3365, 1.3377, 1.3389, 1.3419, and 1.3476, for 0.1 M, 0.5 M, 1.0 M, 2.5 M and 5.0 M, respectively.

As discussed in Section 4.3.5, different morphological events occurred at high concentration of H_2O_2 caused by simultaneous apoptosis and necrosis. Necrotic cells are distinguished from apoptotic cells by the amount of cell swelling, as observed by the increased percentage of confluency after a 5 min exposure time. We investigated this further by visually differentiating necrotic from apoptotic cells using the microscopic images, and re-calculated percent confluency contributed by each condition. The results are shown in Figure 4.20, where we compared confluency of all the cells with confluency from apoptotic (A) and necrotic (N) cells. We observed the cells were all necrotic at 20 min (41% confluency) and possible apoptotic blebs detached from the surface and float into the solution, causing reduced confluency to 36% at 40 min.

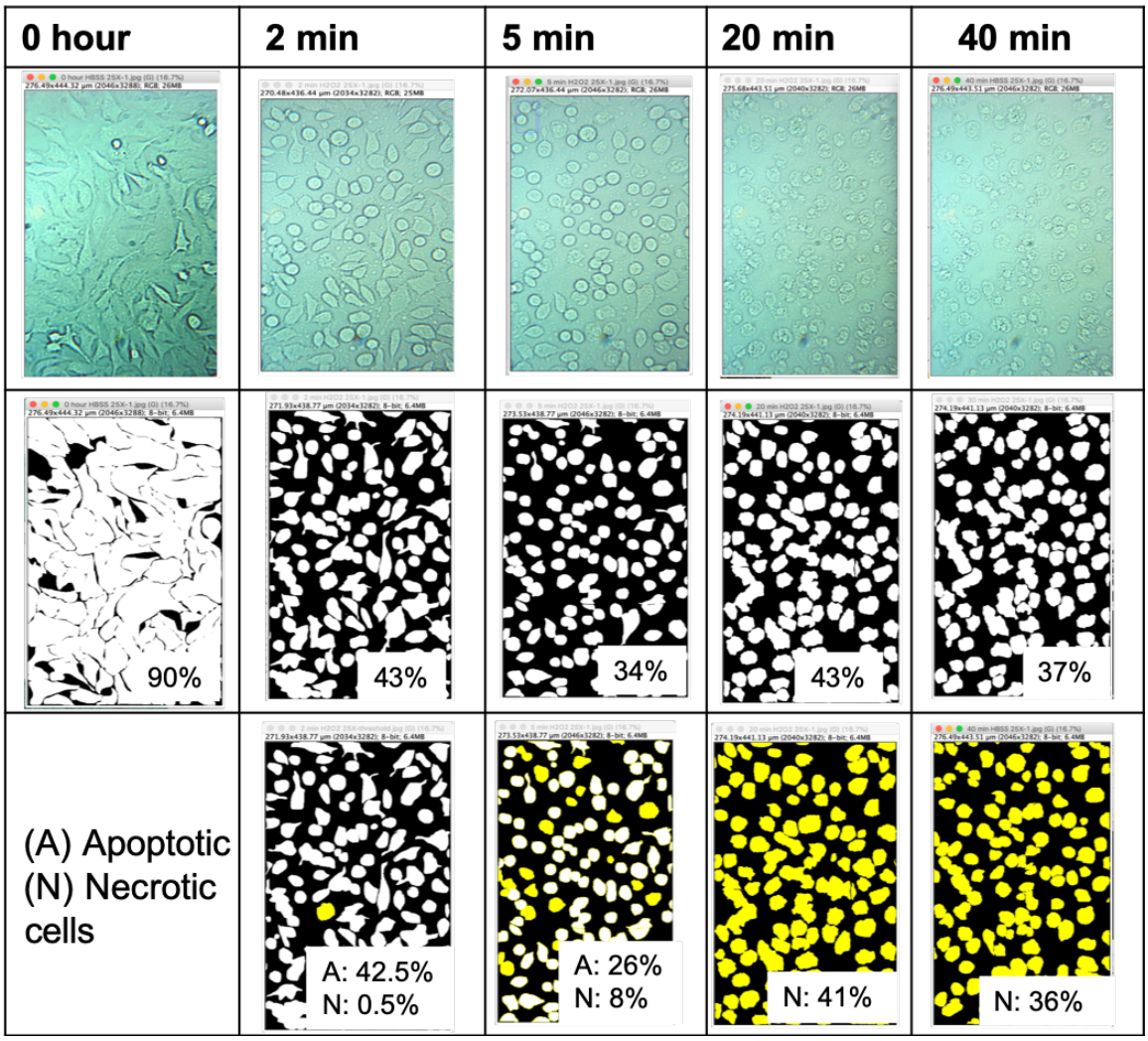

Figure 4.20 Cell confluency according to apoptotic and necrotic HeLa cells exposed to 5.0 M H_2O_2

In a study where HeLa cell morphological changes during apoptosis were observed using AFM,[24] the images provided a better understanding on the size and thickness of the cells at the death stages, which support our observations. During the cell death progression as reported in the paper, the cells initially shrank, and the thickness increased. This explains why confluency decreased initially, before increasing, as the membranes start to become

damaged followed by swelling. At this stage, the thickness keeps decreasing. As the blebs start detaching, the cells shrink again causing less confluency while the thickness increases. Evidently, there is a combination of size and thickness changes that were not able to be observed under the microscope but were detected by SPR due to the sensitivity of this method to minute changes on the surface. In addition, we found that the refractive index inside the cell body changes at different stages of apoptosis, and this change itself is a result of changes to the intracellular biochemical components and volume.[9] Therefore, in addition to cell thickness, the refractive index is also a variable that changes during cell death that directly change SPR response, as indicated in Equation 2. Furthermore, the derivation to achieve Equation 2 can be done in a more complex way for adlayer of cells, by factoring various cell shapes[43] in the formulation of the decay length, $l_{d,}$ instead of assuming the value to be 20% to 50% of the wavelength of the light source.

Although it is a challenge to establish a comprehensive theoretical model interpreting all SPR responses to cell morphological changes, further development is not impossible. A few studies have addressed quantitative issues to study SPR response in cell-based applications.[43-45] For example, a quantitative SPR was applied in a study of cells attachment, spreading and proliferation phase, by modifying the effective refractive index to include cell density and spreading area.[3] However, the experimental SPR response agreed well with the calculated response only in the spreading phase, while the magnitude is largely different in the proliferation phase. Therefore, a revised mathematical model with a better fit between experimental and calculated SPR responses would be desired.

4.4 Conclusions

In conclusion, we have validated the SPR study on the toxicity of cancerous HeLa cell induced by H_2O_2 by monitoring the changes in SPR signal in response to the change in cell confluency and cell detachment caused by the cell death mechanisms. Several important findings were achieved. First, when compared with the microscopic images, we found that SPR signal decreases with decreasing cell confluency after the treatment with H_2O_2. Second, the correlation was valid only at lower concentrations since 5.0 M concentration of H_2O_2 is not proportional to cell confluency because it induces apoptosis and necrosis simultaneously. Quantitative analysis of SPR signal in response to cell confluency was carried out to investigate other factors affecting the shift in SPR signal. The results verified the complexity of cell morphology that cannot be observed just by microscopy technique and that SPR is more sensitive to the changes on the cell-substrate interface. Although the mathematical model equation works in lower H_2O_2 concentrations, more complex derivations and simulation to solve complex mathematical models are needed. This is because cell activities change the morphology in many ways, including thickness of the cell layer, shapes, and refractive index in the cell bodies. Therefore, for more accurate interpretation, the mathematical equation has to include the non-uniform thicknesses, various shapes, and refractive indexes of cell intracellular. Although SPR will not replace conventional cell-based assay to monitor cell responses to biological and chemical stimuli, or cell death inducers, it provides simple screening tools and quantifiable measurements comparable to other methods. This method can find broad applications for

other living cells studies in medical fields, especially in anticancer drug development and clinical diagnosis.

4.5 References

1. Chen, S.; Zhao, M.; Wu, G.; Yao, C.; Zhang, J., Recent advances in morphological cell image analysis. *Computational and mathematical methods in medicine* **2012,** *2012*, 101536-101536.

2. Yanase, Y.; Hiragun, T.; Ishii, K.; Kawaguchi, T.; Yanase, T.; Kawai, M.; Sakamoto, K.; Hide, M., Surface plasmon resonance for cell-based clinical diagnosis. *Sensors (Basel, Switzerland)* **2014,** *14* (3), 4948-4959.

3. Deng, S.; Yu, X.; Wang, P., An irregular-shaped homogeneous refractive index model for interpretation of the surface plasmon resonance response from living cell attachment. *Analytical Methods* **2016,** *8* (16), 3301-3306.

4. Maltais, J. S.; Denault Jb Fau - Gendron, L.; Gendron L Fau - Grandbois, M.; Grandbois, M., Label-free monitoring of apoptosis by surface plasmon resonance detection of morphological changes. (1573-675X (Electronic)).

5. Yanase, Y.; Suzuki, H.; Tsutsui, T.; Hiragun, T.; Kameyoshi, Y.; Hide, M., The SPR signal in living cells reflects changes other than the area of adhesion and the formation of cell constructions. *Biosensors and Bioelectronics* **2007,** *22* (6), 1081-1086.

6. Chen, K.; Obinata, H.; Izumi, T., Detection of G protein-coupled receptor-mediated cellular response involved in cytoskeletal rearrangement using surface plasmon resonance. *Biosensors and Bioelectronics* **2010,** *25* (7), 1675-1680.

7. Chabot, V.; Cuerrier, C. M.; Escher, E.; Aimez, V.; Grandbois, M.; Charette, P. G., Biosensing based on surface plasmon resonance and living cells. *Biosensors and Bioelectronics* **2009,** *24* (6), 1667-1673.

8. Beuthan, J.; Minet, O.; Helfmann, J.; Herrig, M.; Müller, G., The spatial variation of the refractive index in biological cells. *Physics in Medicine and Biology* **1996,** *41* (3), 369-382.

9. Zhang, Q.; Zhong, L.; Tang, P.; Yuan, Y.; Liu, S.; Tian, J.; Lu, X., Quantitative refractive index distribution of single cell by combining phase-shifting interferometry and AFM imaging. *Scientific reports* **2017,** *7* (1), 2532-2532.

10. Robelek, R.; Wegener, J., Label-free and time-resolved measurements of cell volume changes by surface plasmon resonance (SPR) spectroscopy. *Biosensors and Bioelectronics* **2010,** *25* (5), 1221-1224.

11. Moreira, B.; Tuoriniemi, J.; Kouchak Pour, N.; Mihalčíková, L.; Safina, G., Surface Plasmon Resonance for Measuring Exocytosis from Populations of PC12 Cells: Mechanisms of Signal Formation and Assessment of Analytical Capabilities. *Analytical Chemistry* **2017,** *89* (5), 3069-3077.

12. Mir, T. A.; Shinohara, H., Label-free observation of three-dimensional morphology change of a single PC12 cell by digital holographic microscopy. *Analytical Biochemistry* **2012,** *429* (1), 53-57.

13. Zhang, Y.; Huang, T.; Jorgens, D. M.; Nickerson, A.; Lin, L.-J.; Pelz, J.; Gray, J. W.; López, C. S.; Nan, X., Quantitating morphological changes in biological samples during scanning electron microscopy sample preparation with correlative super-resolution microscopy. *PloS one* **2017,** *12* (5), e0176839-e0176839.

14. Bray, F.; Ferlay, J.; Soerjomataram, I.; Siegel, R. L.; Torre, L. A.; Jemal, A., Global cancer statistics 2018: GLOBOCAN estimates of incidence and mortality worldwide for 36 cancers in 185 countries. *CA: A Cancer Journal for Clinicians* **2018,** *68* (6), 394-424.

15. Bethesda, *Cervical Cancer Treatment (PDQ®): Health Professional Version*. National Cancer Institute (US): 2019.

16. Lowe, S. W.; Lin, A. W., Apoptosis in cancer. *Carcinogenesis* **2000,** *21* (3), 485-495.

17. Gordon, J. L.; Brown, M. A.; Reynolds, M. M., Cell-Based Methods for Determination of Efficacy for Candidate Therapeutics in the Clinical Management of Cancer. *Diseases (Basel, Switzerland)* **2018,** *6* (4), 85.

18. Gomez Perez, M.; Fourcade, L.; Mateescu, M. A.; Paquin, J., Neutral Red versus MTT assay of cell viability in the presence of copper compounds. *Analytical Biochemistry* **2017,** *535*, 43-46.

19. Kyrylkova, K.; Kyryachenko S Fau - Leid, M.; Leid M Fau - Kioussi, C.; Kioussi, C., Detection of apoptosis by TUNEL assay. (1940-6029 (Electronic)).

20. Smith, S. M.; Wunder, M. B.; Norris, D. A.; Shellman, Y. G., A Simple Protocol for Using a LDH-Based Cytotoxicity Assay to Assess the Effects of Death and Growth Inhibition at the Same Time. *PLOS ONE* **2011,** *6* (11), e26908.

21. Kosaihira, A.; Ona, T., Rapid and quantitative method for evaluating the personal therapeutic potential of cancer drugs. (1618-2650 (Electronic)).

22. Elmore, S., Apoptosis: a review of programmed cell death. *Toxicologic pathology* **2007,** *35* (4), 495-516.

23. Hacker, G., The morphology of apoptosis. (0302-766X (Print)).

24. Kim, K. S.; Cho, C. H.; Park, E. K.; Jung, M.-H.; Yoon, K.-S.; Park, H.-K., AFM-detected apoptotic changes in morphology and biophysical property caused by paclitaxel in Ishikawa and HeLa cells. *PloS one* **2012,** *7* (1), e30066-e30066.

25. Masters, J. R., HeLa cells 50 years on: the good, the bad and the ugly. *Nature Reviews Cancer* **2002,** *2* (4), 315-319.

26. Clément, M.-V.; Ponton, A.; Pervaiz, S., Apoptosis induced by hydrogen peroxide is mediated by decreased superoxide anion concentration and reduction of intracellular milieu. *FEBS Letters* **1998,** *440* (1), 13-18.

27. Singh, M.; Sharma, H.; Singh, N., Hydrogen peroxide induces apoptosis in HeLa cells through mitochondrial pathway. *Mitochondrion* **2007,** *7* (6), 367-373.

28. Rello, S.; Stockert Jc Fau - Moreno, V.; Moreno V Fau - Gamez, A.; Gamez A Fau - Pacheco, M.; Pacheco M Fau - Juarranz, A.; Juarranz A Fau - Canete, M.; Canete M Fau - Villanueva, A.; Villanueva, A., Morphological criteria to distinguish cell death induced by apoptotic and necrotic treatments. (1360-8185 (Print)).

29. Visagie, M. H.; Jaiswal, S. R.; Joubert, A. M., In vitro assessment of a computer-designed potential anticancer agent in cervical cancer cells. *Biological Research* **2016,** *49* (1), 43.

30. Kumar, R.; Srivastava, R.; Srivastava, S., Detection and Classification of Cancer from Microscopic Biopsy Images Using Clinically Significant and Biologically Interpretable Features. *Journal of Medical Engineering* **2015,** *2015*, 14.

31. Rajbongshi, N.; Bora, K.; Nath, D.; Das, A.; Mahanta, L., Analysis of morphological features of benign and malignant breast cell extracted from fnac microscopic image using the pearsonian system of curves. *Journal of Cytology* **2018,** *35* (2), 99-104.

32. Hemminki, K.; Granström, C., Morphological types of breast cancer in family members and multiple primary tumours: is morphology genetically determined? *Breast Cancer Research* **2002,** *4* (4), R7.

33. Rahmadwati; Naghdy, G.; Ros, M.; Todd, C. In *Morphological Characteristics of Cervical Cells for Cervical Cancer Diagnosis*, Proceedings of the 2011 2nd International Congress on Computer Applications and Computational Science, Berlin, Heidelberg, 2012//; Gaol, F. L.; Nguyen, Q. V., Eds. Springer Berlin Heidelberg: Berlin, Heidelberg, 2012; pp 235-243.

34. GM, C., *The Cell: A Molecular Approach*. 2nd ed.; The Cell: A Molecular Approach: The Cell: A Molecular Approach, 2000.

35. Revel, J. P.; Hoch, P.; Ho, D., Adhesion of culture cells to their substratum. *Experimental Cell Research* **1974,** *84* (1), 207-218.

36. Blikstad, I.; Carlsson, L., On the dynamics of the microfilament system in HeLa cells. *The Journal of cell biology* **1982,** *93* (1), 122-128.

37. McKeague, A. L.; Wilson, D. J.; Nelson, J., Staurosporine-induced apoptosis and hydrogen peroxide-induced necrosis in two human breast cell lines. *British Journal of Cancer* **2003,** *88* (1), 125-131.

38. Troyano, A.; Sancho, P.; Fernández, C.; de Blas, E.; Bernardi, P.; Aller, P., The selection between apoptosis and necrosis is differentially regulated in hydrogen peroxide-treated and glutathione-depleted human promonocytic cells. *Cell Death & Differentiation* **2003,** *10* (8), 889-898.

39. Zeiss, C. J., The apoptosis-necrosis continuum: insights from genetically altered mice. (0300-9858 (Print)).

40. Majno, G.; Joris, I., Apoptosis, oncosis, and necrosis. An overview of cell death. (0002-9440 (Print)).

41. Krysko, D. V.; Vanden Berghe, T.; D'Herde, K.; Vandenabeele, P., Apoptosis and necrosis: Detection, discrimination and phagocytosis. *Methods* **2008,** *44* (3), 205-221.

42. Jung, L. S.; Campbell, C. T.; Chinowsky, T. M.; Mar, M. N.; Yee, S. S., Quantitative Interpretation of the Response of Surface Plasmon Resonance Sensors to Adsorbed Films. *Langmuir* **1998,** *14* (19), 5636-5648.

43. Ramsden, J. J.; Li, S. Y.; Prenosil, J. E.; Heinzle, E., Kinetics of adhesion and spreading of animal cells. *Biotechnology and Bioengineering* **1994,** *43* (10), 939-945.

44. Deng, H.; Wang, C.; Su, M.; Fang, Y., Probing Biochemical Mechanisms of Action of Muscarinic M3 Receptor Antagonists with Label-Free Whole Cell Assays. *Analytical Chemistry* **2012,** *84* (19), 8232-8239.

45. Fang, Y.; Ferrie, A. M.; Fontaine, N. H.; Mauro, J.; Balakrishnan, J., Resonant Waveguide Grating Biosensor for Living Cell Sensing. *Biophysical Journal* **2006,** *91* (5), 1925-1940.

CHAPTER 5 : Conclusion

Biomedical is a broad area of science that looks for ways to prevent and treat diseases that cause illness and death in human. The diagnostic process through laboratory testing has been said to be 60% to 70% of critical decisions in diagnosis and treatment of diseases, and aids in the effective Diseases Management (DM).[1] The diagnostic tests are categorized into general chemistry, immunochemistry, hematology/cytology and microbiology that measures compounds in the body, match antibody-antigen response, blood and cells, and detect disease-causing pathogens. However, despite the advances in biomedical analysis, there is still a need to improve the current diagnostic landscape especially for infectious diseases that would benefit from new technologies that can identify a specific pathogen in a simple and rapid manners.[2] One of the most promising approaches for making early disease diagnosis is to explore the use of biomarkers and molecular nucleic acid based detection. The challenge towards the application is that these target molecules often presence in very low quantities and small sizes, thus requires highly sensitive and specific measurement tools.

SPR biosensors have shown immense potential for application in medical diagnostics, with the label-free capability and versatility to measure the interactions between biomolecules (including various disease biomarkers) and to provide the analysis in real time.[3, 4] However, the main obstacle in achieving high sensitivity and specificity when measuring in real clinical samples has to do with the complexity of the biofluids.

In this dissertation, the overarching goal is to providing solutions in applying SPR biosensors into clinical setting via a design of smart and functional interfaces. For this purpose, various surface modifications and biomolecular binding mechanisms were studied, intended to resolve the issues like the non-specific binding from complex media and the poor signal response from less effective interactions. In Chapter 2, the detection of P. *falciparum* DNA for early detection of Malaria using in-situ DNA hybridization chain reaction (HCR) and AuNPs signal amplification was demonstrated. A linear sensitivity range of target DNA concentrations from 0.1 nM to 0.1 μM was achieved and the signal was amplified 10x after AuNPs enhancement steps. The measurements were repeated in human blood plasma, the results showed that despite the non-specific binding from the plasma sample, the detection of target DNA was not compromised. Some limitations of this study include incomplete test of specificity against other Plasmodium species, and incomplete comparison in terms of sensitivity made to actual clinical methods such as PCR. Moving forward, these are the two areas that will be followed through, in addition to further work on a target DNA directly collected from Malaria patients.

In Chapter 3, supported lipid bilayer membranes (SLBs) were introduced as an antifouling enabled sensitive detection of CT and IgG in undiluted human serum. The use of protein A not only provided a controlled orientation of capture antibody to specifically bind to the analytes, but the strong adsorption on EPC^{+} on protein A/MPO surface lead to a tightly packed structure that plays critical role for reduction of nonspecific binding. A linear sensitivity for CT concentration ranging from 5 to 25 μg/ml was achieved, and in the effort to further increase the sensitivity, the AuNPs enhancement step enabled detection at

lower concentrations, from 0.01 to 0.05 μg/ml of CT. The addition of this membrane caused no reduction in SPR signal when compared to a detection carried out via a traditional coupling scheme (i.e. EDC/NHS coupling over a mercaptoundecanoic acid). Although the FRAP analysis verified the strong charge-based interaction between EPC^+ and protein A/MPO surface, it does not provide the information of the actual structure of the lipids formed on the surface. Therefore, more surface characterizations will be performed as future works.

In Chapter 4, the potential of SPR for studying cancer cells toxicity was explored and the findings led to a more understanding of the complex cell-substrate interface. HeLa cells was chosen as model system, while H_2O_2 induced morphological changes to the cells with different behaviors as the concentrations of H_2O_2 increases. The theoretical equation that governed the effect of refractive index and adsorbed layer thickness to SPR signal has to be further expanded for the calculated signal to more precisely match the actual SPR signal. Other recommendations include improvement on the microscopic imaging technique, ideally the images of the actual cells on SPR chip used for the morphological observations. This can potentially be done by constructing an in-house high-resolution microscope camera attached to the SPR cell holder. Future work will be focused on studying more clinically relevant toxics or drugs related to cancer cells and treatment.

References

1. Regan, M.; Forsman, R., The Impact of the Laboratory on Disease Management. *Disease Management* **2006,** *9* (2), 122-130.

2. Caliendo, A. M.; Gilbert, D. N.; Ginocchio, C. C.; Hanson, K. E.; May, L.; Quinn, T. C.; Tenover, F. C.; Alland, D.; Blaschke, A. J.; Bonomo, R. A.; Carroll, K. C.; Ferraro, M. J.; Hirschhorn, L. R.; Joseph, W. P.; Karchmer, T.; MacIntyre, A. T.; Reller, L. B.; Jackson, A. F.; Infectious Diseases Society of, A., Better tests, better care: improved diagnostics for infectious diseases. *Clinical infectious diseases : an official publication of the Infectious Diseases Society of America* **2013,** *57 Suppl 3* (Suppl 3), S139-S170.

3. Patel, S.; Nanda, R.; Sahoo, S.; Mohapatra, E., Biosensors in Health Care: The Milestones Achieved in Their Development towards Lab-on-Chip-Analysis. *Biochemistry research international* **2016,** *2016*, 3130469-3130469.

4. Sin, M. L. Y.; Mach, K. E.; Wong, P. K.; Liao, J. C., Advances and challenges in biosensor-based diagnosis of infectious diseases. *Expert Review of Molecular Diagnostics* **2014,** *14* (2), 225-244.